JAERI-M
91-007

STUDIES ON DEVELOPMENT OF PRESSURE MEASUREMENT METHODS FOR A LARGE FUSION EXPERIMENTAL DEVICE

February 1991

Norio OGIWARA

日本原子力研究所
Japan Atomic Energy Research Institute

JAERI-Mレポートは，日本原子力研究所が不定期に公刊している研究報告書です。
入手の問合わせは，日本原子力研究所技術情報部情報資料課（〒319-11茨城県那珂郡東海村）あて，お申しこしください。なお，このほかに財団法人原子力弘済会資料センター（〒319-11 茨城県那珂郡東海村日本原子力研究所内）で複写による実費頒布をおこなっております。

JAERI-M reports are issued irregularly.
Inquiries about availability of the reports should be addressed to Information Division, Department of Technical Information, Japan Atomic Energy Research Institute, Tokai-mura, Naka-gun, Ibaraki-ken 319-11, Japan.

編集兼発行　日本原子力研究所
印　　刷　㈱原子力資料サービス

JAERI-M 91-007

Studies on Development of Pressure Measurement Methods for a Large Fusion Experimental Device

Norio OGIWARA

Department of JT-60 Facility
Naka Fusion Research Establishment
Japan Atomic Energy Research Institute
Naka-machi, Naka-gun, Ibaraki-ken

(Received January 18, 1991)

This report describes the studies on development of the pressure measurement methods, which are necessary to develop and confirm the particle control method for a long-pulse break-even plasma.

We first developed a new type of hot cathode ionization gauge with spherical symmetry to measure the neutral gas pressure in a high magnetic field. The gauge has a linear relation between the ion current and the pressure ranging from 10^{-4} to 1 Pa for N_2 and Ar. The changes in the sensitivity are small; within + 20% in a field of 0 - 1.2 T.

Then we describe a new method for using a Penning gauge to measure pressure in high magnetic fields. The intensity of the H_α and H_β Balmer lines emitted from a Penning discharge is a function only of the discharge ion current: their intensity is independent of anode voltage and magnetic fields from 0.1 to 2.0 T. The light intensity is proportional to the ion current below $\sim$ 0.1 Pa. In addition, we demonstrated the possibility of the partial pressure measurement with the light emitted from the Penning discharge. The line intensities are individually linear to the partial pressure in the gas mixture of H_2 and He.

Next we have constructed the fast pressure monitoring system with the newly developed gauges. The gauges are used to monitor the pressure near the JT-60 plasma. The response time is fast (less than

10 ms) because of the Penning discharge which is sustained by the confining magnetic field of the plasma. Because the structure is very simple, the gauges are reliable for use in severe conditions in a fusion device.

Finally, the usefulness of the fast response gauge is demonstrated. The outgassing mechanisms are studied in the JT-60 tokamak. Large amounts of gases are abruptly released during the disruption of the plasma. The disruptions of 1 MA plasmas outgas a surface area of $\sim$10 m^2. The gases of 30-80 Pam^3 are released within 30 ms. Then three quarters of them return to the wall. This return of the gases to the wall clearly reveals the wall pumping of the graphite first wall.

Keywords: Fusion Device, Pressure Measurement, Ionization Gauge, Penning Gauge, Light Intensity, Fast Response, Outgassing Mechanism, JT-60 Tokamak, Wall Pumping, Particle Control

JAERI－M　91－007

大型核融合実験装置における圧力測定法の開発に関する研究

日本原子力研究所那珂研究所 JT－60 試験部
荻原　徳男

（1991 年 1 月 18 日受理）

本論文は，臨界プラズマを長時間維持するための粒子制御技術の開発にとって必要なプラズマ近傍での圧力測定法の開発に関する研究をまとめたものである。

最初に 1 T 程度の強磁場中で使用しうる球対称形の電離真空計を開発した。この真空計においては，10^{-4} Pa から 1 Pa までの圧力範囲でイオン電流は圧力に比例する。また，1.2 T までの磁場に対する感度変化は ＋20 % 以下である。

次に強磁場中での分圧測定を行うためのペニング型真空計を開発した。ペニング放電から発せられる水素の H_α および H_β 線強度はアノード電圧および磁場には依存せず，イオン電流のみの関数であり，しかも，0.1 Pa 以下では，その線強度はイオン電流に比例する。また，線スペクトルの分析から水素雰囲気下において微量のヘリウムを検知することも可能である。

以上の開発に基づき JT－60 においてプラズマ近傍での圧力を高速でモニタする真空計を実用化した。応答速度は 10 ms 以下である。本真空計は，核融合装置での使用に対して十分な信頼性を有する。

高速応答の圧力測定を行うことにより JT－60 において放電終了直後の放出ガス特性を調べた。プラズマディスラプションに伴って多量のガス放出がおこる。1 MA プラズマのディスラプションでは約 10 m^2 の第一壁表面から 30 － 80 Pam^3 のガスが放出される。このうち 3 ／ 4 は再び壁に戻るが，これは黒鉛第一壁の排気作用を示すものである。

那珂研究所：〒 311－01　茨城県那珂郡那珂町大字向山 801－1

Contents

目　　次

1. General introduction

1.1 Outline of nuclear fusion research

Nuclear fusion reactions are the source of the enormous power radiated from the sun. They have the potential of providing an essentially inexhaustible source of energy for the future.

Great efforts have been devoted on building miniature suns on earth for over thirty years. The variety of approaches can be classified into closed system (tokamak, stellarator), open system (mirror), theta pinch and inertia fusion.

In the closed system, fusion plasmas are confined by toroidal magnetic lines of force forming an enclosed system. Open systems utilize magnetic mirrors which push back plasma particles outside the loss cone. Pinches are plasmas carrying large current capable of generating sufficient magnetic fields to confine and heat the plasma. In inertia fusion, the laser or ion beams are focused onto a pellet or a gaseous column of DT to ignite, compress and heat it. Among these approaches, the tokamak device originally developed in the USSR has been the most successful[1] and has received the most attention.

The scientific feasibility of fusion will be established when it is demonstrated that plasmas can be heated to thermonuclear temperatures and confined sufficiently well under conditions which lead to a positive energy balance. These conditions are represented by the Lawson criterion on plasma density, confinement time and temperature.[2]

Experimental progress with tokamak plasmas has been considerable in recent years. Following a number of medium-sized tokamaks constructed in the 1970's, most of which are now in operation, three large tokamaks have been in operation since the

early 1980's: the Tokamak Fusion Test Reactor (TFTR) started plasma operations at Princeton Plasma Physics Laboratory (USA) in Dec. 1982,[3] the Joint European Torus (JET) at Culham Laboratory (England) obtained the first plasma in June 1983,[4] and the first plasma of the JT-60 was obtained at Naka-site of JAERI in Apr. 1985.[5] All three of these large tokamaks aim at achieving the break-even conditions, plasma conditions in which the energy necessary to be put into plasma to yield the thermonuclear fusion reaction balances the energy released from the plasma, corresponding to the plasma temperature of ~10 keV and the product of the plasma density and the plasma energy confinement time of $\sim 10^{20}$ m^{-3} s.[6]

The best value so far of the triple product of T_i, n, and τ_E, 8×10^{20} m^{-3} s keV, was achieved recently on JET.[7] It is less than a factor of 10 away from ignition. This means that break-even conditions have almost been established. However, the duration was less than 1 s. This is mainly because the first wall is the most influential part in both reducing the impurities and increasing the density limit.

Together with the experimental research aimed at achieving break-even conditions, conceptual design studies have been performed on the next-step machines such as the Fusion Experimental Reactor (FER) in Japan,[8] the Next European Torus (NET) in EC,[9] and the International Thermonuclear Experimental Reactor (ITER) which has been designed by Japan, EC, USA, and USSR in collaboration under the auspices of International Atomic Energy Agency (IAEA).[10] These next-step machines aim to achieve a long ignited and controlled DT burn. Table 1.1 shows the parameters and performances for the ITER. The main specific areas

to be covered are as follows: 1) power and particle exhaust physics (i.e., the combined fields of the physics of the plasma edge and plasma-wall interaction as well as impurity control), 2) disruption control and operational limits, 3) enhanced confinement, 4) heating and fueling physics, 5) long-pulse operation (including noninductive current drive), and 6) physics of burning plasma.

In order to realize the performance of the next-step machines, it is of the utmost importance to arrive at an overall optimization of tokamak discharge conditions which can be extrapolated to those of the next-step machines. Therefore, with the present machines, we must complete the database necessary for taking the decision to start construction. From the viewpoint of technology, noninductive current drivers and particle control devices such as pumped divertor and pump limiter will be more urgently developed and examined in order to ensure steady-state operation.

1.2 Significance of pressure measurement

As shown in Table 1.2, pressure measurement is needed in various fields for fusion devices.[11] First, the vacuum vessel is evacuated. The performance is measured with commercial pressure gauges. Then the first wall is cleaned by the discharge (discharge cleaning). Its purpose is to remove light impurities such as oxygen and carbon. Certain types of discharge cleaning are applied.[12-14] Usually, the discharge is carried out in a rather weak magnetic field. Therefore, the commercial residual

gas analyzer (RGA) is applicable to monitor the cleaning efficiency, if necessary, with magnetic shielding.

Neutral beam injection is very effective in heating the ohmically heated plasma.[15] However, its efficiency is strongly reduced if the high energy atomic hydrogen (and its isotope) is reionized in the transition tube before entering the plasma. The reionizing rate is dependent on the pressure in the tube. The experience gained at PLT (Princeton Large Tokamak) was valuable. Unless the pressure in the tube is low enough, the reionized high-energy particles hit the tube wall and cause the abrupt gas release. Therefore, monitoring of the pressure in the transition tube is very important for neutral beam injection.

Ion temperature is measured by the charge-exchange method. In this case, the reionization probability of fast neutrals is essential to evaluate the ion temperature. Thus, the pressure should be measured to within an accuracy of ±5%.

In the DT burning experiment, the retention of tritium will be one of the main problems.[16] Total gas flow should be measured with pressure measurement. In addition, the leak hunting method in D_2 atmosphere will be developed.[17,18]

Gas pressure measurement is necessary to consider particle balance.[19] Assuming $Z_{eff} \approx 1$, the variation of the total number of electrons in the discharge, N_e, is described by the equation

$$\frac{dN_e}{dt} = q + (R - 1)\frac{N_e}{\tau_p} - \frac{dP}{dt}(V_T - V_p) - PS, \qquad (1)$$

where q = gas injection rate,

P = gas pressure around the plasma case,

R = recycling coefficient, i.e. the ratio of atoms coming from the wall to the number of particles incident upon the wall,

τ_p = gross particle lifetime,

V_T = volume of the vacuum torus,

V_p = plasma volume,

S = pumping speed.

In addition, the effective particle confinement time τ_A is defined as $\tau_A = \tau_p / (1-R)$, which is obtained if we measure N_e, q, and P;

$$\tau_A = N_e \Big/ \left\{ q - \frac{dN_e}{dt} - \frac{dP}{dt}(V_T - V_p) - PS \right\}. \qquad (2)$$

Equation (2) shows the relation of effective particle confinement time to the gas pressure around the plasma column. More detailed investigation into particle confinement requires that R should be evaluated.

To realize a fusion reactor, various techniques for particle control must be developed. We show in Table 1.3 the relation of pressure measurements to the techniques which must be developed. Fuel gas pressure should be monitored to ensure particle control. In the steady-state reactor, unloaded fuel gas should be removed efficiently from the reactor chamber in order to control the plasma density.[20,21] As described before, JET has achieved a world record in the Q-value (~0.8) due to the introduction of the beryllium limiter. The limiter tiles have the following two effects: a) oxygen virtually disappeared from the plasma, and b) the hydrogenic species are strongly pumped out. These pumping effects not only reduce the radiation loss to ~10% of the input

power but also permit the use of the heavy gas fueling to control impurities and the plasma with Z_{eff} ~1.5 during the additional heating phase. However, the duration was less than 1 s. This is because the first wall was saturated with fuel particles. Moreover the first wall saturated with the particles may be the source of refueling. Since we must operate the plasma within the density limit in order to realize a steady-state reactor, we need an active particle control method instead of the passive wall pumping. In other words, we must develop methods and confirm the performance for removing the fuel and ash particles from the boundary of a break-even plasma over a prolonged period. In the future, the pressure gauges near the plasma boundary will be sensors which will control the reacting plasma.[21]

Impurity gases should also be removed to maintain a high temperature plasma.[22,23] Graphite is widely used in the present fusion devices.[24-26] The carbon has two possible ways of entering the plasma; one is by physical sputtering and the other is by chemical sputtering. If the chemical sputtering is dominant, the partial pressure of the hydrocarbon, which is believed to be produced on the graphite first wall in reaction with hydrogen atom, should be removed. Furthermore, in a fusion reactor, the He ash should be removed.[27,28] The design study of ITER shows that the partial pressure of He should be less than 10^{-2} Pa. Therefore, the partial pressure measurement near the plasma is also important in order to control impurities and not to dilute the fuel.

Next, the time response of the pressure measurement is discussed. An important concern in attempts to obtain pressure measurements on the first-generation plasma devices was the need

for a high transient response. Since the duration of the discharge was only of the order of 1 ms, gauge response times of 10-100 μs were desired to infer the neutral density temporal behavior during the discharge.[29,30] In contrast, the discharge duration has been extended to beyond 1 s for the present generation of large tokamaks, and relaxing response requirements to 1-10 ms for pressure measurement in the vacuum vessel.[11] In addition, the programmed gas-injection systems for plasma density control have required gas-flow measurement with a similar response time (~10 ms).[31] Here we discuss the response time in order to develop the technique for removing the particles from the plasma boundary. From the experiment of JET, heavy fueling by pellet injection and gas feed is needed to achieve a break-even plasma. After injection into the plasma, the particles will be released from the plasma with a time constant of τ_p (particle time constant). Thus the particle density (pressure) near the plasma changes with an almost unchanging time constant. Therefore, the response time of the pressure measurement should be less than the particle time constant. Because τ_p of the JT-60 is in the order of 100 ms, we must measure the pressure with the time constant of ~10 ms.

Relatively few types of gauges have been applied to pressure measurements in fusion devices,[11,32] mainly because of the response time requirements. They are listed in Table 1.4. The most commonly applied gauge types are the various forms of hot-filament ionization gauges because of their large pressure range and short-transient response. The conventional triode, Bayard-Alpert, and Schultz-Phelps gauges have been utilized. The most troublesome application problems are the effects of magnetic

fields and plasma-induced spurious signals. Generally, ion-gauge operation is quite sensitive to an arbitrarily applied magnetic field because of the effect on the low electron trajectories.[33,34] For operation of the triode or BA gauge in fields higher than 0.01 T, external magnetic shielding is required.

The Schultz-Phelps gauges can be operated in magnetic fields without external shielding if the field is oriented parallel to the electric field in the gauges. In general, the sensitivity will not be independent of the ambient field because of the lengthened electron path. Martin[33] has shown that a Schultz-Phelps gauge with 0.2 cm electrode spacings is independent of a parallel applied magnetic field up to 0.15 T. A more recent test by Mioduszewski and Edmonds[35] showed a sensitivity which was independent of the field up to 0.02 T and then decreased by 70% at 0.07 T.

An alternative to the hot-filament ionization gauge is the cold-cathode ionization gauge. However, this type of gauge sacrifices accuracy and reproducibility for the simplification of hardware.[36] A disadvantage of cold-cathode discharge is that the discharge current is not a linear function of the pressure. The sensitivity changes depending on the electrode geometry, applied fields, and pressure range. In spite of this disadvantage, this type of gauge recently has been used in an attempt to measure pressures in high magnetic fields.[11,37]

The present generation of capacitance-diaphragm manometers has been tested in fusion devices.[38] It was found that the sensor heads are insensitive to magnetic fields up to 0.6 T. However, the electronics package is quite sensitive to magnetic fields.

Thus the package would require magnetic shielding. For the application of the capacitance-diaphragm gauge in fusion devices, the vibration must be isolated almost completely because the sensor heads are microphonic. This would limit the use of this type of gauge.

Quadrupole-type mass filters have been used for partial pressure measurements.[39] However, their use is almost restricted to the diagnosis of discharge cleaning effectiveness. The most troublesome problems are the effects of magnetic fields and plasma-induced spurious signals. In general, magnetic fields produce severer effects on the mass filters than on the hot-filament ionization gauges. Usually, the mass filters are employed only with magnetic shielding.

The above discussion shows that the pressure measurement near the plasma will be more important in future fusion devices and that the application of commercial pressure gauges will be restricted mainly because of the effects of high magnetic fields and plasma-induced spurious signals.

1.3 Outline of the present work

As mentioned above, the pressure measurement near the plasma will be more important for next-step fusion research. Thus we have developed new pressure measurement methods in a high magnetic field. They are suitable for any type of magnetically confined fusion devices.

First, in chapter 2, a new type of hot filament ionization gauge is described for the measurement of neutral gas density in a high magnetic field. A notable feature of the gauge is its spherical symmetry. The ion current varies linearly with the pressure from 10^{-4} to 1 Pa for N_2 and Ar. The sensitivity changes by no more than + 20% in a magnetic field of up to 1.2 T. The main reasons for this small change in sensitivity are as follows: (1) the probability of ionization of gas molecules is almost independent of a high magnetic field because the spherical symmetry causes electrons to be emitted from the filament to the region in which the electric field is almost parallel to the magnetic field; (2) the probability of the ion collection is independent of the magnetic field.

In chapter 3, we propose and demonstrate a new type of partial pressure gauge for use in a high magnetic field. It is a type of Penning configuration gauge. A Penning discharge in the cell is sustained by the magnetic field which confines the plasma. The light emitted from the Penning discharge is analyzed. This gauge enables us to measure He and D_2 independently. First, the principle of the gauge is described. Then the new type of gauge is experimentally demonstrated. The experiment is divided into two parts; one deals with hydrogen pressure measurement in a high magnetic field, and the other with the gas mixture of H_2 and He.

The newly developed gauges are used to measure the pressure near a plasma in JT-60. The gauges are controlled by a personal computer. The main features of the gauges are as follows: (a) the

response time is fast ($\lesssim$10 ms), and (b) the structure is so simple that the gauges are reliable for use in the severe conditions of JT-60. In chapter 4, the details of this fast pressure monitoring system are described. The performance of the gauges is shown.

In chapter 5, an application of the fast response pressure measurement is shown. The outgassing from the first wall made of graphite has been investigated. The pressure near hydrogen plasmas is measured in a fast response time (<10 ms). Large amounts of gases are found to be abruptly released in two stages during a disruption of the plasma. The first gas release occurs at the same time as the soft x-ray crash. This is ascribed to the heat flux due to the loss of the plasma thermal energy (thermal quench). The second appears during the current decay phase. This is caused by the heat flux due to the loss of the plasma magnetic energy. The disruption of a 1 MA plasma outgases a surface area of ~10 m^2. The typical disruption releases 30-80 Pa m^3 of gases in ~30 ms. Then three quarters of them return to the wall. In the case of a normal discharge, the outgassing occurs after the end of the plasma.

Finally, we summarize the concluding remarks of these studies.

References

[1] L. A. Artsimovich, Nucl. Fusion 12, 215 (1972).

[2] J. D. Lawson, Proc. Phys. Soc. (London) B70, 6 (1957).

[3] J. Sinnis, Proc. 10th Symp. on Fusion Engrg., Philadelphia (1983) p. 2096.

[4] M. Huguet, Proc. 10th Symp. on Fusion Engrg., Philadelphia (1983) p. 834.

[5] JT-60 team (presented by M. Yoshikawa), Plasma Physics and Controlled Fusion 28, 165 (1986).

[6] B. J. Green, Nucl. Fusion 19, 515 (1979).

[7] P. R. Thomas for the JET Team, in Proc. 9th International Conference on Plasma Surface Interactions in Controlled Fusion Devices, Bounemouth, 1990.

[8] FER Design Team, JAERI-M 88-090 (1988).

[9] NET Design Group, EUR-FU/XII-361/85/34 (1985).

[10] ITER Concept Definition vol.1 and vol.2, Vienna, IAEA, 1989.

[11] H. F. Dylla, J. Vac. Sci. Technol. 20, 119 (1982).

[12] R. S. Calder, Vacuum 24, 437 (1974).

[13] L. Oren and R. J. Taylor, Nucl. Fusion 17, 1143 (1977).

[14] Y. Sakamoto, Proc. IX Inter. Vac. Congress & Inter. Conf. on Solid Surface, Madrid, p. 716 (Asociacion Espanola del Vacioy Sus Aplicaciones, Madrid, 1983).

[15] H. Eubank et al., Proc. 7th Inter. Conf. Plasma Physics and Controlled Nuclear Fusion Research (1979) p. 167.

[16] K. L. Wilson and W. L. Hsu, J. Nucl. Mater. 145/147, 121 (1987).

[17] W. R. Blanchard, R. B. Krawchuk, and H. F. Dylla, J. Vac. Sci. Technol. 20, 1162 (1982).

[18]T. Winkel and J. L. Hemmerich, J. Vac. Sci. Technol. A5, 2637 (1987).

[19]TFR Group, J. Nucl. Mater. 93 & 94, 272 (1980).

[20]G. M. McCracken, Proc. of an IAEA Workshop on Fusion Reactor Design Problems, p. 471.

[21]A. Miyahara, Kakuyugo-kenkyu 55, 7 (1986).

[22]D. Düchs et al., J. Nucl. Mater. 53, 102 (1974).

[23]G. M. McCracken and P. E. Stott, Nucl. Fusion 19, 889 (1979).

[24]A. E. Pontau et al., J. Vac. Sci. Technol. A4, 1193 (1986).

[25]J. Ehrenberg et al., IPP-JET Report No. 29 (1985).

[26]T. Arai et al., J. Nucl. Mater. 162/164, 743 (1989).

[27]Y. Seki et al., Nucl. Fusion 20, 1213 (1980).

[28]M. Sugihara and T. Abe, Nucl. Fusion 21, 1024 (1981).

[29]J. Jacquinot, C. Deck, and J. Godarert, Rev. Sci. Instrum. 43, 905 (1972).

[30]G. Lewin and G. Martin, Rev. Sci. Instrum. 33, 447 (1962).

[31]G. Schilling et al., Proc. 11th Symp. on Fusion Technol., Oxford, Sept. 1980 (Pergamon, Oxford) p.967.

[32]Y. Tuzi, Kakuyugo-kenkyu 55, 461 (1986).

[33]G. D. Martin Jr., in 1961 Transactions of 8th Vacuum Symposium and 2nd International Congress of the American Vacuum Society (Pergamon, New York, 1962), p. 476.

[34]A. Berman, J. Vac. Sci. Technol. 18, 1017 (1981).

[35]P. K. Mioduszewski and P. H. Edmonds, presented at 2nd Annual Symposium of the Tenn-Valley Chapter of the Vacuum Society, Knoxville, Oct. 1981, (unpublished).

[36]W. Schuurman, Physica 36, 136 (1967).

[37]S. R. Thomas Jr. et al., J. Vac. Sci. Technol. A4, 1736 (1986).

[38]D. O. Overski, Phys. Rev. Lett. 46, 177 (1981).

[39] Y. Matsuzaki et al., J. Nucl. Mater. **145/147**, 704 (1987).

Table 1.1 ITER parameters and performance

Nominal fusion power	1 GW
Pulse length	> 200 s
Energy multiplication	Q > 5
Plasma major radius	6.0 m
Plasma half-width at midplane	2.15m
Maximum plasma current	22 MA
Toroidal field on axis	4.85 T
Toroidal coil outer radius	11.5 m

Table 1.2 Pressure measurements in fusion device

Measurement	Object
Plasma performance	
pressure near a plasma	particle balance
Supporting diagnostics	
NBI transition duct pressure	reionization efficiency
CX diagnostic duct pressure	ion temperature measurement
Vacuum system operation	
base pressure	vacuum system performance
total gas flow	fuel gas retention (tritium)
leak rate	He in D_2

Table 1.3 Pressure measurement related to plasma performance.

To be measured	To be examined	Technology
fuel gas	particle confinement	density control
light impurity	origin of impurity	impurity control
He partial pressure	He accumulation	He ash exhaust

Table 1.4 Application problems associated with the use of various types of gauges.

Type of gauge	Problem
Hot-filament ionization gauges triode Bayard-Alpert Schulz-Phelps	effects of magnetic fields and plasma-induced spurious signal
Cold-cathode gauges Penning magnetron inverted magnetron	nonlinearities erratic
Capacitance-diaphragm gauge	effect of vibration (sensor head) quite sensitive to magnetic fields (electronics package)
Quadrupole mass filters	effects of magnetic fields and plasma-induced spurious signals

2. A spherical ionization gauge

2.1 Introduction

The assessment of the neutral gas density in the vicinity of a plasma is important for fundamental considerations of particle balance.[1-3] The various forms of ionization gauges are most commonly applied for pressure measurement in fusion devices because of their linearity over a very broad range. Customary gauge heads of the Bayard-Alpert (B-A), Schultz-Phelps, and cold magnetron type have been utilized by making certain provisions.[4-7] Several workers used specially designed ionization gauges.[2,3,8,9] With the use of ionization gauges, the most troublesome problems are the effects of magnetic field and spurious currents induced by the plasma.[6,10] Several techniques have been used to reduce the value of the spurious currents.[10] There have been many works on the behavior of a B-A gauge in a magnetic field,[5,7,11-13] but there have been few approaches to the development of a gauge insensitive to a magnetic field.[14]

We have developed a new type of hot-filament ionization gauge, which is a kind of triode-type gauge. The notable feature of the gauge is its spherical symmetry. This spherical ionization (SI) gauge was found to have small changes in the sensitivity (+ 20% for N_2) in a magnetic field of up to 1.2 T. The gauge is also insensitive to the direction of the magnetic field.

In the first section, the motion of electrons is analyzed to show how it affects the sensitivity. Then the description of the gauge is presented. Next the gauge characteristics in a magnetic field are given. Finally the experimental results are discussed.

2.2 Description of the gauge

2.2.1 Simulation of the electron trajectories

In this part we simulate the electron trajectories for the gauge head with the spherical symmetry in magnetic fields. Both the average path length of electrons and their kinetic energy then are shown to be almost independent of a high magnetic field for this type of gauge.

First the qualitative picture is given of the motion of electrons in a magnetic field based on Berman's[10] and Martin's[11] analyses. The following picture is useful for all types of hot filament ionization gauges. The motion of electrons can be considered as the resultant of two components: a drift along the cathode due to E_n x B and a translation parallel to the lines of the electric field due to E_z. Here, E_n and E_z refer to the components of an electric field E perpendicular and parallel to B. In the region with a high E_n/E_z ratio, no electrons can move away from the filament. Notwithstanding the long path length that the electrons travel in spiraling, the ionization yield is reduced by the lack of the kinetic energy. Electrons starting from the filament with a low E_n/E_z ratio are accelerated along the electric field lines, and they gain enough kinetic energy to yield efficient ionization. Thus, both the average path length and the kinetic energy depend on the electrode geometry of the gauge head as well as the magnetic field strength. Martin[11] applied this picture to evaluation of the sensitivity of gauge heads with planar and cylindrical symmetry. Practically, electrons are emitted in space from the hot filament at different angles. Therefore, we have to consider how all the electrons with

different E_n/E_z ratios contribute to the ionization yield.

Next, the gauge head with the spherical symmetry is dealt with by simulating the electron trajectories in a magnetic field. It is a triode-gauge head with spherical symmetry as shown in Fig. 2.1. The diameters of the elements are as follows: the filament (F), 10 mm; the anode grid (G), 30 mm; the collector (C), 60 mm. This gauge is assumed to be operated with F at ground potential, G at + 100 V, and C at - 20 V. The origin of the coordinates is placed in the center of the gauge head. The magnetic field B is assumed to be parallel to the z axis because the gauge characteristics are in principle independent of the direction of B. Figure 2.1 shows the electron trajectories for magnetic fields of 0.005, 0.01, and 0.05 T. They are seen from the direction of the x axis. Here, we assume that electrons with a thermal energy of 0.2 eV are emitted to the normal direction of the spherical filament. The effect of the space charge is also neglected. The electron trajectories for 0.005 T are complicated because of E_n x B drift as shown in Fig. 2.1(a). In the field of 0.01 T the electrons are forced to move parallel to the magnetic field, although the trajectories are still in a spiral. We find, however, the paths of the electrons at B = 0.05 T are almost parallel to the magnetic field. As a result, electron trajectories become almost straight lines as the strength of B is increased. Thus the average path length of electrons becomes almost equal to that in zero magnetic field. Moreover, the electrons are found to move in the ion-collection region with a low E_n/E_z ratio. Therefore, they have almost same kinetic energy in the ion-collection region as that in zero magnetic field. Where, the "ion-collection region" is defined as the one both in

which electrons gain enough energy by **E** to ionize molecules and in which the produced ions are gathered by the collector in zero magnetic field.

We also simulated the trajectories of electrons with a thermal energy of 10 eV. The results are almost equal to those for the electrons with a thermal energy of 0.2 eV. Although space charge may work to divert the electron trajectories, a higher magnetic field compensates for this effect. These simple simulations show that the electrons have almost the same average path length and kinetic energy in a high magnetic field as those in zero magnetic field.

2.2.2 Description of the SI gauge

The SI gauge, which is of the triode-type, is composed of five concentric spherical grids with a round-shaped filament in the center. The cross-sectional view of the SI gauge is shown in Fig. 2.2. Main parts of the SI gauge are the filament, the grids for extracting electrons and for giving them enough kinetic energy, and the grid for ion collection. In order to study the ion collection probability two potential configurations of the electrodes as given in Table 2.1 are examined. We use G4 and G5 as the electron repeller and the ion collector for the configuration 1. For configuration 2, G4 and G5 serve as the ion collector and the ion repeller, respectively. In both cases, G1 extracts electrons from the hot filament and G2 controls the average energy of the electrons.

Each grid is made of type 304 stainless steel mesh with a transparency of 90%. Each spherical grid is made of a pair of

semispherical grids. All the semispherical grids are attached to the same four quartz plates 6 mm wide and 30 mm long as shown in Fig. 2.2. Lead wires are guided out through the small quartz tubes. In order to avoid the electro-magnetic force, the tungsten filament, 0.2 mm in diameter and 50 mm in total length, is heated by 1 kHz ac, which value has been adopted from the estimation of the resonant frequency. The measured resonant frequency was several hundred Hz at B = 0.1 T and was in good agreement with the estimation. The ~ 1000 hr operating life time of the filament with 1 kHz ac heating in the magnetic field was equal to the one in zero magnetic field. The SI gauge is bakable up to 250^{o}C and is degassed by electron bombardment.

2.3 Performance of the gauge

2.3.1 Experimental procedure

The experimental apparatus is schematically shown in Fig. 2.3. The experiments were carried out in a chamber of 150 mm diameter, which was evacuated through an orifice of 1 mm diameter (0.09 l/s for N_2) by a 200 l/s turbomolecular pump. The SI gauge was monitored with a Bayard-Alpert (B-A) gauge. The pressure difference between them was less than 1% because of the large conductance (13.5 l/s for N_2) of the chamber. After the chamber was baked out for 10 hr at 250^{o}C, a pressure of 3 x 10^{-5} Pa was obtained. Before each run of the measurements, the SI gauge was degassed until the chamber was evacuated below 5 x 10^{-5} Pa. The currents of all the electrodes were measured as functions of both the working gas pressure and the magnetic field strength. An emission current was controlled at the filament so as to be 3 mA.

The magnetic field B was produced by a pair of electromagnets. The direction and magnitude of B at the SI gauge head were monitored by a Hall effect gaussmeter. The uniformity of the magnetic field was within ± 5% over the volume occupied by the SI gauge head. The stray magnetic field at the B-A gauge was less than 0.015 T, while a magnetic field of up to 1.2 T was generated at the SI gauge.

The procedure of the pressure measurements was as follows: (1) The B-A gauge was calibrated by a standard ionization gauge (VS-1)[15] in a calibration stand without the magnetic field; (2) The B-A gauge when mounted in the chamber was calibrated against the stray magnetic field (< 0.015 T); (3) Total calibration factors were given by the product of above two calibration ones. The experimental error is mainly due to the uncertainty of the pressure measurement. Neglecting the error of the sensitivity of the VS-1 gauge, the uncertainty of the pressure measurement was estimated to be less than 15% for pressures above 5×10^{-4} Pa. At 1×10^{-4} Pa it increased to 25% because of the residual gases. Moreover, the uncertainty around 0.1 - 0.2 T increased to 20% because the changes in the sensitivity of the B-A gauge were the largest with the stray magnetic fields.

Preliminary experiments were carried out in order to apply proper potentials to the electrodes. The values for all the electrodes are chosen as shown in Table 2.1. The ion current is unaffected by small variations of the electrode potentials around the values given in Table 2.1. This feature is almost independent of the magnetic field strength.

2.3.2 Results

Figure 2.4 shows the typical variations of the ion current I_i with the pressure P of N_2 and Ar for the configuration 1. The solid lines refer to the linear relation calculated by the least-squares method for all the data obtained below 1.2 T. Almost all the data are found to be included within ± 10% deviation from the relation shown by the solid line for N_2, and within ± 12.5% deviation for Ar. The linear relation between I_i and P is well established over the pressure range less than 1 Pa. Deviations from the linear relation below 1×10^{-4} Pa were observed for these gases despite the large experimental error (± 25% at 1×10^{-4} Pa). This is due to residual currents of ~ 1 nA at the collector. Although the linearity persisted above 1 Pa in zero magnetic field, the gauge characteristics became unstable above 1 Pa with B: (1) The emission current was erratic; (2) Sometimes a discharge occurred.

The sensitivity factors S for the configuration 1 are summarized in Table 2.2 over the pressure and field ranges of less than 1 Pa and below 1.2 T. The factors S are given by $I_i/(I_eP)$. Where, I_i and I_e are the collector and emission currents, respectively. Pressure P was measured directly for N_2 by the calibrated B-A gauge. For Ar the relative ionization efficiency to N_2 was selected to be 1.31.[16]

Figure 2.5 shows the normalized sensitivity S_B/S_0 plotted as a function of the magnetic field strength for the configuration 1. Here, S_B and S_0 are the sensitivity factors in the magnetic field B and in zero magnetic field, respectively. The value of S_B/S_0 has a maximum around 0.1 T and gradually decreases with B.

Then this value increases again with B to a saturated one. The changes of the normalized sensitivity on the magnetic field are similar for N_2 and Ar.

The typical variations of I_i on P of N_2 and Ar are shown in Fig. 2.6 for the configuration 2. The solid lines have the same meaning as that in Fig. 2.4. Almost all the data are included within ± 20% deviation for N_2 and within ± 13% for Ar. The linear relation between I_i and P is maintained up to 1 Pa. Deviations from the the linear relation below ~ 5×10^{-5} Pa was observed. The gauge characteristics became unstable above 1 Pa in the magnetic field. These features are similar to those for the configuration 1. Figure 2.7 shows the changes in the normalized sensitivity S_B/S_0 on the magnetic field strength. They also change in a similar way to those for the configuration 1. The sensitivity factors S change as shown in Table 2.2.

The effect of the field direction on the changes in the sensitivity was also studied. The relation between the ion current and the pressure was the same within the experimental errors for the two directions shown in Fig. 2.2. The same emission current in the magnetic field needed more heating power for the direction of (a) in Fig. 2.2 than that for the direction of (b). In addition, the heating power with B increased by ~ 12% for the direction of (a) and by ~ 6% for the direction of (b). The dependence of the heating power on the field direction shows that the number of electrons starting with a high E_n/E_z ratio decreases with B.

2.4 Discussion

2.4.1 Sensitivity changes with the magnetic field

We are able to measure the gas pressure by the SI gauge, if the gauge is once calibrated in zero magnetic field. In this section we examine the effect of the magnetic field on the sensitivity of this gauge. The sensitivity depends mainly on two factors: (1) The probability of ionization of gas molecules by the emitted electrons within the ion-collection region; (2) The probability of the collection of these ions.

First, the ion collection is discussed. Martin[11] analyzed qualitatively the motion of ions in a magnetic field and showed that they are relatively free to reach any part of the gauge allowed by the electric field. Hsueh[13] also showed by experiment that the changes in the collection of ions are negligible for a B-A gauge in a weak field less than 0.01 T. Let us now look into the result of the SI gauge. There is a difference only in the ion collection between the two configurations shown in Table 2.1; the conditions for the electrons are all the same. Moreover, the ion-collection region is the same for both the configurations. All the ions are collected for the configuration 2. On the other hand, some of them run through the collector grid for the configuration 1. Experimental results show little change with B of the normalized sensitivity between the two configurations (see Figs. 2.5 and 2.7). On the basis of these facts, the probability of ion collection is independent of B. As a result, the motion of electrons in the ion-collection region is mainly responsible for the change in sensitivity with the magnetic field.

Next, the probability of the ionization of gas molecules is discussed. When the emission current is controlled to be constant, the ionization of gas molecules by the emitted electrons in the ion-collection region is determined by the product of the average path length of electrons and the average ionizing probability per electron.

A local maximum at ~ 0.1 T in the normalized sensitivity is probably due to increase of the path length of electrons. In a weak field the electron trajectories are complicated as shown in Fig. 2.1(a) and (b). The average path length in the weak field is larger than that in zero magnetic field. On the other hand, the average kinetic energy appears not to change so drastically. Thus the electrons have more efficient ionization probability of gas molecules.

As the magnetic field increases, the electron trajectories become straight and the electrons have a low E_n/E_z ratio in the ion-collection region: Both the average path length and the kinetic energy of the electrons in the ion-collection region are almost equal to those in zero magnetic field. Thus the sensitivity decreases gradually to that in zero magnetic field.

Above discussion is useful in a magnetic field of up to 0.4 T. However, the normalized sensitivity above ~ 0.4 T becomes larger than unity and then appears to reach saturation (B > 1.0 T). This is probably due to the decrease of the capture rate of electrons by the grids, although we have implicitly assumed that each emitted electron has a constant life time until it is captured by the grids. If the life time of electrons is longer than that in zero magnetic field, the average path length becomes larger and then the sensitivity increases. Following observation

implies the decrease of the capture rate of electrons in magnetic fields above ~ 0.4 T:

(1) All the ions made in the ion-collection region increased with increasing magnetic field above ~ 0.4 T, because both the currents at the collector (- 40 V) and at the grid G3 (grounded) increased for the configuration 2.

(2) In magnetic fields from 0 to 0.4 T, the emission current flowed into G1 and G2 at a constant ratio. Above 0.4 T, the current at G1 increased and decreased at G2. The changes of the ratio were similar to those in the normalized sensitivity.

The effects of a magnetic field on the sensitivity have been widely studied for B-A gauges.[5,7,11-13] The B-A gauges have rather large changes in the sensitivity. The difference of the sensitivity changes between the SI gauge and B-A gauges shows that symmetry plays an important role for the sensitivity changes in a magnetic field.

2.4.2 Pressure range

The SI gauge has a linear relation to within ± 5% between the pressure and the ion current over the ranges of 10^{-4} to 1 Pa and 0 up to 1.2 T. The lower and upper pressure limits are well explained by the "x-ray limit" and the collective motion of ions, respectively.

At first, the lower pressure limit P_x is estimated in accordance with the equation $P_x = Y_a \ Y_c \ G/S$, where Y_a denotes the number of x rays emitted from the grids except the collector, Y_c is the number of electrons released from the collector per absorbed x ray, and G is a geometric factor.[17] The value of P_x is

estimated to be 1 x 10^{-4} Pa for the configuration 1 and 3 x 10^{-5} Pa for the configuration 2. Here, the values of Y_a and Y_c are 10^{-5} x ray/electron[18] and ~0.1 electron/x ray,[19] respectively, and the factor G is evaluated to be ~0.2. The estimated values of P_x are in good agreement with the ones which are determined from residual currents of ~ 1 nA at the collector. Although the x-ray limit for the SI gauge is rather larger than that for the B-A gauge, it is principally unaffected by a magnetic field because the factor G is always unity.

Next, we discuss the upper limit of the pressure at which the linearity between the pressure and the ion current breaks down. This limit is evaluated from the pressure where the collective motion of ions is prevalent. The collective motion of ions is probably accelerated in a magnetic field if the mean free path for the collisions of ions is smaller than the distance between the grids. Then the discharge likely occurs. While the ions collide with both other ions and neutral molecules, the mean free path for these collisions is simply assumed to be equal to that of the neutral particles. The upper pressure limit is evaluated to be ~ 1 Pa for N_2 from the pressure at which the mean free path of nitrogen molecules is equal to the distance between the grids. This value of ~ 1 Pa for N_2 is well agreed with the observations.

Negative values and oscillatory components in the collector current have been observed by Filippelli[12] for a B-A gauge in a magnetic field, but no negative currents were observed in the SI gauge. This is probably due to the short distance between the grids in the SI gauge.

2.4.3 On the use in a fusion device

In order to use the SI gauge in a fusion device, we consider the noise level due to various effects.[6,10] The following phenomena produce the noise signal:

--radiation from a plasma

--a fast particle which has escaped from a plasma

--β radiation from tritium

--the high power facility for NBI and RF heating

Soft x-ray from a plasma hits the collector and then produces the spurious collector current. The effect of the soft x-ray is well recognized in the field of pressure measurement with the hot filament gauge.[20] When the photon with energy of greater than ~20 eV hits the collector, electrons are produced at the rate of ~0.1 electron/x-ray. Fast particles escape from the plasma. If they hit the surroundings of the gauge, they sputter the gases and/or particles which are absorbed on the surface. In the D-T burning experiment, we must use a large amount of tritium. Tritium on the surface emits electrons due to the β-decay mechanism. Therefore these electrons act as the noise source on the gauge. High power facilities for NBI and RF heating produce the electromagnetic pulse.

Various kinds of blinds (e.g. Venetian) are very useful for eliminating the effect of fast particles. Even when fast particles hit the metal surface several times, the effect is almost completely suppressed. In addition, the blind is useful to reduce the effect of soft x-ray radiation. If the photon hits the metal surface once, the effect becomes ~100 times smaller because of the small reflectivity of the soft x-ray.[20] Assuming that the radiation loss of the plasma is 10 MW over the whole volume of

the plasma (100 m^3), we can easily measure the pressure of 10^{-4} Pa. The tritium effect has been examined by Dylla.[6] From his estimation, the effect of β radiation from tritium is negligible. As shown in Fig. 2.2, we have five grids in the SI gauge. By modulating the electrical potential of the second grid, we can eliminate the noise with the modulation technique.[2] In this case, the third grid will cut the capacitance coupling between the second grid and the ion collector. If we measure the collector current with the modulation frequency, we will easily detect the true signal in a ~10^3 times larger spurious signal.

Thus we hope that we can measure the pressure near a plasma.

2.5 Conclusions

We have developed a new type of hot cathode ionization gauge with spherical symmetry to measure the neutral gas pressure in a high magnetic field. Its performance is summarized as follows:

(1) The gauge has a linear relation between the ion current and the pressure ranging from 10^{-4} to 1 Pa for N_2 and Ar.

(2) The changes in the sensitivity are small; within + 20% in the field of 0 - 1.2 T. The main reasons are that the collection probability of ions is unaffected by the magnetic field, and that the emitted electrons have almost the same probability of ionizing gas molecules as in zero magnetic field, owing to the spherical symmetry.

(3) The lower pressure limit is ascribed to the x-ray limit. On the other hand, the collective motion of ions explains the upper pressure limit.

(4) With the aid of the blind and the modulation technique we can eliminate the spurious signals from the collector current and then use the gauge in a fusion device.

References

[1] E. P. Gorbunov, Yu. N. Kotel'nikov, G. P. Kutukov, and V. A. Simonov, Sov. Phys.-Tech. Phys. **11**, 1363 (1967).

[2] J. Jacquinot, C. Deck, and J. Godaert, Rev. Sci. Instrum. **43**, 905 (1972).

[3] D. R. A. Webb, J. Phys. E7, 453 (1974).

[4] S. S. Butuzov, V. F. Zubarev, V. P. Konyaev, E. A. Maslennikov, A. N. Nekrasov, Yu. M. Pustovoit, V. S. Svishchev, and I. A. Chukhin, Sov. Phys.-Tech. Phys. **13**, 207 (1968).

[5] D. P. Hammond and A. C. Riviere, J. Phys. E**4**, 650 (1971).

[6] H. F. Dylla, J. Vac. Sci. Technol. **20**, 119 (1982).

[7] W. L. Pickles and A. L. Hunt, J. Vac. Sci. Technol. A**4**, 1732 (1986).

[8] G. Lewin and G. Martin, Rev. Sci. Instrum. **33**, 447 (1962).

[9] G. Lewin and G. Martin, Rev. Sci. Instrum. **34**, 942 (1963).

[10] A. Berman, J. Vac. Sci. Technol. **18**, 1017 (1981).

[11] G. D. Martin Jr., in 1961 Transactions of the 8th Vacuum Symposium and 2nd International Congress of the American Vacuum Society (Pergamon, New York, 1962), P.476.

[12] A. R. Filippelli, J. Vac. Sci. Technol. A5, 249 (1987).

[13] H. C. Hseuh, J. Vac. Sci. Technol. **20**, 237 (1982).

[14] B. L. Stansfield, B. Bergevin, and J. M. Larsen, J. Vac. Sci. Technol. A**4**, 2284 (1986).

[15] M. Hirata, M. Ono, H. Hojo, and K. Nakayama, J. Vac. Sci. Technol. **20**, 1159 (1982).

[16] H. Ishii and K. Nakayama, Shinku (J. Vac. Soc. Jpn.) **3**, 77 (1960).

[17] F. Watanabe, J. Vac. Sci. Technol. A5, 242 (1987).

[18] J. van Ark and J. van de Rutte, Vak. Tech. **17**, 173 (1968).

[19] J. J. Grodski and B. W. Schumacher, Rev. Sci. Instrum. **39**, 702 (1968).

[20] P. A. Redhead, J. P. Hobson, and E. V. Kornelsen, The Physical Basis of Ultrahigh Vacuum, London, Chapman and Hall Ltd., 1968.

Table 2.1 Potential configurations.

	G1	G2	G3	G4	G5
Configuration 1	+ 160 V (extraction of electrons)	+ 170 V (control of electron energy)	Grounded	- 70 V (electron repeller)	- 40 V (ion collector)
Configuration 2				- 40 V (ion collector)	+ 220 V (ion repeller)

Table 2.2 Sensitivity factors S of the SI gauge over the pressure and field ranges of less than 1 Pa and below 1.2 T.

	$S(N_2)$ $(10^{-3}\ Pa^{-1})$	$S(Ar)$ $(10^{-3}\ Pa^{-1})$
Configuration 1	1.9 - 2.3	2.3 - 2.8
Configuration 2	5.7 - 8.5	6.8 - 8.8

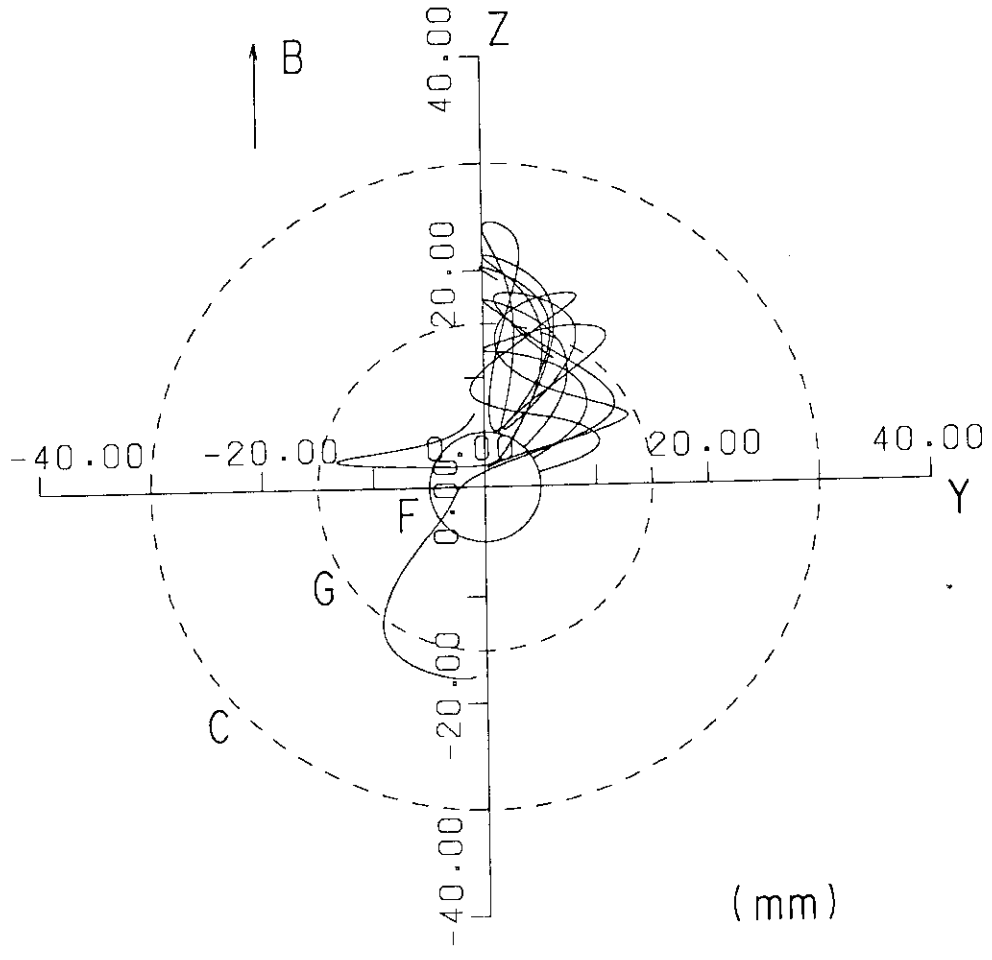

(a) 0.005 T

Fig. 2.1 Electron trajectories in the magnetic fields of 0.005 T (a), 0.01 T (b), and 0.05 T (c). The diameters of the filament (F), the grid (G), and the collector (C) are 10 mm, 30mm, and 60 mm, respectively. Three electrodes are biased as follows: F, 0 V; G, + 100 V; C, - 20 V. Electrons with a thermal energy of 0.2 eV are assumed to be emitted normally to the filament sphere at intervals of 15° from the z axis.

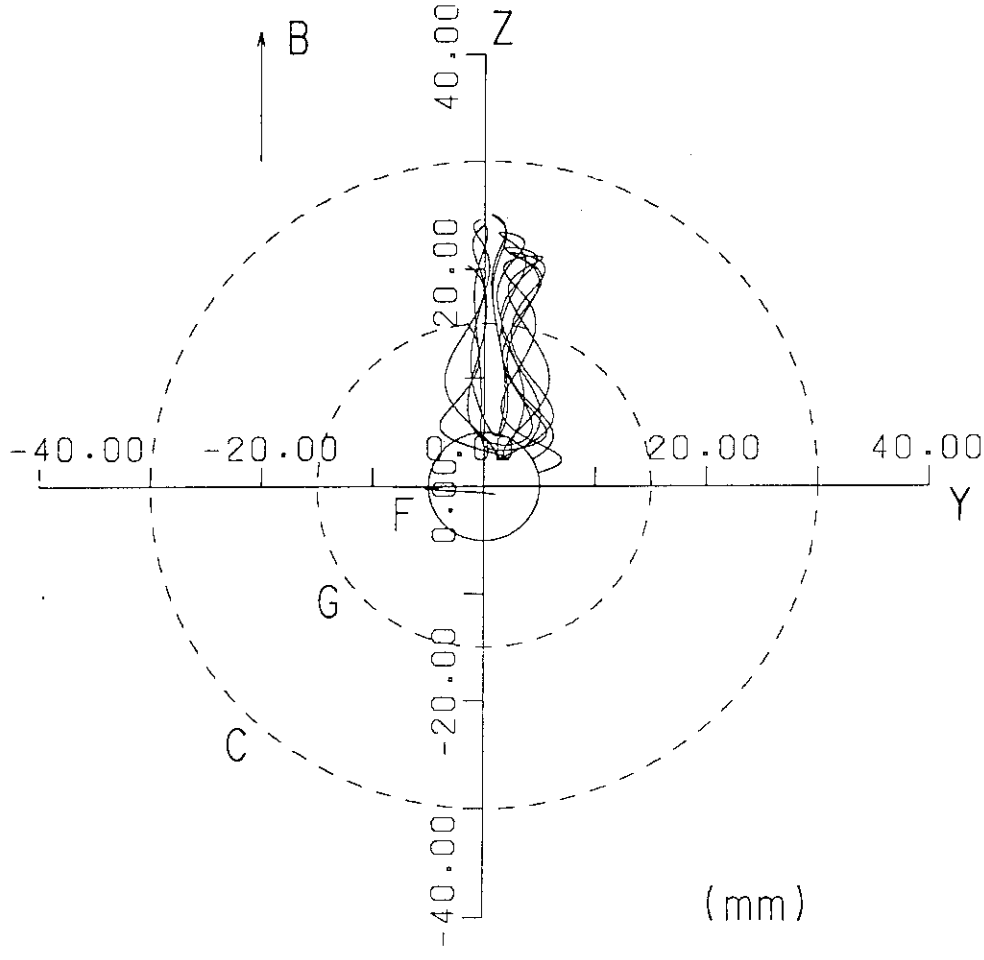

(b) 0.01 T

Fig. 2.1 (Continued)

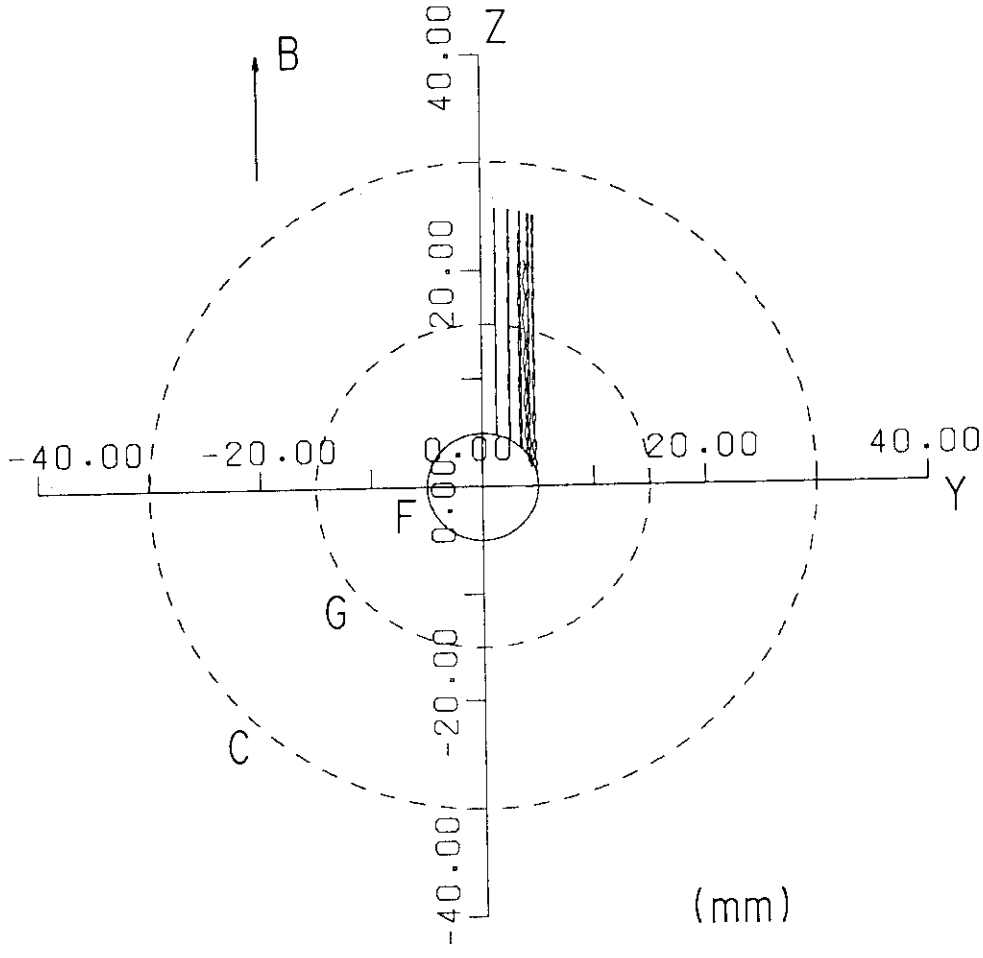

(c) 0.05 T

Fig. 2.1 (Continued)

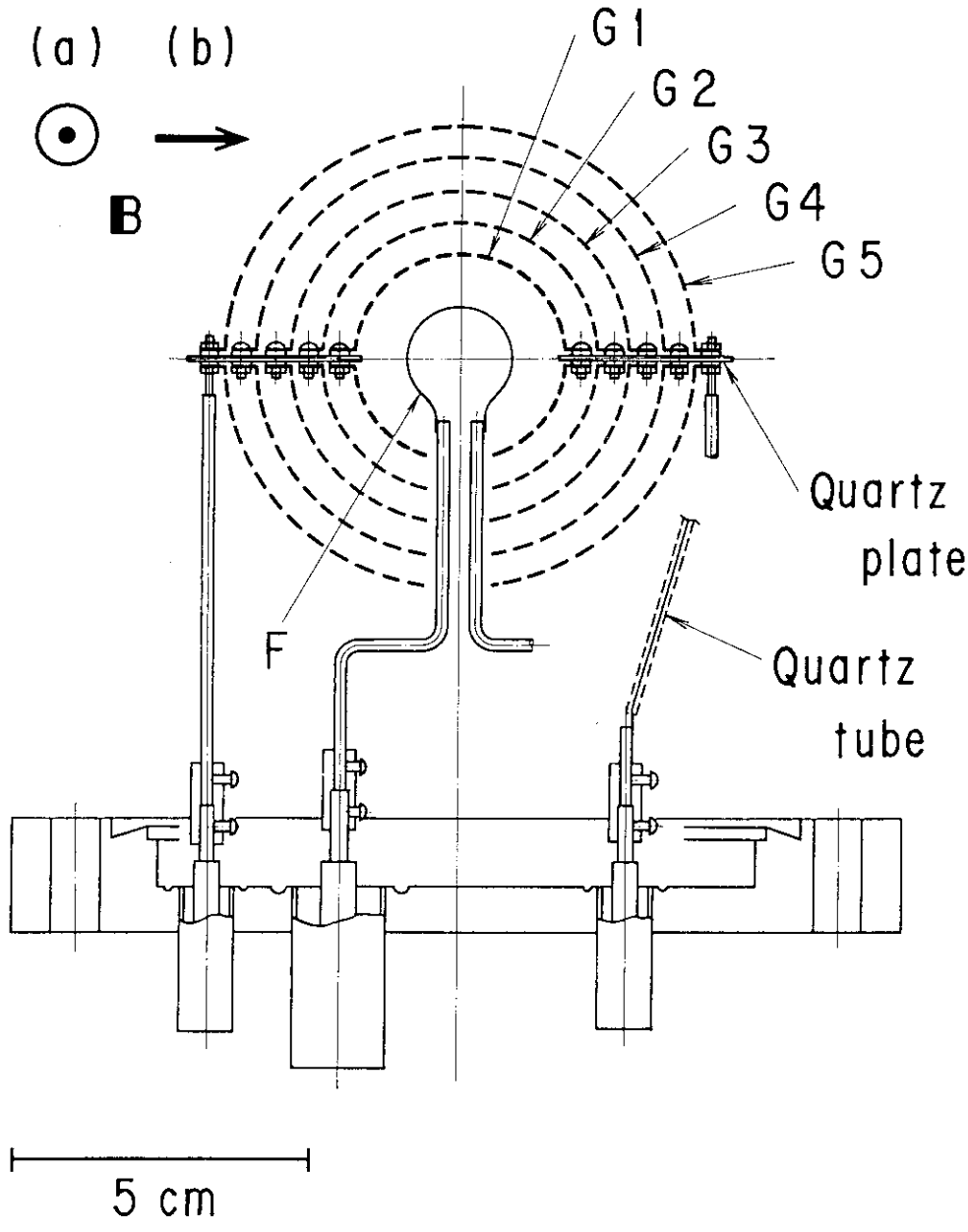

Fig. 2.2 Cross sectional view of the spherical ionization gauge. There are five grids (G1 - G5) with radii of 18 mm, 23.5 mm, 34.5 mm, and 40 mm. The potentials are given in Table 2.1. The directions of the magnetic field are also shown.

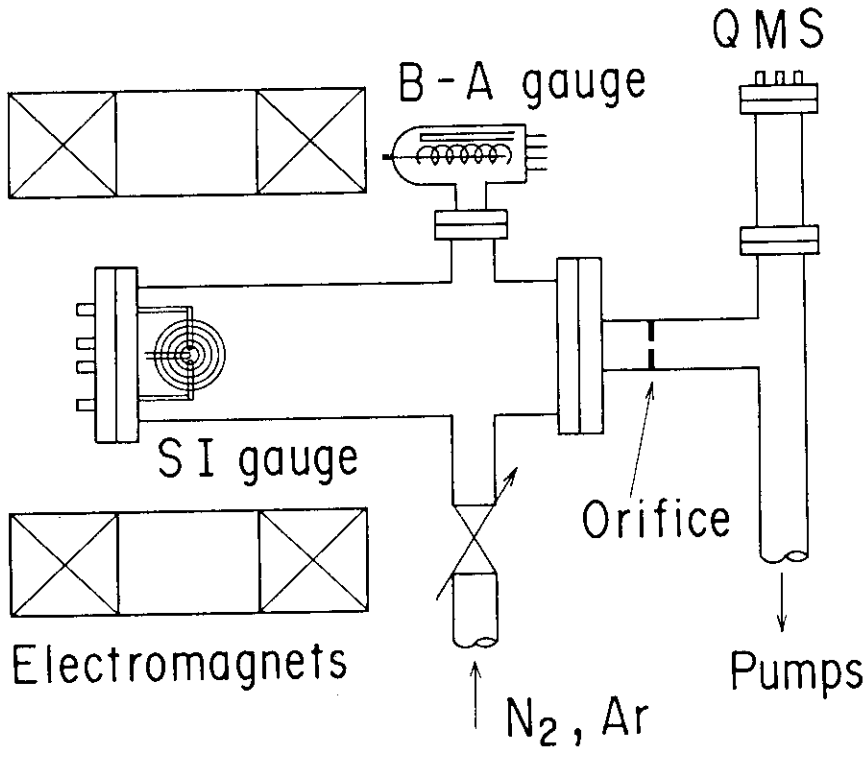

Fig. 2.3 Schematic of experimental apparatus. The SI gauge is placed in the center of the electromagnets. Pressure is measured by the calibrated B-A gauge. Purity of gases is monitored by a quadrupole mass spectrometer (QMS).

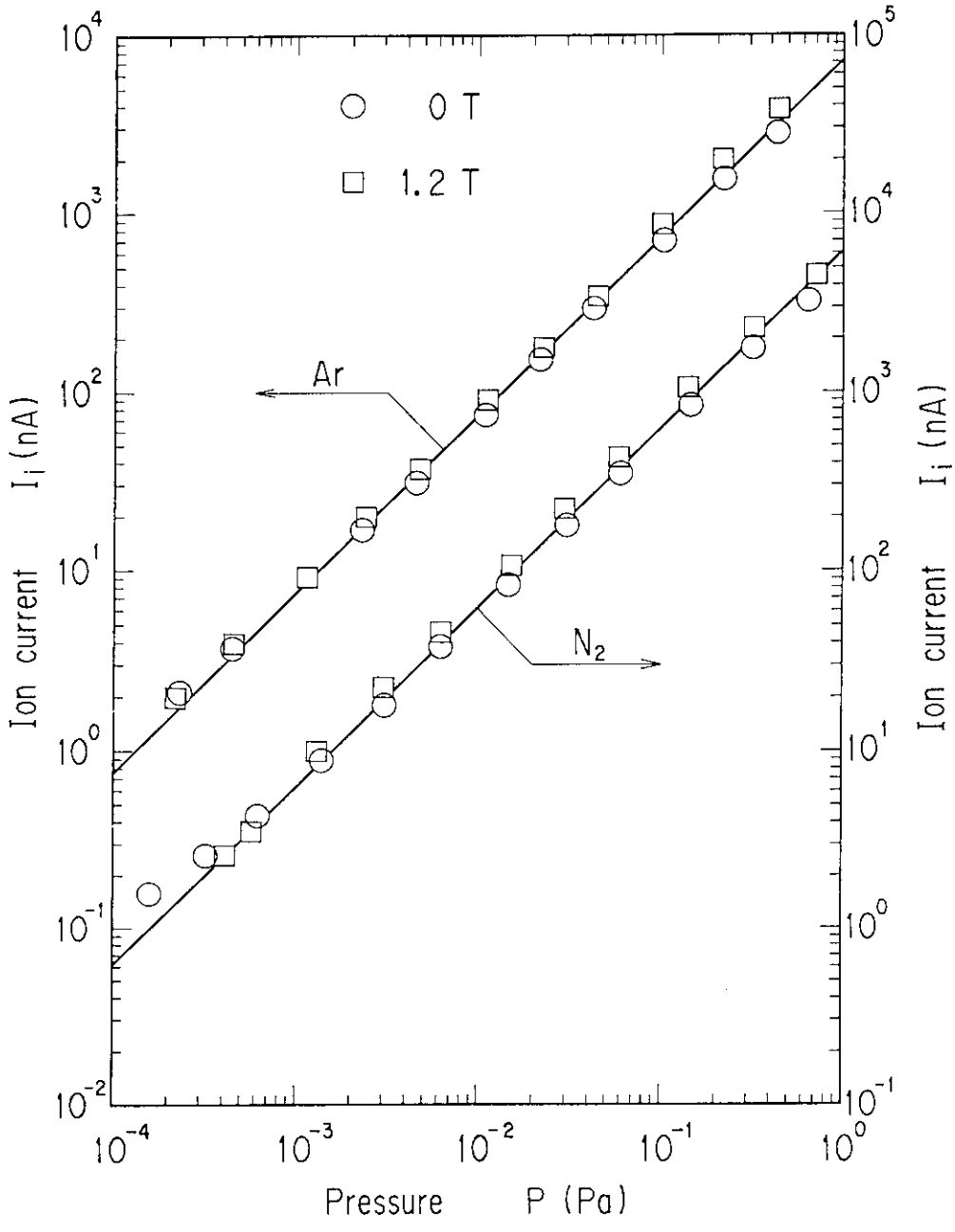

Fig. 2.4 Typical ion current I_i as a function of pressure P for N_2 and Ar at the magnetic field of 0 and 1.2 T for the configuration 1. The emission current is controlled at the filament so as to be 3 mA.

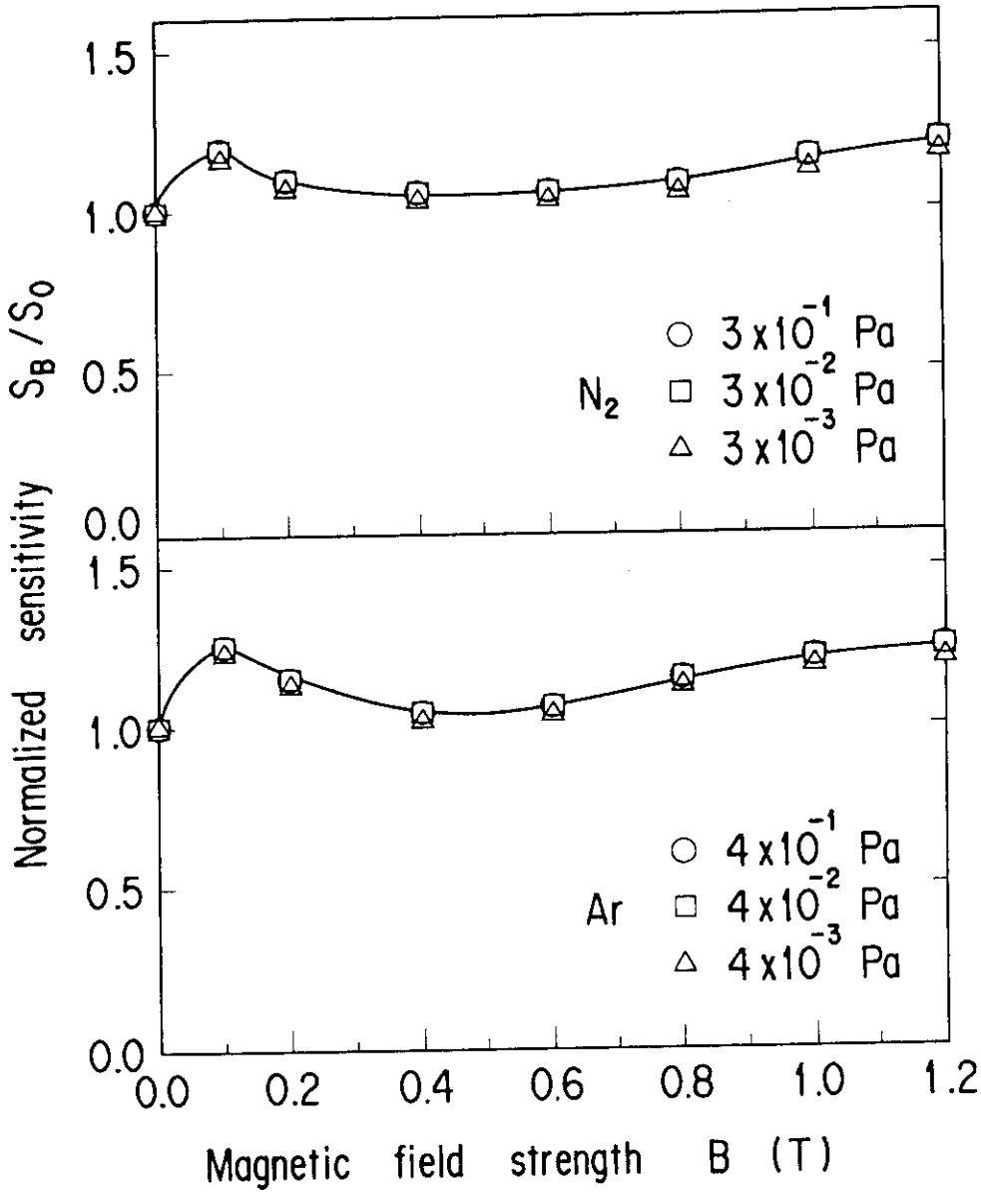

Fig. 2.5 Variation of the normalized sensitivity S_B/S_0 as a function of the magnetic field strength B for N_2 and Ar. The electrode potentials are those for the configuration 1 in Table 2.1.

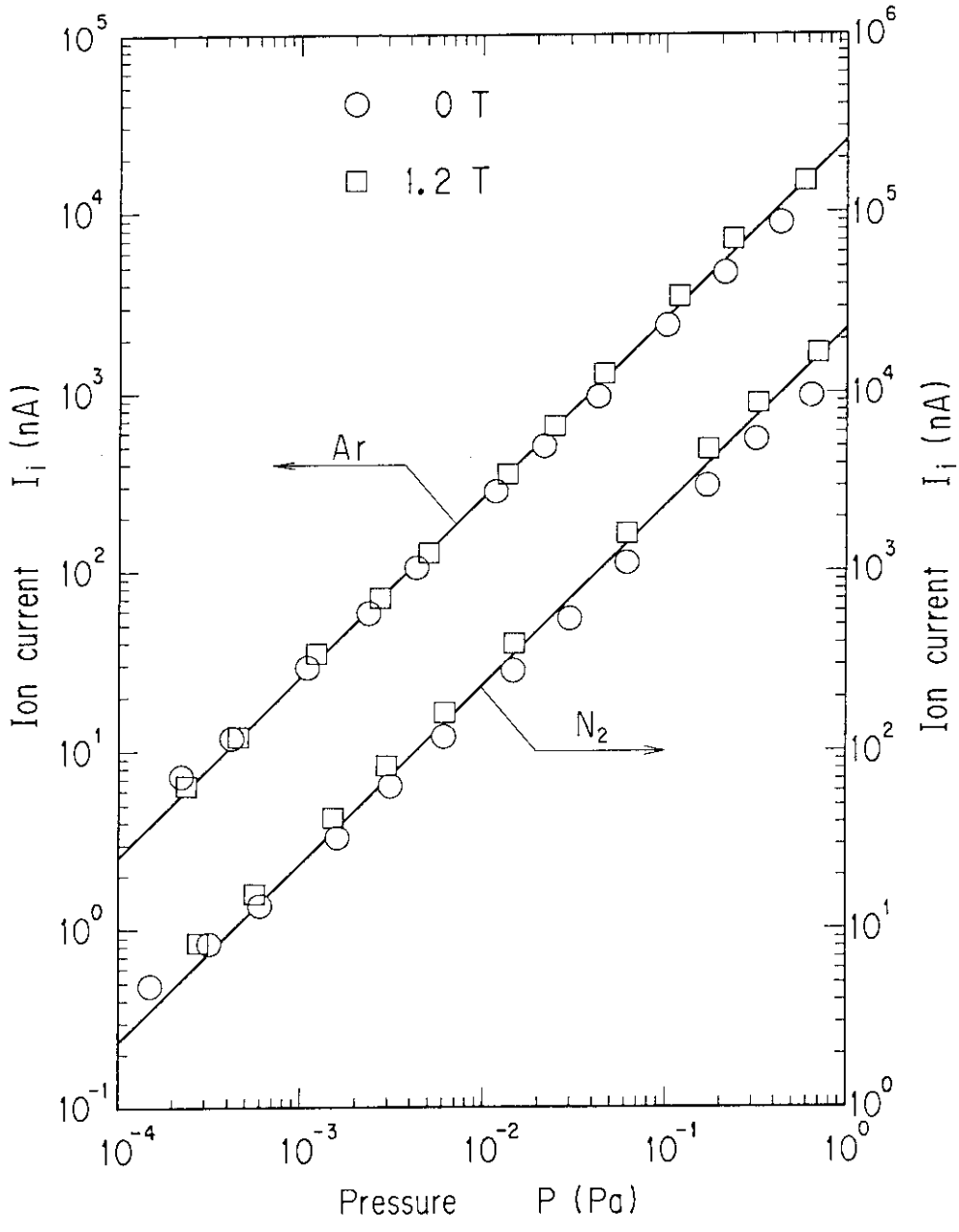

Fig. 2.6 Typical ion current I_i as a function of pressure P for N_2 and Ar at the magnetic field of 0 and 1.2 T for the configuration 2. The emission current at the filament is 3 mA.

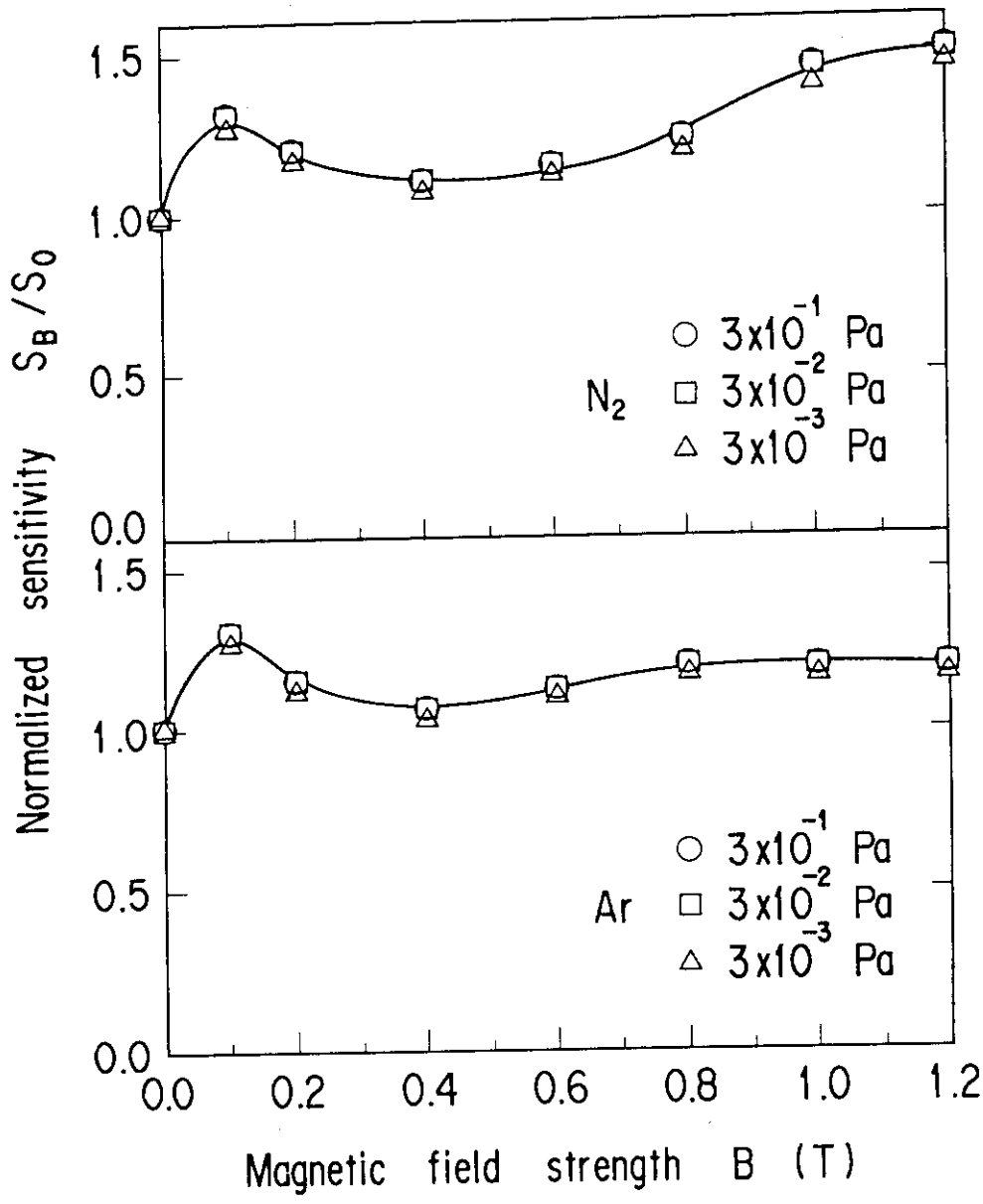

Fig. 2.7 Variation of the normalized sensitivity S_B/S_0 as a function of the magnetic field strength B for N_2 and Ar. The electrode potentials are those for the configuration 2.

3. Penning-type partial pressure gauge

3.1 Introduction

Direct pressure measurements close to a plasma are rarely made because of the presence of the high magnetic field required to confine the plasma. As for the total pressure measurement, we have developed the new type of ionization gauge described in chapter 2.[1] However, partial pressure is more difficult to measure because disturbance of the trajectories of the ions should be avoided. Matsuzaki et al. have examined the performance of a quadrupole mass spectrometer (QMS) in a magnetic field.[2] They showed that without the magnetic shield, the QMS (Balzers, QMA-112) could measure the partial pressure with a sensitivity change of less than ±20% only below a magnetic field of 0.01 T. Recently, Akaishi et al.[3,4] developed a new type of partial pressure gauge for He and D_2 in a pump-limiter experiment in TEXTOR.[5] However, it is difficult to measure the partial pressure with a short response time because their gauge must be operated far from the magnetic field in order to avoid disturbance of the ion trajectories.

In this chapter, we propose and demonstrate a new method of measuring partial pressures.[6,7] Its features are as follows:
(1) This gauge has Penning-type configuration which utilizes the plasma-confining magnetic field.
(2) The light from the plasma glow in the Penning discharge is analyzed. The wavelength of the spectral lines reveals the gas species, and their intensity tells us the partial pressures.

In the first section, the principle of this gauge is described. Then two types of experiments are shown. Finally, the experimental results are discussed.

3.2 Principle of the gauge

We use a Penning discharge sustained by a high magnetic field such as a toroidal field for tokamaks. A schematic configuration of the Penning discharge is shown in Fig. 3.1.[8] A high voltage between the cathode plates and anode cylinder provides an electric field with radial and axial components. Electrons trying to escape towards the anode are restricted to the magnetic field lines. Thus electrons move in trochoidal paths superimposed on the oscillation in the axial potential well. Because of the lengthened path, the discharge can be self-sustaining at pressures far below the operating pressures of a normal glow discharge. The discovery of the Penning discharge by Phillips[9] dates back to 1898, but the experimental development began in 1936 with the construction of an ionization gauge by Penning.[10] In the field of plasma research, the Penning configuration gauge has long been used to measure pressure near a plasma.[11-13]

Although previous researchers used the discharge current as a measure of the pressure, we analyze the light emitted from the plasma glow which exists in the Penning discharge near an axis of the Penning cell. In the Penning discharge, the electrons have enough energy and density to ionize the gas molecules and to excite neutral atoms. In the collision of electrons with gas molecules, various particles are produced. Those are electrons, ions, and neutrals at electronically excited states. Elementary processes are shown in Fig. 3.2. The excited neutrals and the ions will emit the spectral lines. The processes which emit the lines are spontaneous radiation and radiative recombination. The

spectral lines are emitted through the spontaneous radiation process. On the other hand, the radiative recombination emits the continuous radiation. Thus by analyzing the spectral lines, the partial pressure will be obtained.

The emitted light intensity is a function of electron density, electron energy, molecule density, and ion density.[14] If the electron density and the potential configuration are unchangeable, the light intensity of the spectral lines is thought to increase linearly with the gas pressure. Only if the ratio between the spectral line intensities for each gas species is almost constant for various conditions can we achieve the partial pressure with a combination of the spherical ionization gauge[1] described previously. However, a disadvantage of the Penning discharge is that the discharge current is not necessarily a linear function of the pressure, depending also on the electrode geometry, applied fields, and pressure range.[15,16] Therefore, the characteristics of the emitted light from the Penning discharge must be examined theoretically and experimentally.

Here we consider the relation of the discharge current and the emitted light intensity.

First the cathode current is dealt with. There are two methods of evaluation. One is to evaluate the electron (anode) current through electron diffusion across the magnetic field.[17] The other is to calculate the ion (cathode) current.[18] Here, we estimate the cathode current because we are interested in the relation between the ions and the excited neutrals. In the Penning cell, there is an electron cloud, as schematically shown in Fig. 3.1. Electrons are confined by the electric field and the

magnetic field. Ions and excited neutrals are produced by the collision of gas molecules with electrons. Because the confinement time of the ions in the Penning cell is short, all of the ions produced in it are justifiably assumed to be collected completely to the cathodes. That is, the electron recombination process is negligible for evaluating the cathode current. Here, the ionization process in the small volume dv is examined. The number of ions Jdv produced in it is expressed by the equation

$$Jdv = n_e \, dv \, f_c \, P_i, \qquad (3)$$

where n_e is the electron density, f_c is the collision frequency of electrons with gas molecules, and P_i is the ionization probability per collision. The value of f_c is expressed by the equation

$$f_c = v_e/\lambda_e. \qquad (4)$$

Here, v_e and λ_e are the average velocity and the mean free path of electrons, respectively. Moreover, the mean free path λ_e is related to that of the gas molecules λ_g by the following equation:[19]

$$\lambda_e = 4\sqrt{2}\,\lambda_g = 4/(\pi\, n(1)\, r_g^{\,2}), \qquad (5)$$

where $n(1)$ and r_g are the density (at ground state) and effective radius of gas molecules, respectively. From equations (3)-(5), the number of ions produced in the small volume dv is

$$Jdv = dv\, n(1)\, n_e\, [v_e\, P_i(v_e)/A], \qquad (6)$$

$$A = 4/\pi\, r_g^{\,2}.$$

Since the ionization cross section σ_{ion} is expressed by the equation $\sigma_{ion} = P_i(v_e)/A$, the equation (6) is reformed as the following equation:

$$Jdv = v_e\, \sigma_{ion}\, n_e\, n(1)\, dv. \qquad (7)$$

Next the spectral line intensity emitted from the Penning discharge is evaluated. Elementary processes including radiation are spontaneous radiative transition and radiative recombination. These two processes are illustrated in Fig. 3.2. Because we are interested in the spectral lines, the population of excited states should be calculated. For simplicity, we consider hydrogenic ions with nuclear charge z. The temporal variation of the population density of a level with the principal quantum number p is described by a set of rate equations:[20]

$$\begin{aligned}\frac{d}{dt}n(p) = & \sum_{q<p} C(q,p)\, n_e\, n(q) \\ & - [\{\sum_{q<p} F(p,q) + \sum_{q>p} C(p,q) + S(p)\}\, n_e \\ & \quad + \sum_{q\neq p} A(p,q)]\, n(p) \\ & + \sum_{q>p} \{F(q,p)\, n_e + A(q,p)\}\, n(q) \\ & + \{\alpha(p)\, n_e + \beta(p)\}\, n_z\, n_e, \quad \text{for } p = 1, 2, \cdots, \end{aligned} \tag{8}$$

where C(p,q) and F(q,p) are the excitation rate coefficient by electron collisions from level p to q and its reverse de-excitation rate coefficient, respectively. A(p,q) is the spontaneous transition probability from p to q. S(p) and $\alpha(p)$ are the ionization rate coefficient and the three-body recombination rate coefficient for level p, respectively. $\beta(p)$ is the radiative recombination rate coefficient, and n_z is the particle density of the fully stripped ion. The solution of the set of equations (8) gives us exact populations n(p) for all p with given n_e and average kinetic energy T_e. However, it is difficult to solve the equations and many assumptions are needed.

In the case of the Penning discharge, the corona approximation[21] is valid, because the plasma is almost equal to the ionizing plasma and the electron density n_e is low.

The ionizing plasma is defined as that with the ion density of $n_z = 0$. The ions in the Penning discharge can easily escape to the cathodes. Even if the parallel velocity of the ions would be a thermal one, the mean lifetime τ_{ion} is $\sim 10^{-5}$ s. The discharge current I is roughly expressed by the linear relation of $I = C\,P$ with $C \lesssim 0.1$ A/Pa (see section 4.4). Thus the ion density is estimated as follows:

$$n_z \sim (1/V)(I/e)\,\tau_{ion} \lesssim 10^{12}\,P\ \ cm^{-3}\ (P:Pa), \qquad (9)$$

where the volume of the discharge is less than ~ 10 cm^3. On the other hand, the neutral gas density n(1) is $\sim 3\times 10^{14}$ P cm^{-3} (P:Pa). Therefore, the density n_z is negligible and the population density n(p) is independent of n_z.

By solving the set of equations (8), Fujimoto has examined the population density n(p) in the ionizing plasma as a function of the electron density n_e.[21] It is found that the density n(p) ($p \lesssim 5$) is proportional to the electron density n_e if the value of n_e is less than 10^{11} cm^{-3} and the electron temperature is high ($\gtrsim 10^5$ K). In the Penning discharge, Knauer and Lutz[22] found the electron density to be less than $\sim 1.6\times 10^{10}$ cm^{-3}.

Thus the corona approximation is valid for dealing with the Penning discharge. In corona equilibrium, the population density n(p) is written by the simple equation:[21]

$$n(p) = n(1)\,C(1,p)\,n_e \,/\, {}_{q\lesssim p}\Sigma A(p,q). \qquad (10)$$

The rate coefficient C(1,p) is given by the product of the average velocity v_e and the excitation cross section $\sigma_{1\to p}$. That is, $C(1,p) = \sigma_{1\to p}\,v_e$. The rate coefficient A(p,q) is constant for given values of p and q.

From equation (10), the intensity L(p→q) of the spectral line for the transition from p to q is described by the following:

$$L(p\to q) = A(p,q)\, n(p)$$

$$= A(p,q)\, \sigma_{1\to p} v_e \frac{n(1)\, n_e}{{}_q\Sigma_p A(p,q)}. \qquad (11)$$

Therefore, the ratio of the spectral line intensity L(p→q)dv to the ions produced in the small volume dv is approximated as follows:

$$\frac{L\, dv}{J\, dv} = \frac{A(p,q)}{\sigma_{ion} v_e\, n(1)} \frac{\sigma_{1\to p} v_e\, n(1)\, n_e}{{}_q\Sigma_p A(p,q)}$$

$$= \frac{A(p,q)}{{}_q\Sigma_p A(p,q)} \frac{\sigma_{1\to p}}{\sigma_{ion}}. \qquad (12)$$

From this equation, the spectral line intensity is thought to increase linearly with the increasing discharge current if the ratio of the excitation cross section to the ionization cross section is constant. Figure 3.3 shows excitation and ionization cross sections from the ground 1s state as a function of kinetic energy of electrons reduced by the square of nuclear charge z. At the reduced kinetic energy higher than ~$60/z^2$ eV, the ratio is nearly constant.

In conclusion, the spectral line intensity is assumed to be nearly proportional to the discharge current with the Penning discharge. This should be confirmed by experiments.

3.3 Experiment (I)

Hydrogen pressure measurement using the intensity of the light emitted from a Penning discharge

3.3.1 Introduction

In this part, we examine the dependence of the emitted spectral line on the magnetic field strength, the electrode geometry, and the pressure. The experiments are carried out in a hydrogen atmosphere. The intensity of the H_α and H_β Balmer lines emitted from a Penning discharge is a function only of the discharge ion current: their intensity is independent of the anode voltage and magnetic fields from 0.1 to 2.0 T. The light intensity is proportional to the ion current below ~ 0.1 Pa. The ratio of the light intensity to the ion current increases by 40% for pressures above ~ 0.1 Pa because of a change in the type of discharge. The higher pressure discharge probably has a lower electron temperature.

3.3.2 Experimental procedure

Penning discharge occurs in a hydrogen atmosphere at a pressure below 0.5 Pa. The light emitted from the discharge and the ion current are measured as functions of the anode voltage V, the magnetic field strength B, and the pressure P. Various sizes of Penning cells are used (see Table 3.1). The cathode and anode of the cells are made of Mo (99.9%) and type 304 stainless steel, respectively. The hydrogen pressure is measured with a Bayard-Alpert gauge, which is calibrated by a standard ionization gauge

(VS-1).[23] The accuracy of the pressure measurement is within ± 15%. The uniformity of B is within ± 5% over the volume occupied by the Penning cell. A high dc voltage up to 5 kV is supplied to the anode through a 50 kΩ resistor to stabilize the Penning discharge (see Fig. 3.4). The light from the Penning discharge is viewed through a 16 mm diameter viewing port by a monochromator (Nikon, G500-II). The light is detected by a photomultiplier. It is placed far from the light source (i.e., the Penning cell) to avoid the stray magnetic field: the solid angle of the light is 1 x 10^{-5} sr. This sets a lower limit of the pressure for which the light can be measured to be ~ 10^{-3} Pa. The relative light intensity is measured within ± 30% error. The H_{α} (656.3 nm) and H_{β} (486.1 nm) lines of Balmer series are examined in this experiment.

3.3.3 Results

3.3.3.1 The light intensity as functions of discharge current, anode voltage, and magnetic field strength

The light intensity emitted from the Penning discharge was investigated as a function of the discharge current. The anode voltage V varied from 3 to 5 kV, and the magnetic field B from 0.1 to 1.4 T. Figure 3.5 shows a typical variation of the intensity of the H_{β} line with the discharge current for the cell of type I. The intensity of the H_{β} line is proportional to the discharge current within the accuracy of the experiment. The light intensity reduced by the discharge current is more useful to examine the dependence of the light intensity on the anode

voltage and the magnetic field strength. Figure 3.6 shows the reduced light intensity for the data shown in Fig. 3.5. As shown in Fig. 3.6(a), the light intensity is independent of anode voltages from 3 to 5 kV. Figure 3.6(b) shows that the light intensity is also independent of magnetic fields from 0.1 to 1.4 T. The light intensity of the H_β line is a function only of the discharge current. The ratio of the light intensity to the current is almost constant below a current of ~ 2 mA. The intensity of the H_α line varies in a way similar to that of the H_β line as shown in Fig. 3.7. These features were also observed for all the other cells shown in Table 3.1.

A glow with a diameter less than that of the anode appears along the discharge axis. Its diameter increases with the current (i.e., the pressure). At a current of ~ 2 mA, which corresponds to a pressure of ~ 0.1 Pa, the region of light emission suddenly fills the entire volume of the cell. This is ascribed to a mode transition to the glowlike discharge.[17]

The intensity of the H_α line was measured for the cell of type IX in a fusion device JT-60.[24] The accuracy of the measurement of the light intensity increased to within ± 10%. The magnetic field and the anode voltage were 1.3 to 2.0 T and 5 kV, respectively. Figure 3.8 shows clearly that a mode transition occurs at 1.8 mA. In the glowlike discharge, the ratio of the intensity of the H_α line to the ion current increases to ~ 1.4 times that before the transition. Below 1.8 mA, the ratio is almost constant within the accuracy of the experiment.

In the glowlike discharge above ~ 0.1 Pa, the enhancement of the light intensity to the ion current is explained by a decrease in the electron temperature. The reason is that the electric

field in the glowlike discharge is almost zero over the whole volume except the vicinity of the anode.[25]

3.3.3.2 The discharge current as a function of pressure in a high magnetic field

Next the variation of the Penning-discharge current with the magnetic field was investigated for all the sizes of the cells at pressures below 0.5 Pa. Figure 3.9 shows a typical variation of discharge current with B at the same pressure for the cell of type I. The discharge current is almost independent of the magnetic field above 0.6 T, and it increases with increasing the anode voltage. All the cells have the similar variation of the discharge current with the magnetic field. Moreover, the relation between the discharge current I and the pressure P is approximated well by the equation $I = AP^{\gamma}$, where both A and γ are constant. This is efficient over the pressure and field ranges of less than 0.5 Pa and above 0.6 T. All the cells have the value of γ between 1.0 and 1.5. These features of the discharge current are consistent with the works for a sputter ion pump by many researchers.[15-17]

3.4 Experiment (II)

Partial pressure measurement in the gas mixture of H_2 and He

3.4.1 Introduction

As shown in previous section, the pressure of H_2 can be measured by the light emitted from the Penning discharge. In this

section, the gas mixture is studied. In the future, the He ash exhaust is one of the inevitable problems.[26] In order to develop the means for exhausting the He ash efficiently, the partial pressure of He in the D_2 atmosphere must first be known. The simulation of detection of He in D_2 has been carried out in the gas mixture of He and H_2 because the light emitted from deuterium is almost equal to that of hydrogen as shown in Table 3.2. The experiment shows that the spectral line intensity increases linearly with the partial pressure and that is independent of the other gas pressure.

3.4.2 Experimental procedure

The setup of the experiment is shown schematically in Fig. 3.10. The Penning discharge is operated under the conditions as shown in Fig. 3.11. Light emitted from the discharge is viewed by a monochromator through a quartz window, quartz lenses, and a bundle of quartz fibers. Then the light is detected by a photomultiplier. An analog lock-in technique is employed for increasing the signal-to-noise ratio. Pressure measurement is made by a Bayard-Alpert gauge (BAG), a spinning rotor gauge (SRG), and a quadrupole mass spectrometer (QMS) surrounded by a 77 K trap. An anode of the cell, which is made of SUS 304, is a cylinder 10 mm long and 20 mm in diameter. Cathodes are Mo squares which are 50 mm long and 1 mm thick. A dc voltage of 3 to 5 kV is supplied to the anode through a stabilizing 50 kΩ resistor. The discharge current is measured by an electrometer between the cathodes and the earth. The sustaining magnetic field of 0.11 T is supplied to the Penning cell by a pair of permanent

magnets. The variation of the magnetic field is less than ±0.005 T within the whole volume of the cell. A test chamber of ~ 10 l is evacuated through an orifice (0.5 mm in diameter) by a 350 l/s turbomolecular pump. A base pressure of ~ 1 x 10^{-7} Pa is obtained after baking at 250°C for 10 hr. Residual gases are mainly H_2 and CO. Hydrogen at 7-9 degree and helium at 6.5-9 degree are used in this experiment. Before the experiment, the cell is cleaned by the discharge at ~ 10^{-2} Pa until the ratio of the peak height of the working gas to that of the other gases becomes larger than 1000 with the QMS.

Both the intensity of the spectral lines and the discharge current are measured as a function of the pressure. Here the pressure is controlled so as to be constant with time within the variation of ± 10%. Then the pressure is changed. The above procedure is routinely repeated.

Pressure in a gas of monospecies was measured with the SRG above 10^{-3} Pa and with the BAG below 10^{-3} Pa. The stray magnetic field is perhaps the reason that the spurious pressure of the SRG is so high (~ 10^{-4} Pa). The BAG was calibrated by the SRG above 10^{-3} Pa before each run of the experiment. Partial pressure was measured with the QMS in combination with the BAG. The ratio of the partial pressure was determined with the QMS. The partial pressure was then obtained from the BAG measurement using the relative sensitivity determined in the experiment in the mono-species gas.

The experimental error is caused mainly by the uncertainty of the pressure control. Error of the data for the pressure and the discharge current is less than ± 10%. Residual current of the photomultiplier limits the lower level of the light intensity

measurement. Data with a larger than ± 10% error are exhibited with the error bar.

3.4.3 Results

3.4.3.1 Cathode current as a function of pressure

The cathode current was measured as a function of the pressure. A typical change of the cathode current in the pressure is shown in Fig. 3.12. In this case, the anode voltage is 4 kV. The linearity between the current and the pressure is well established for hydrogen and helium. With a constant anode voltage (3-5 kV) this linearity is obtained. This means that the distribution of the electron cloud is rather constant over a wide range of pressure with a constant anode voltage.

3.4.3.2 Spectral line intensity as a function of the pressure (in the gas of monospecies)

In this experiment, the light from 350 nm to 800 nm is analyzed. The lines shown in Table 3.3 are detected for hydrogen and helium Penning discharges. For hydrogen, the lines originate from the state of the principal quantum number n=4 and 3. For helium, the spectral lines originate from n=5,4, and 3 to n=2. The lines from n=5 are rather weak, however. In addition, the lines from He^+ cannot be detected. This is probably because the kinetic energy of the electrons in the cell is rather low.

The line intensities as a function of the pressure are shown in Figs. 3.13 and 3.14 for H_2 and He, respectively. In all cases,

the anode voltages are 4 kV. For helium, the lines of 388.9 nm, 667.8 nm, and 706.5 nm are shown. All the lines are obtained assuming the linear relation between the line intensities and the pressure. The real lines refer to the region where the measurement was carried out. Figures 3.13 and 3.14 clearly show that the line intensities increase with the pressure for H_2 and He. In addition, the intensity of all the other lines was revealed to be proportional to the pressure for He.

3.4.3.3 The line intensities as a function of the pressure (in the gas mixture of H_2 and He)

The gas mixture of H_2 and He was studied. The spectral line intensities were measured as a function of each partial pressure. The hydrogen pressure ranged from ~10^{-5} Pa to 10^{-1} Pa. Here, the helium pressure was less than 10^{-4} Pa. Figure 3.15 shows the line intensities of H_α and 667.8 nm of helium. The intensity of H_α is shown as a function of the hydrogen pressure. The intensity of H_α increases with the hydrogen pressure in the same manner as shown in Fig. 3.13. The intensity of 667.8 nm, which is normalized as the helium pressure, is also plotted as a function of the hydrogen pressure. Its intensity keeps constant; nevertheless, the hydrogen pressure ranges over 4 orders. From this observation, the line from the helium is not modified by the hydrogen. These characteristics are suitable to measure the partial pressure.

3.5 Discussion

3.5.1 Enhancement of the light intensity due to the transition to the glowlike discharge

The ion current is dependent on the density n_e and the average kinetic energy T_e of the electrons. The density n_e and/or the kinetic energy T_e are not necessarily constant for a wide range of the Penning discharge because the discharge current is not always proportional to the pressure and the discharge current increases with the anode voltage. The experimental results in which the spectral line intensity increases linearly with the discharge current shows that the density n_e is less than 10^{11} cm^{-3} and the energy T_e is greater than ~60 eV under the corona approximation. The enhancement of the spectral line intensity can be explained by the reduction of the kinetic energy T_e of the electrons (see section 3.2).

We can evaluate the average kinetic energy T_e with the electric field E and the magnetic field B in the Penning cell. The electrons in the cell move cycloidally. The guide center of the cycloidal rotation is determined by the ExB drift. This is analyzed in detail by Asamaki.[27] The guide center is well approximated as a circle around the axis of the cell. Here, we assume that electrons lose the kinetic energy every cycloidal rotation. The cycloidal height D is related in MKS units to E and B through

$$D = (2m/e)\ E/B^2, \qquad (13)$$

where m and e refer to the mass and the charge of the electron. Thus the value of T_e is estimated as follows:

$$T_e \approx 2\ e\ E\ D \quad (J)$$

$$\approx \frac{2\ m\ E^2}{e\ B^2} \quad (eV). \qquad (14)$$

Dow has observed the change in the potential in the cell through the transition to the glowlike discharge.[25] The potential configuration changes from parabolic to flat. This is a qualitative explanation of the light enhancement. Before the transition to the glowlike discharge, the value of T_e is estimated from the observation of Knauer and Lutz. They have shown that the electric field strength E at B = 0.015 T is to be ~ 5.5×10^5 V/m. The value of T_e is calculated to be ~ 75 eV. This is consistent with the condition for the kinetic energy of electrons. In addition, on the basis of the calculation by Johnson and Hinnov,[28] we deduce the average kinetic energy of ~ 10 eV in the glowlike discharge from the light enhancement factor of 1.4. Nevertheless, the above discussion would need to be confirmed by a detailed investigation of the density and the kinetic energy of electrons.

3.5.2 How can the spectral lines from He II (He^+) not be detected?

The spectral lines from He II cannot be detected although the electron temperature is sufficiently high.

The reason is that the confining time of ions is very short. Since the ground state for He II is $He^+(1s\ ^2S_{1/2})$, the population of the ground state for He II will be much lower than that of the ground state for He I (He ($1s^2\ ^1S_0$)). As a result, the spectral lines from He II will be difficult to detect. Only the excited neutrals are likely to emit the spectral line from the Penning discharge.

3.6 Conclusions

We have demonstrated a new partial pressure measurement method by analyzing the light from the Penning discharge.

(1) The intensity of H_α and H_β Balmer lines from the Penning discharge in H_2 is a function only of the discharge ion current. Their intensity is independent of the anode voltage and magnetic fields from 0.1 to 2.0 T.

(2) The light intensity of the H_α and H_β lines is proportional to the ion current below ~0.1 Pa. The ratio of the light intensity to the ion current increases by 40% for pressures above ~0.1 Pa because of a change in the type of discharge.

(3) The possibility of the partial pressure measurement by analyzing the light is demonstrated in the gas mixture of H_2 and He. The spectral line from He is a function only of the He partial pressure and independent of the H_2 pressure.

(4) Only the spectral line from the excited neutrals is measurable. That is, the spectral lines from the ions are difficult to detect because the confining time of ions is very short.

(5) Characteristics of the light intensity are rather well evaluated from the corona approximation.

As a result, this method is applicable to measure partial pressure near a plasma. Since the use of the quartz fibers and lenses increases the solid angle for the collection of the light, it is anticipated that a pressure from 10^{-5} to ~ 0.5 Pa can be measured in the vicinity of a magnetically confined plasma of JT-60.

References

[1] N. Ogiwara and M. Maeno, J. Vac. Sci. Technol. A6, 2870 (1988).

[2] Y. Matsuzaki et al., Shinku [J. Vac. Soc. Jpn.] **30**, 355 (1987).

[3] K. Akaishi, A. Uritani, Y. Kubota, and Y. Hori, J. Vac. Sci. Technol. A5, 2444 (1987).

[4] A. Uritani, K. Akaishi, Y. Kubota, Y. Hori, and A. Miyahara, Jpn. J. Appl. Phys. 25, L403 (1986).

[5] R. W. Conn, J. Nucl. Mater. **128/129**, 407 (1984).

[6] N. Ogiwara and M. Maeno, J. Vac. Sci. Technol. A7, 2804 (1989).

[7] N. Ogiwara and M. Maeno, Shinku [J. Vac. Soc. Jpn.] **32**, 292 (1989).

[8] J. C. Helmer and R. L. Jepsen, Proc. I.R.E. **49**, 1920 (1961).

[9] L. E. S. Phillips, Proc. Roy. Soc. A64, 172 (1898).

[10] F. M. Penning, Physica 3, 873 (1936).

[11] D. R. A. Webb, J. Phys. E7, 453 (1974).

[12] H. F. Dylla, J. Vac. Sci. Technol. **20**, 119 (1982).

[13] S. R. Thomas Jr., D. A. Goerz, and W. L. Pickles, J. Vac. Sci. Technol. A4, 1736 (1986).

[14] H. R. Griem, Plasma Spectroscopy (McGraw-Hill, New York, (1964).

[15] H. Hartwig and J. S. Kouptsidis, J. Vac. Sci. Technol. 11, 1154 (1974).

[16] A. Dallos, Vacuum **14**, 79 (1969)

[17] W. Schuurman, Physica **36**, 136 (1967).

[18] R. L. Jepsen, J. Appl. Phys. **12**, 2619 (1961).

[19] H. Kumagai, G. Tominaga, Y. Tuzi, and G. Horikoshi, Vacuum Science and Engineering, (Shokabo, Tokyo, 1970) p.48.

[20]D. R. Bates, A. E. Kingston, and R. W. P. McWhirter, Proc. Roy. Soc. A267, 297 (1962).

[21]T. Fujimoto, J. Phys. Soc. Jpn. **47**, 273 (1979).

[22]W. Knauer and M. A. Lutz, Appl. Phys. Lett. **2**, 109 (1963).

[23]M. Hirata, M. Ono, H. Hojo, and K. Nakayama, J. Vac. Sci. Technol. **20**, 1159 (1982).

[24]M. Yoshikawa, Nucl. Fusion **25**, 1081 (1985).

[25]D. G. Dow, J. Appl. Phys. **34**, 2395 (1963).

[26]Y. Seki, Y. Shimomura, K. Maki, M. Azumi, and T. Takizuka, Nucl. Fusion **20**, 1213 (1980).

[27]T. Asamaki, Oyobutsuri **41**, 451 (1972).

[28]L. C. Johnson and E. Hinnov, J. Quant. Spectros. Radiat. Transfer **13**, 333 (1973).

Table 3.1 Twelve sizes of Penning cells.
Diameter d of the anodes is 20 mm.

Distance L between the cathodes (mm)	Anode length l (mm)			
	40	20	10	5
45	I	II	III	IV
35		V	VI	VII
25		VIII	IX	X
15			XI	XII

Table 3.2 Spectral lines between 400 nm and 700 nm of H, D, and T.

Transition	Wavelength (nm)		
	H	D	T
$2p\ ^2P^0 - 3d\ ^2D$	(H_α) 656.3	(D_α) 656.1	(T_α) 656.0
$2p\ ^2P^0 - 4d\ ^2D$	(H_β) 486.1	(D_β) 486.0	(T_β) 486.0
$2p\ ^2P^0 - 5d\ ^2D$	(H_γ) 434.0	(D_γ) 433.9	(T_γ) 433.9
$2p\ ^2P^0 - 6d\ ^2D$	(H_δ) 410.2	(D_δ) 410.1	(T_δ) 410.0

Table 3.3 Spectral lines between 350 nm and 800 nm detected in a Penning discharge. Intensity of the lines 402.6 nm and 412.1 nm from the He discharge is rather weaker than that of other lines.

Gas	Wavelength (nm)	Transition*
H_2	H_α 656.3	$2p\ ^2P^0 - 3d\ ^2D$
	H_β 486.1	$2p\ ^2P^0 - 4d\ ^2D$
He	388.9	$2s\ ^3S - 3p\ ^3P^0$
	396.5	$2s\ ^1S - 4p\ ^1P^0$
	402.6	$2p\ ^3P^0 - 5d\ ^3D$
	412.1	$2p\ ^3P^0 - 5s\ ^3S$
	447.1	$2p\ ^3P^0 - 4d\ ^3D$
	471.3	$2p\ ^3P^0 - 4s\ ^3S$
	492.2	$2p\ ^1P^0 - 4d\ ^1D$
	501.6	$2s\ ^1S - 3p\ ^1P^0$
	504.8	$2p\ ^1P^0 - 4s\ ^1S$
	587.6	$2p\ ^3P^0 - 3d\ ^3D$
	667.8	$2p\ ^1P^0 - 3d\ ^1D$
	706.5	$2p\ ^3P^0 - 3s\ ^3S$
	728.1	$2p\ ^1P^0 - 3s\ ^1S$

*The symbol 1s is omitted for He. For example, 3d refers to (1s)(3d).

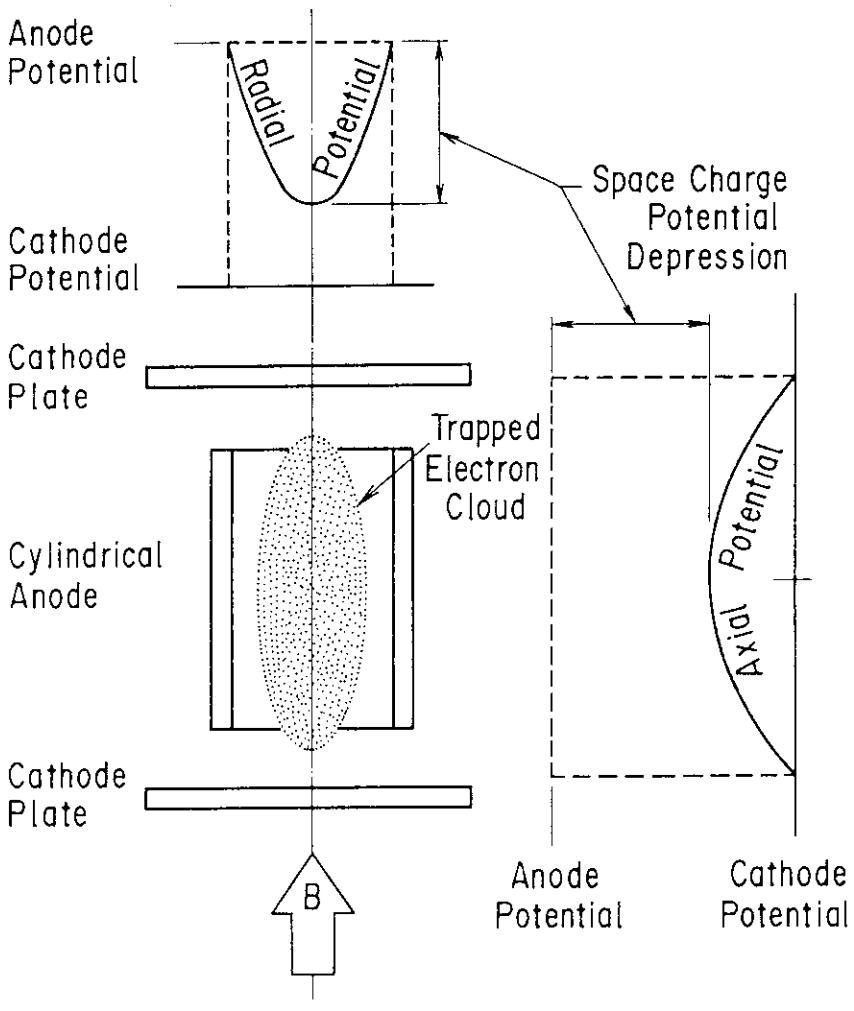

Fig. 3.1 Schematic configuration of the Penning discharge.

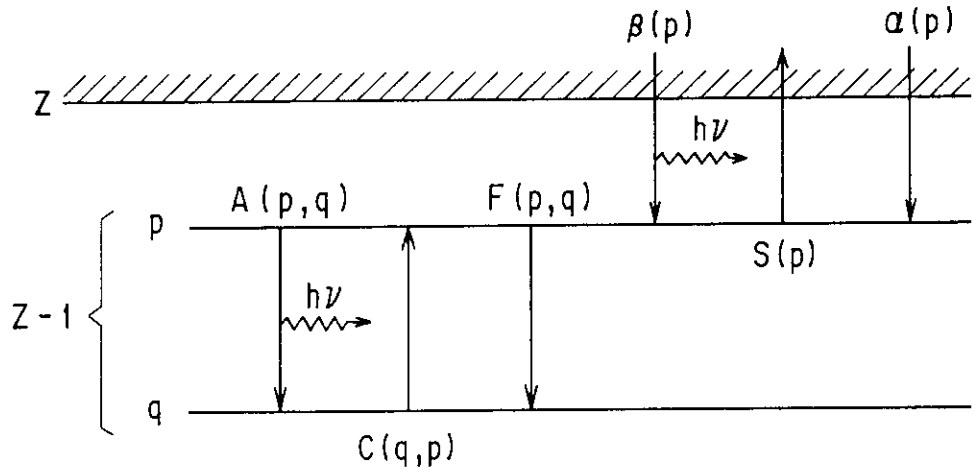

$p \xrightarrow{A(p,q)} q + h\nu$: spontaneous radiative transition

$q + e \xrightarrow{C(q,p)} p + e$: excitation by electron collisions

$p + e \xrightarrow{F(p,q)} q + e$: deexcitation by electron collisions

$z + e \xrightarrow{\beta(p)} p + h\nu$: radiative recombination

$p + e \xrightarrow{S(p)} z + e + e$: ionization by electron collisions

$z + e + e \xrightarrow{\alpha(p)} p + e$: three-body recombination

Fig. 3.2 Elementary processes in the Penning discharge.

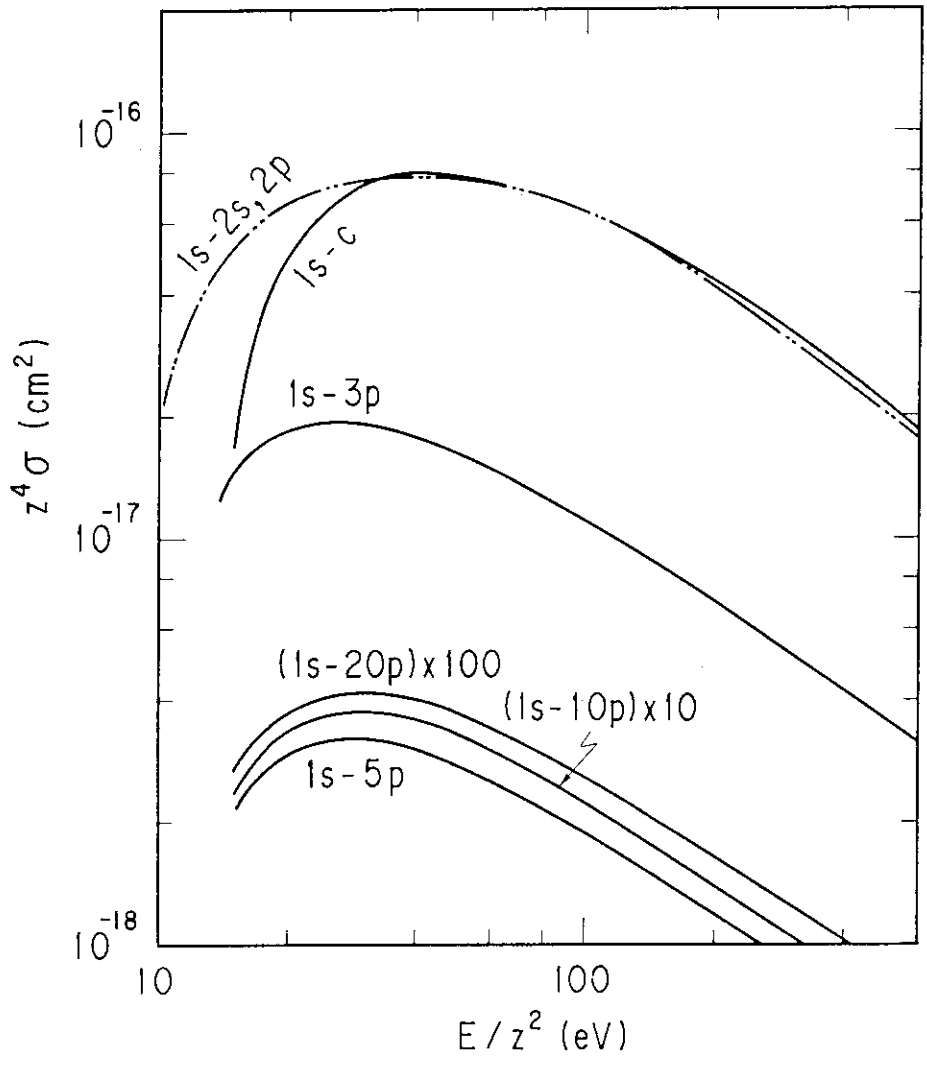

Fig. 3.3 Excitation and ionization cross sections for hydrogenic ions with nuclear charge z from the ground 1s state as a function of electron kinetic energy reduced by the square of nuclear charge.

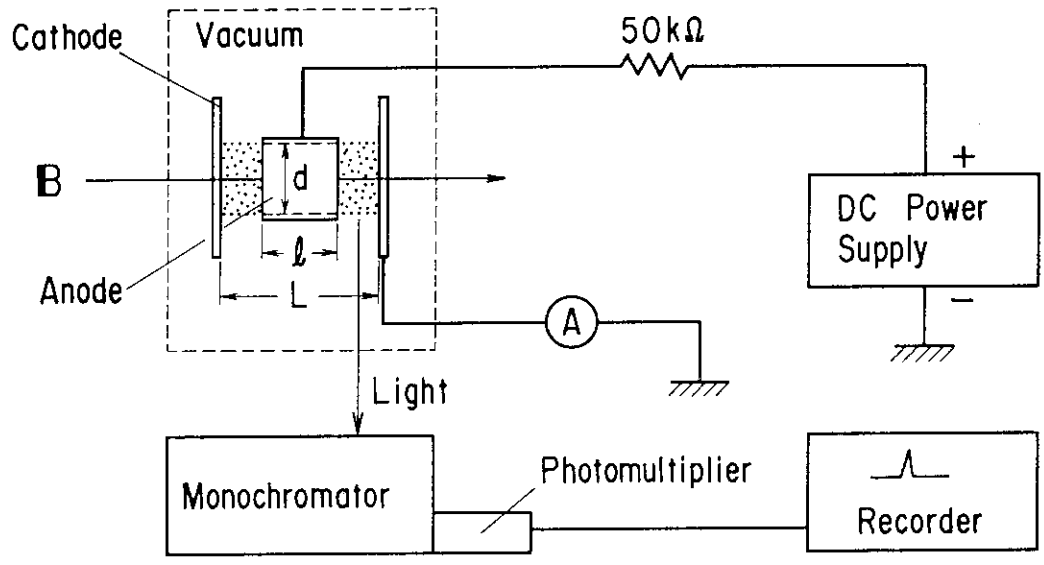

Fig. 3.4 Schematic diagram of the essential parts of the experimental apparatus. The cells are classified as shown in Table 3.1 by the distance L between the cathodes and the length l of the anode. Diameter d of the anode is 20 mm.

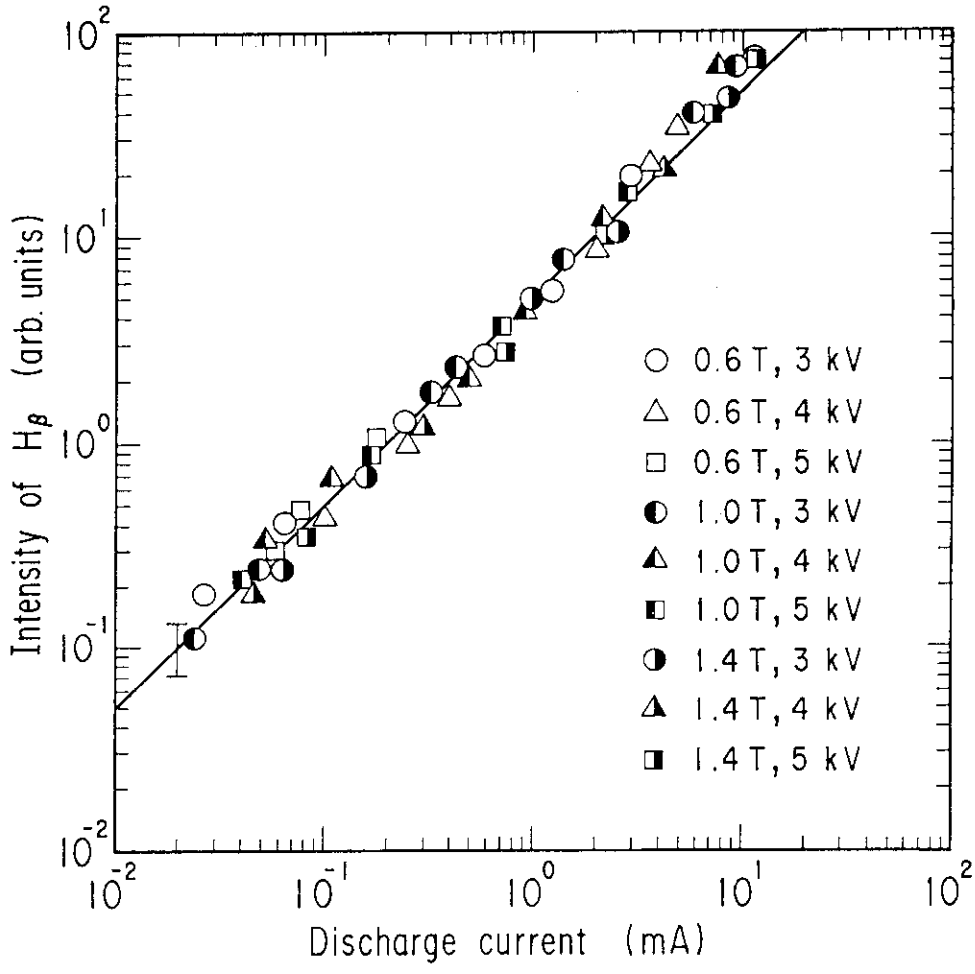

Fig. 3.5 Typical variation of the intensity of H_β Balmer line (486.1 nm) with the discharge current. The cell is type I.

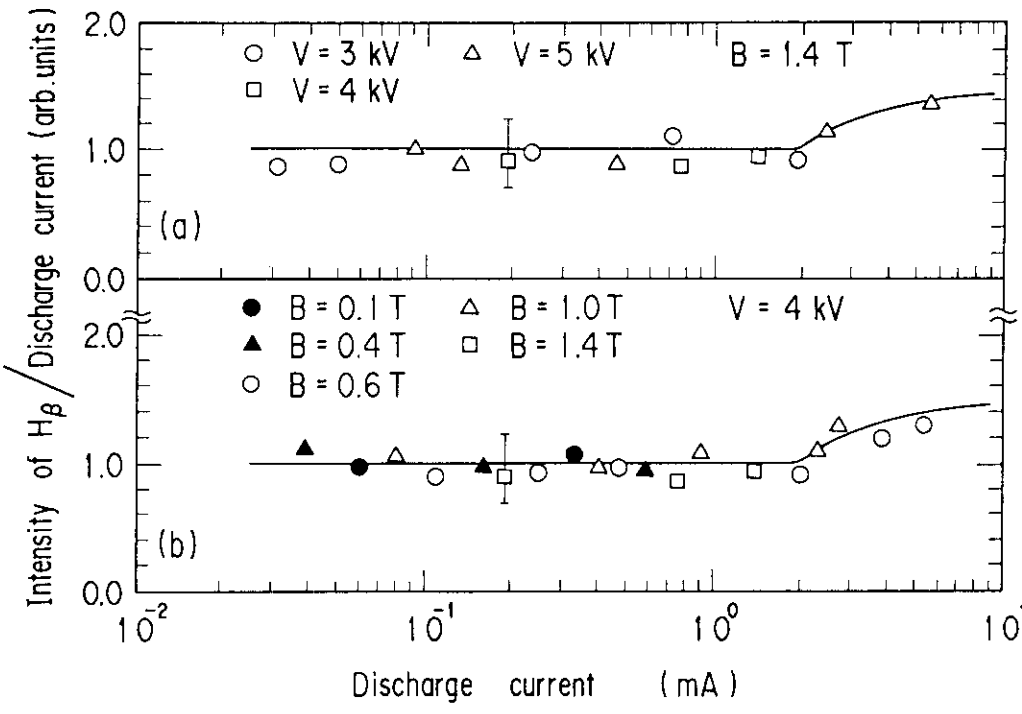

Fig. 3.6 The H_β line intensity reduced by the discharge current is plotted as a function of the discharge current. The cell is type I. (a) dependence on the anode voltage; (b) dependence on the magnetic field.

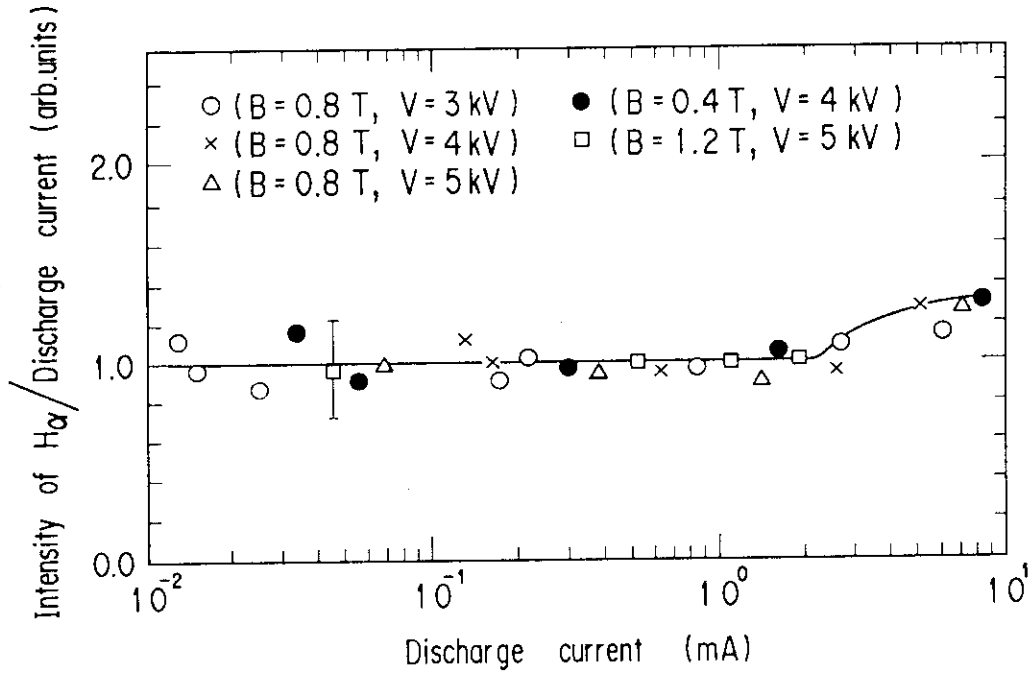

Fig. 3.7 Typical variation of the reduced intensity of the H_α line (656.3 nm) with the discharge current. The cell is type I. Parameters are the magnetic field and the anode voltage.

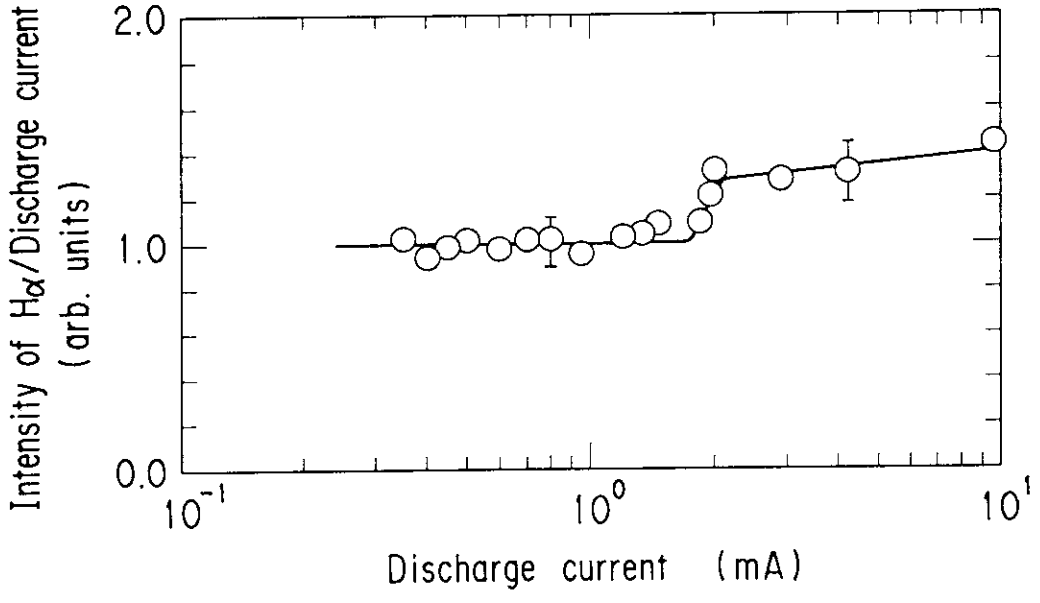

Fig. 3.8 Ratio of the intensity of the H_α line to the discharge current. These data are taken for the cell of type IX in a fusion device JT-60.

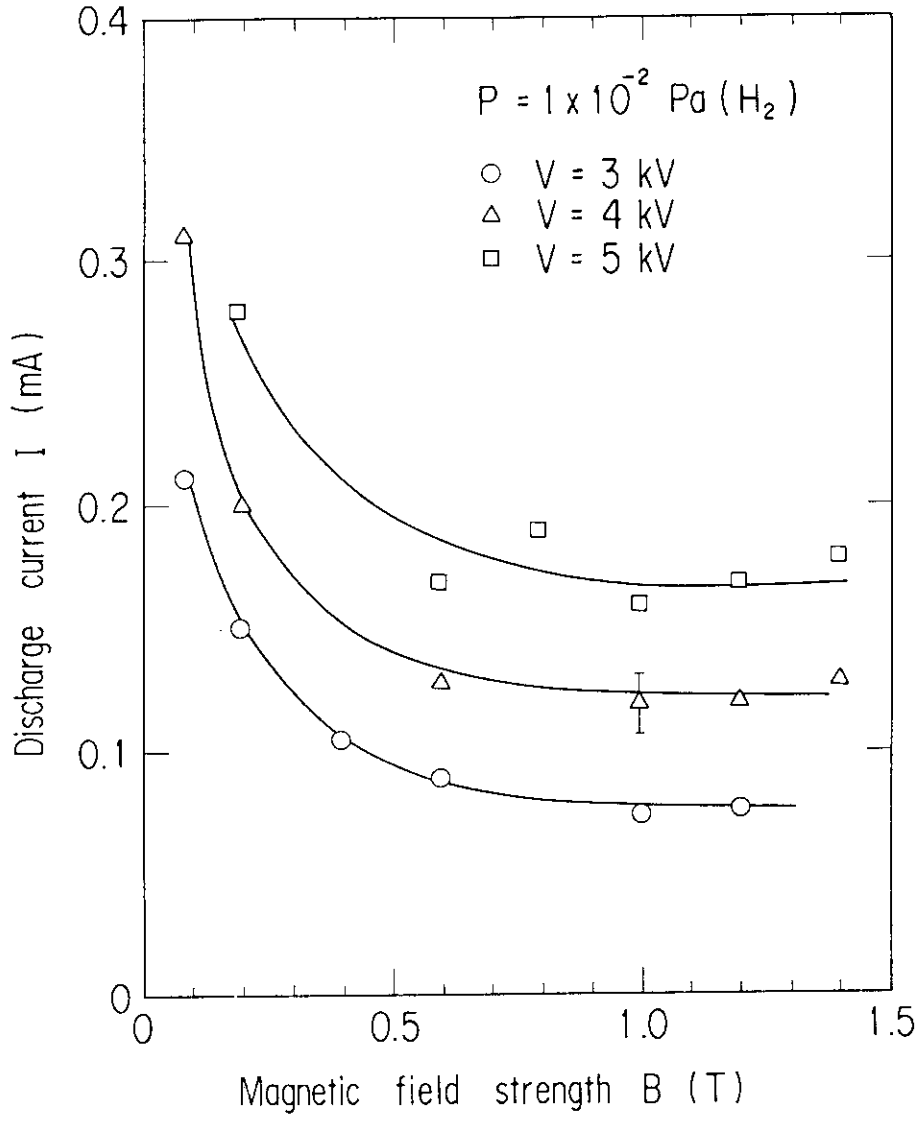

Fig. 3.9 Typical variation of the discharge current with the magnetic field strength at a pressure of 10^{-2} Pa (H_2). The cell is type I.

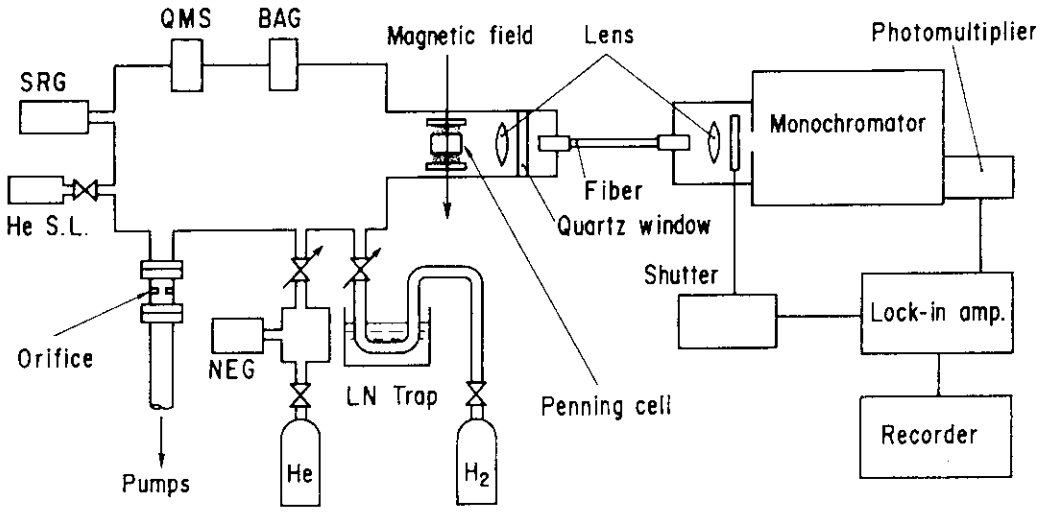

Fig. 3.10 Schematic view of the experimental apparatus. Pressure is measured by a Bayard-Alpert gauge (BAG), a spinning rotor gauge (SRG), and a quadrupole mass spectrometer (QMS). The introduced gases (H_2 and He) have the purity of higher than 99.99%. Light from a Penning discharge is guided to a monochromator through a quartz window, quartz lenses, and a bundle of quartz fibers. Standard leak of helium (He S.L.) is mainly used for the calibration of the QMS. A liquid-nitrogen trap to remove impurities in a main chamber is omitted from this figure.

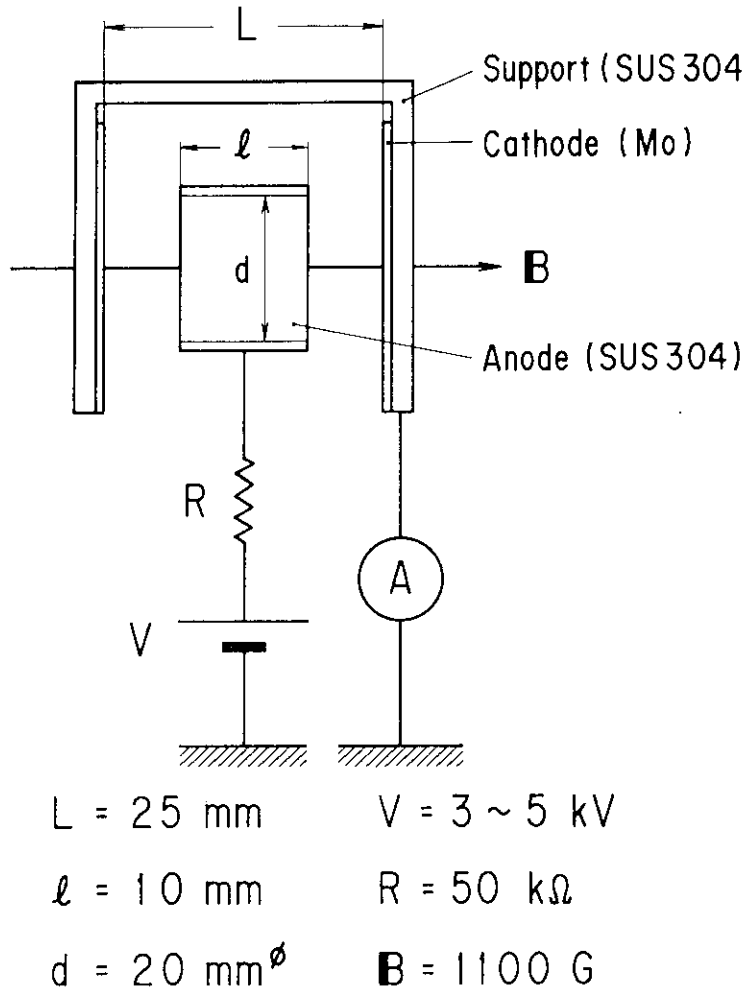

Fig. 3.11 Dimensions of the Penning cell and the discharge conditions.

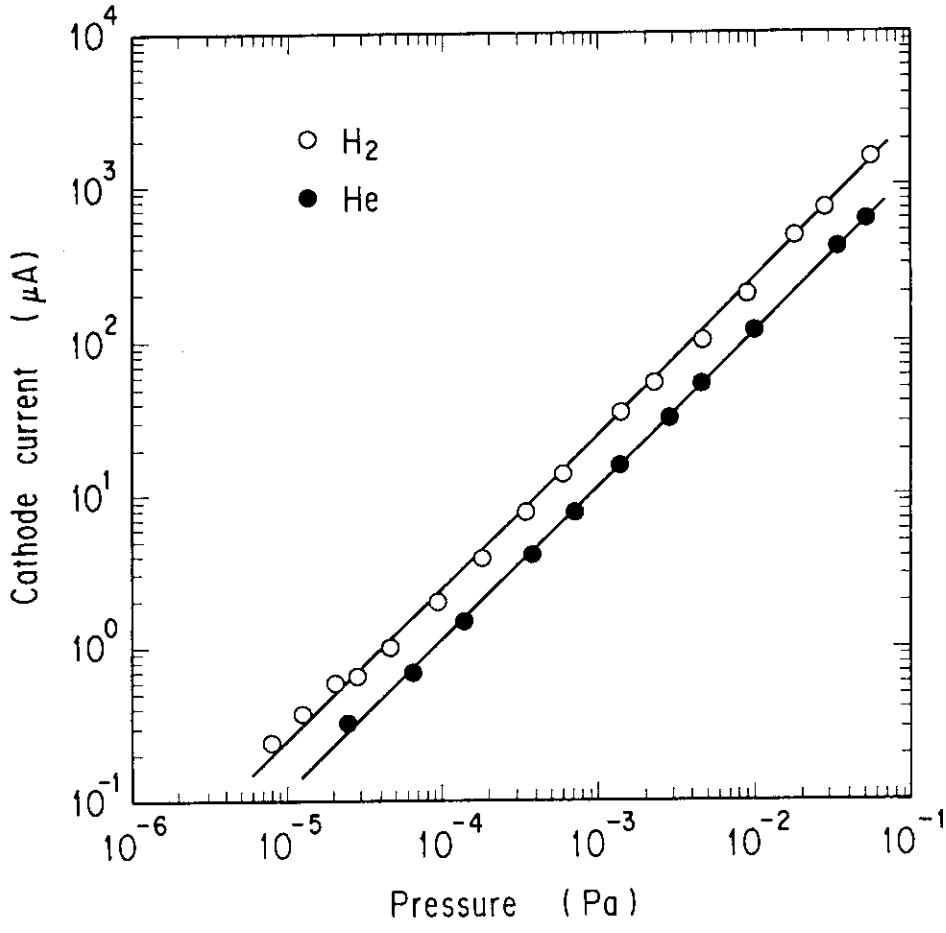

Fig. 3.12 Typical variation of the cathode current with the pressure of H_2 and He. The anode voltage V is 4 kV.

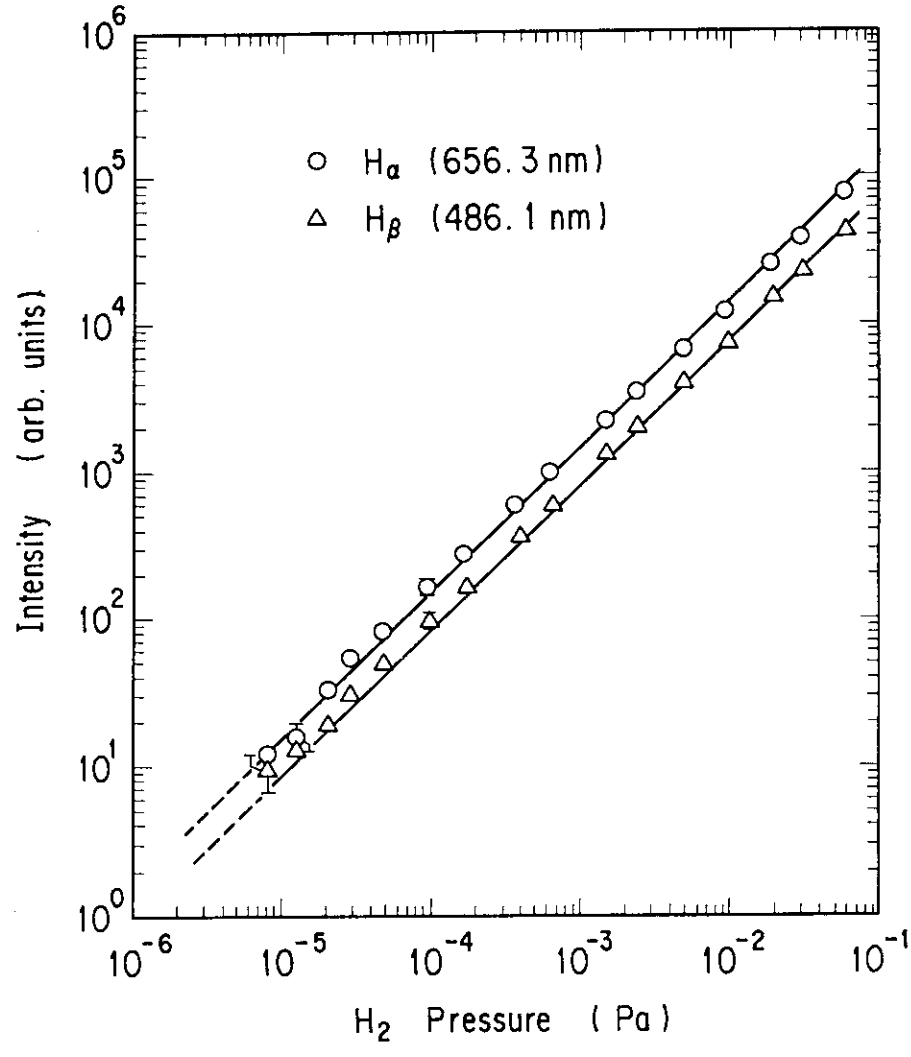

Fig. 3.13 The intensity of H_α and H_β as a function of H_2 pressure. The anode voltage V is 4 kV.

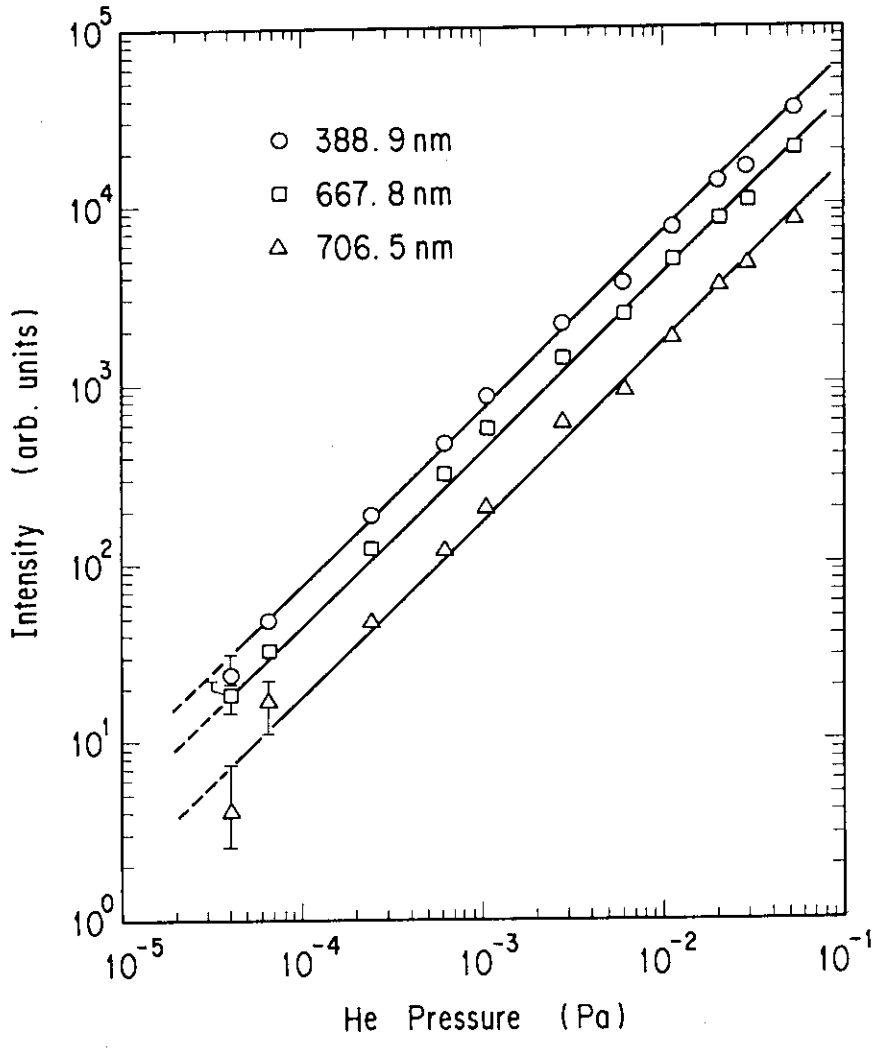

Fig. 3.14 The intensity of the lines 388.9 nm, 667.8 nm, and 706.5 nm as a function of He pressure. The anode voltage V is 4 kV.

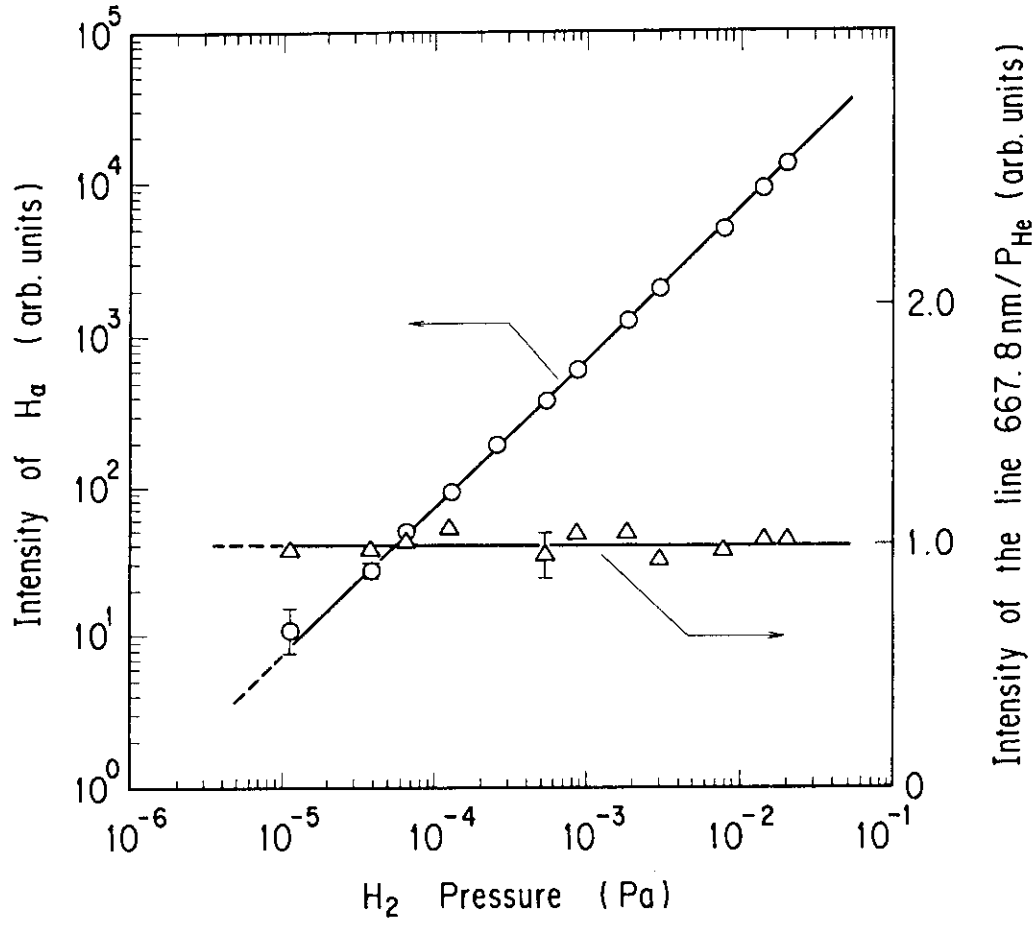

Fig. 3.15 The intensity of H_α and the line 667.8 nm from He as a function of the partial pressure of H_2 in the gas mixture of H_2 and He. The partial pressure of He (P_{He}) is varied from 4×10^{-5} Pa to 10^{-4} Pa. The intensity of the line 667.8 nm is normalized with P_{He}. The anode voltage V is 4 kV.

4. The fast pressure monitoring system on JT-60

4.1 Introduction

Pressure measurement near a plasma is necessary to control the plasma density, especially in current build-up phase. Recently, the build-up of the plasma on JT-60 has been found to be successful only in a fixed range of the fuel gas pressure.[1] In a large tokamak such as JT-60, the response time of the pressure measurement for density control must be less than 10 ms.[2]

Several researchers have utilized the confining magnetic field of the fusion device to measure pressure near a plasma.[2-4] We have also developed a new type of gauge for use in a fusion device JT-60.[5-7] It is a type of Penning configuration gauge, which utilizes the magnetic field for confining the plasma. Merits of this Penning configuration gauge are as follows:

(a) The response time is very short. Since the sustaining magnetic field is mainly the toroidal magnetic fields, the gauge head can be installed inside the toroidal magnetic field coils. Thus we can measure the pressure with a response time of less than 10 ms.

(b) The structure is very simple. Only two electrodes are necessary: an anode tube and two cathode plates. Therefore, the mechanical reliability is large.

(c) The partial pressure can be measured.

On the other hand, the disadvantage is that it is a little noisy and erratic.

The gauges are successfully used to monitor the pressure near the plasma over a year. Some of the gauge characteristics have been described previously (in chapter 3). In this part, the details of this fast pressure monitoring system are described and

the performance of the gauge is shown.

4.2 Outline of the JT-60 tokamak

First we show the outline of the JT-60 tokamak. JT-60 is one of the three large tokamaks now in operation in the world. Its main objectives are as follows:[8]

(1) achieving and investigating Q~1 hydrogen plasma,

(2) making an integrated test of fusion technologies to develop scientific and technical basis for the next stage of advancement.

Figure 4.1 shows a bird's-eye view of the JT-60 tokamak, which is composed of a vacuum vessel, toroidal field coils, poloidal field coils, supplementary heating devices (neutral beam injectors and RF heating equipment), and other additional components. The main device parameters are listed in Table 4.1. The vacuum vessel is a toroidal chamber to confine the 60 m^3 plasma. It is made of Inconel 625 alloy and its volume is ~160 m^3. Inside the vacuum vessel attached are a number of first walls such as limiters, liners, and magnetic limiter plates. It has a maximum baking temperature of 500^{o}C and contains discharges at temperatures of up to 400^{o}C. The vacuum vessel is evacuated to less than $1X10^{-6}$ Pa by a pumping system. Eighteen toroidal field coils are located around a torus axis at a regular interval of 20 degrees, and produce a magnetic field intensity of 4.5 T at a plasma axis of 3 m. The poloidal field coils, which are placed inside the toroidal field coils, consist of five kinds of coils, each with a separate function: the current transformer, the vertical, the horizontal, the quadrupole, and the divertor coils.

The neutral beam injectors, fourteen in total, are paired into a vertical stack and placed at seven azimuthal positions. RF waves are introduced through four units (three for lower hybrid wave and one for ion cyclotron wave).

Figure 4.2 shows the ports where the gauge heads are placed. In order to measure the pressure with a fast response time, the gauge heads are installed inside the toroidal magnetic field coils. The pressure is measured at three points in the same poloidal section because the pressure around the plasma is not necessarily uniform. At the IN2LS port, the pressure near an open divertor is measured. The changes in the pressure far from the divertor are studied at the ports of S4U and S4L.

4.3 Description of the gauge

4.3.1 Constitution of the system

The whole system of these gauges is schematically shown in Fig. 4.3. All the gauges shown in Fig. 4.2 are controlled by a personal computer. They are independent of JT-60's host computer, "ZENKEI". The operational sequence is shown in Fig. 4.4. The whole system is first waiting in the mode of "standby". The toroidal magnetic field, which is a main component of the magnetic fields, is always monitored by a Hall effect gaussmeter. If the magnetic field strength becomes greater than the threshold value (usually 0.5-0.7 T), the power supplies are switched on. Thus the Penning discharge is fired. At the same time, the data are acquired. After the time T_1 (usually 60 s), the power

supplies are turned off and the data are then stored in the memory. The gauges are reset in the standby mode after the time T_2 (~5 min). The data of the discharge current are acquired with four kinds of linear amplifiers in order to cover a wide range of pressure (10^0-10^{-4} Pa). Here, the time constant of the amplifiers is a total of less than 100 μs. Thus the time constant of the electric circuit is confirmed to be less than 1 ms. On the other hand, the light emitted from the Penning discharge is guided to a monochromator in a diagnostic room through 300-m quartz fibers and then analyzed. The data about the light are stored in a micro-computer in the diagnostic room. The time constant of the electric circuit for analyzing the light is also designed and confirmed to be less than 1 ms.

The origin of the time is set at the time of the "marker" signal, which is sent from the host computer through an optical fiber. Usually, the time of the build-up of the plasma current is used as the marker signal. The data of the discharge current are individually sent to the host computer "ZENKEI" at time intervals of 20 ms through a CAMAC system. The data are visually shown on the display after every discharge.

As the high dc voltage is supplied, current leak is very dangerous. Therefore the system is designed to stop in the case of even a small leak of current. The current leak is monitored not only by the personal computer but also by an electrometer between the power supply and the earth line.

4.3.2 Gauge head

The schematic configuration of the head is shown in Fig.

4.5. An anode is a 20 mm diameter ring with a length of 10 mm. It is made of SUS 304, and is supported by an electrical feedthrough. Cathodes are made of Mo plates with a depth of 1 mm and are mounted on a frame made of SUS 304. The frame is also supported by the feedthroughs. Bias potentials of the anode and cathode are individually introduced by the electrical feedthroughs which also work as supports. A Venetian blind is placed between the plasma and the Penning cell to prevent the fast particles from impinging into the cell. The flange on which the feedthroughs are mounted will be differentially pumped out in the case of an unexpected vacuum trouble. In addition, the gauge head has a viewing port through which the light emitted from the Penning discharge is guided out to the monochromator. The viewing port will be also differentially pumped out. The response time of the gauge head is designed to be less than 1 ms.

The gauge head is supported by the support arm. Figure 4.6 shows the support structure for the heads at S4U and S4L. The gauge head is electrically isolated from the support by the insulator. The vibrations of the vacuum vessel are broken by the bellows, which are placed between the head and the flange.

The center axis of the anode is set to be parallel to the direction of the toroidal magnetic field. The influence of the direction of the magnetic field is described later.

4.3.3 Response time vs. magnetic field

The gauge heads must be placed in or very near the vacuum vessel in order to measure the pressure with a fast response time. Figure 4.7 shows the rough relation of the response time to

the magnetic field strength (mainly the toroidal magnetic field). Here, the connecting pipe is a 100 mm diameter tube and the gas is hydrogen. Point "A" is a place where the flange is fixed for an IN2LS port. When we measure the pressure with a response time of less than 10 ms, we cannot place the gauge heads far from the flanges. More precise estimation of the response time is carried out. The response time is estimated to be ~8 ms.

4.3.4 Vibration of the port due to plasma disruption

The port is excessively vibrated by the impulsive force due to the plasma disruption.[9] We have measured the vibration at the three connecting flanges for a month before the installation of the gauges. Figure 4.8 shows the typical acceleration and frequency components in the vibration of IN2LS port just after the disruption of the 2 MA plasma. The maximum acceleration in all the disruptions was 40 G at IN2LS port and 25 G at S4U and S4L ports. The main component of the oscillation frequencies is 400 Hz for IN2LS and 200 Hz for S4U and S4L ports.

We have vibrated the prototype gauge head with an acceleration of 40 G. The electrodes can withstand more than ten thousand vibrations. However, the welded part of the housing was destroyed after several thousand oscillations. Since extensive research and development are needed in order to increase the toughness of the housing against the vibration, we have installed a bellows between the gauge head and the flange. As the bellows have a spring coefficient of 0.88 kgf/mm, the force due to the vibration of 200 and 400 Hz with the acceleration of 40 G is weakened to less than 0.5 kgf, which is

negligibly small. However, it is doubtful whether the bellows have sufficient strength and fatigue may necessitate their exchange after a certain period of operation.

4.4 Performance

4.4.1 Calibration

The gauge is calibrated at JT-60 for H_2. The procedure is as follows:

(a) The pressure in the vacuum vessel is held at a constant flow of hydrogen. The flow rate for gas-supply equipment is previously calibrated. Moreover, the rate is doubly checked with the pressure measurement and the pumping speed in a pumping duct.

(b) The pressure in the vacuum vessel is calculated by the equation $P = q/S$.

Here, q and S refer to the flow rate and the pumping speed for hydrogen at the pumping port.

(c) Then the magnetic field is supplied without plasma discharge. Thus the Penning discharge current is measured as a function of magnetic field strength with a fixed hydrogen pressure.

(d) For various values of flow rate, the above procedures from (a) to (c) are repeated.

Figure 4.9 shows the typical variation of the Penning discharge current I with the strength of the toroidal magnetic field B_T. The discharge current reaches a steady value with the increasing magnetic field strength. The current is almost

independent of magnetic fields above 0.7 T. Figure 4.10 shows the relation of the discharge current I above 0.7 T to the hydrogen pressure $P(H_2)$. The current I is approximated by the following equation:

$$P(H_2) = CI. \quad (15)$$

Here, the constant C is 21.5 Pa/A. The deviation of the data is within ±20 % from equation (15).

The discharge current is also investigated at a test stand and is found to be almost independent of the small angle (less than 8 degrees) between the anode axis and the magnetic field. The Penning cell is set to be parallel to the toroidal direction. The ratio of the poloidal magnetic field B_P to the toroidal field B_T is estimated from the safety value q at the plasma surface. The safety factor q at the plasma surface is written by the equation:

$$q = (B_T/B_P)\ (a/r). \quad (16)$$

Here, a and r refer to the minor and major radius, respectively. From equation (16), the ratio B_P/B_T is less than 1/7.5 because we operate the plasma at $q \geq 2.5$. Since the angle is less than 7.5 degrees, the influence of the angle is negligible.

4.4.2 Performance

Figure 4.11 shows a typical change in pressure for 30 s including the plasma discharge. The top and bottom of the figure are the changes in the pressure measured by a BA gauge with a magnetic shield and by the Penning configuration gauge, respectively. The BA gauge is placed ~5 m from the plasma. The response time is ~300 ms.[10] The following features are made clear

only with the Penning configuration gauge.

(a) The gas fueled before burning of the plasma is exhausted by the plasma at the same time of the burn-up of the plasma.

(b) The abrupt rise of the pressure is observed at almost the same time of the disruption of plasma current.[11]

(c) The pressure becomes lower after the mode of the plasma changes from the L- to the H-mode[12] (not shown in Fig. 4.11).

Time response was estimated using the abrupt change in the pressure due to the plasma-wall interaction. Figure 4.12 shows the change in the discharge current just after 1 ms contact of a plasma with the inner wall near the gauge at the IN2LS port. From this data, the time response of the gauge is evaluated to be less than 10 ms.

JT-60 is usually operated with hydrogen. Figure 4.13 illustrates the equivalence of the H_α line intensity to the discharge current for pressure measurement with the Penning configuration gauge. The details are discussed in the previous chapter. The pressure can be measured by either the discharge current or the spectral line intensity.

When the plasma current is disrupted at the rate of ~200 MA/s, the large spurious voltage and current are induced. Figure 4.14 shows the noise level of the Penning configuration gauge. The change in the current for the two gauges is measured. The gauge at S4U is operated at the anode voltage of 5 kV. The other at IN2LS is not ignited. Thus it measures the spurious current. The plasma disruption occurs at t= ~5.5 s for the discharge shown in Fig. 4.14. It is found that the spurious current is less than $\sim 10^{-2}$ mA, the value of which corresponds to the pressure of $\sim 10^{-4}$ Pa.

4.5 Conclusions

We have developed and installed the fast response gauge in JT-60. The gauges are used to monitor the pressure near the plasma. The main features of the gauges are as follows:

(1) The response time is fast (less than 10 ms) because of the Penning discharge which is sustained by the confining magnetic field of the plasma.

(2) The gauges cover a wide range of pressure from 1 to 10^{-4} Pa. The accuracy of the measurement is within ±20% although the plasma disruption induces the spurious signal corresponding to ~10^{-4} Pa.

(3) The gauges are controlled by the personal computer. The measurement is carried out for ~60 s including a plasma discharge.

References

[1] R. Yoshino, Y. Neyatani, H. Ninomiya, N. Hosogane, H. Nakamura, T. Arai, K. Itami, N. Nishino, M. Sato, T. Fukuda, and JT-60 Team, J. Nucl. Mater. **162/164**, 527 (1989).

[2] H. F. Dylla, J. Vac. Sci. Technol. **20**, 119 (1982).

[3] D. R. A. Webb, J. Phys. E7, 453 (1974).

[4] S. R. Thomas, Jr., D. A. Goertz, and W. L. Pickles, J. Vac. Sci. Technol. A4, 1736 (1986).

[5] N. Ogiwara, Y. Yamashita, H. Yokomizo, M. Maeno, T. Shimada, and F. Kimijima, Shinku [J. Vac. Soc. Jpn.] **31**, 406 (1988).

[6] N. Ogiwara and M. Maeno, J. Vac. Sci. Technol. A7, 2804 (1989).

[7] N. Ogiwara, M. Maeno, and M. Matsukawa, in Proc. 13th Symp. on Fusion Technol., Knoxville, IEEE, 1989.

[8] Y. Yoshikawa and K. Tomabechi, Nuclear Technol./Fusion **4**, 299 (1983).

[9] H. Ninomiya, Y. Nakamura, T. Ozeki, A. Kameari, N. Tsuzuki, T. Sometani, and Y. Suzuki, Proc. 8th Symp. on Engrg. Problems of Fusion Research, San Francisco (1979) 1863.

[10] N. Miya, H. Nakamura, S. Tsuji, T. Ando, S. Hiroki, T. Nishitani, K. Nagashima, S. Koide, and JT-60 Team, J. Nucl. Mater. **162/164**, 618 (1989).

[11] This is studied in detail in chapter 5.

N. Ogiwara and M. Maeno, Shinku [J. Vac. Soc. Jpn.] **33**, 381 (1990).

[12] M. Shimada et al., to be published.

Table 4.1 Main device parameters of the JT-60 tokamak machine

Parameter	Design value
Major radius	3.03 m
Minor radius	0.9 m
Plasma current	3.2 MA
Toroidal field at plasma axis	4.5 T
Plasma current duration	10 s
Repetition time	600 s
Additional heating power	
Neutral beam injection	20 MW
Radio frequency heating	10 MW

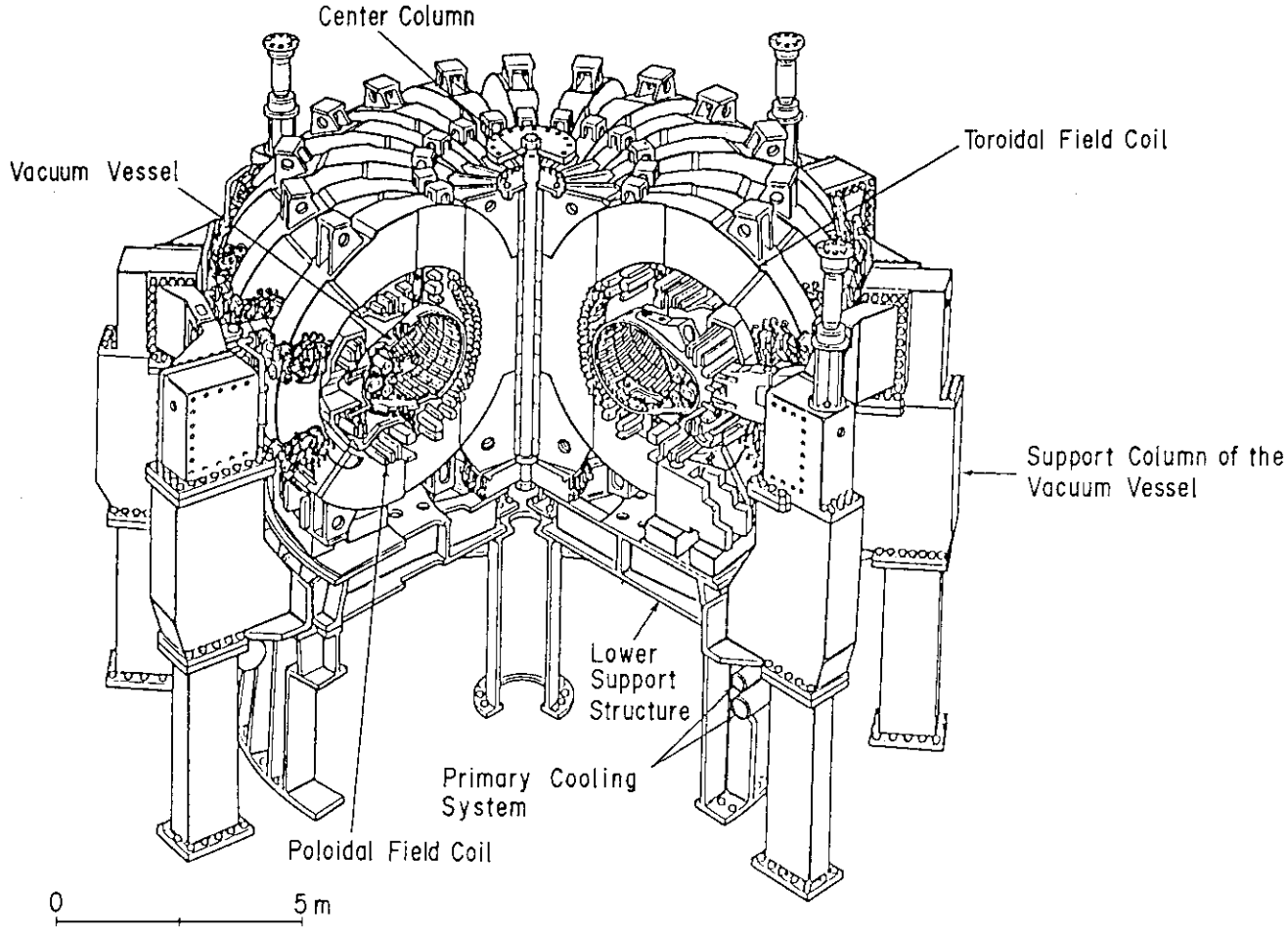

Fig. 4.1 Bird's-eye view of the JT-60 tokamak machine.

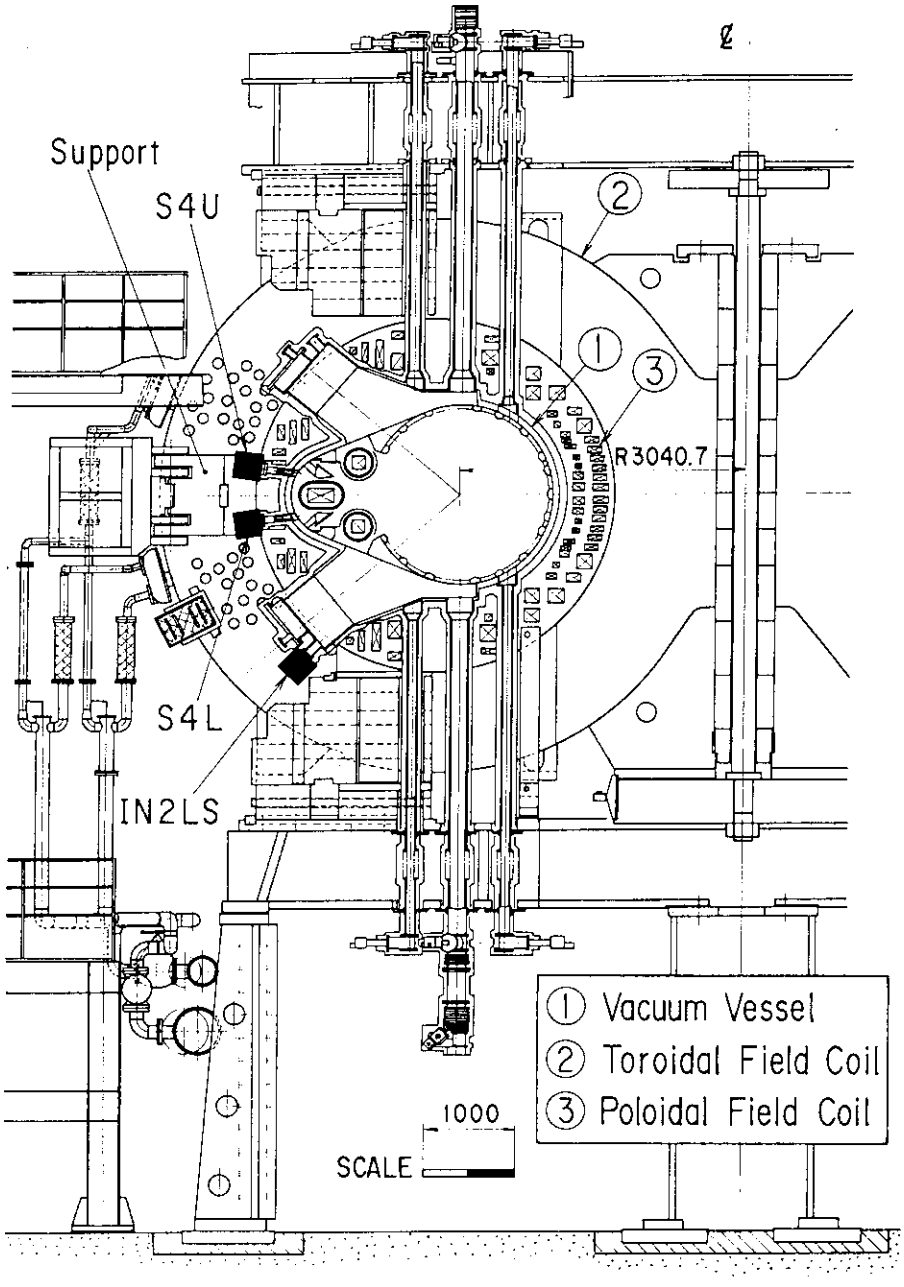

Fig. 4.2 Cross sectional view of JT-60. The gauge heads are fixed to the flanges of S4U, S4L, and IN2LS ports.

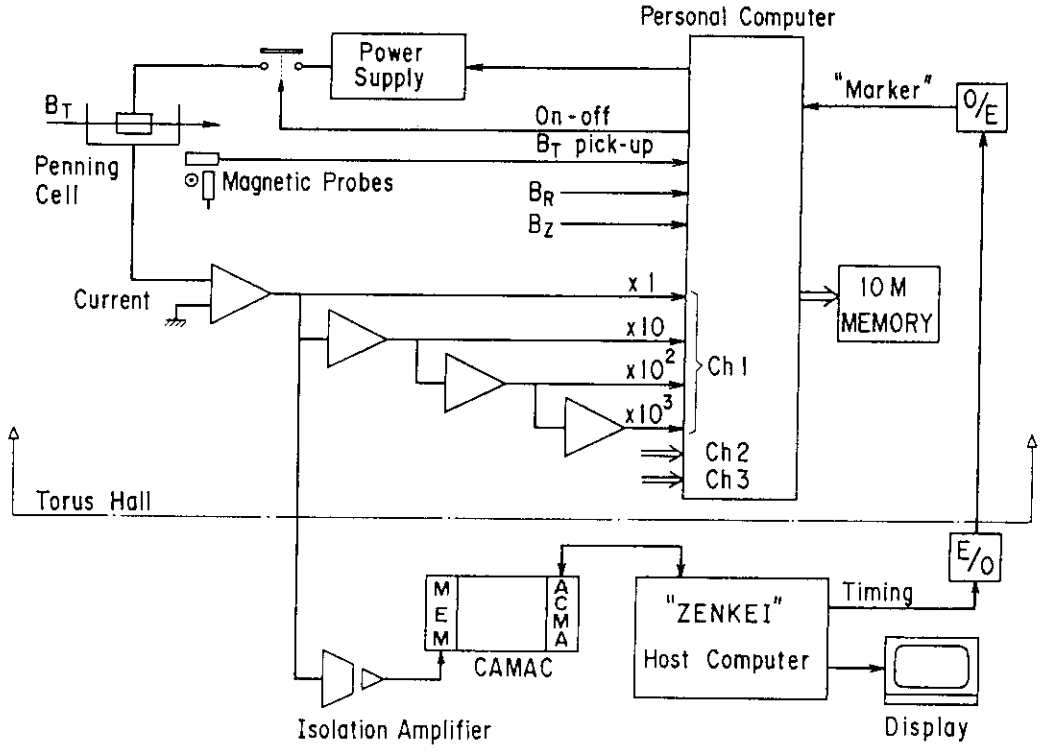

Fig. 4.3 Schematic diagram of the fast pressure monitoring system.

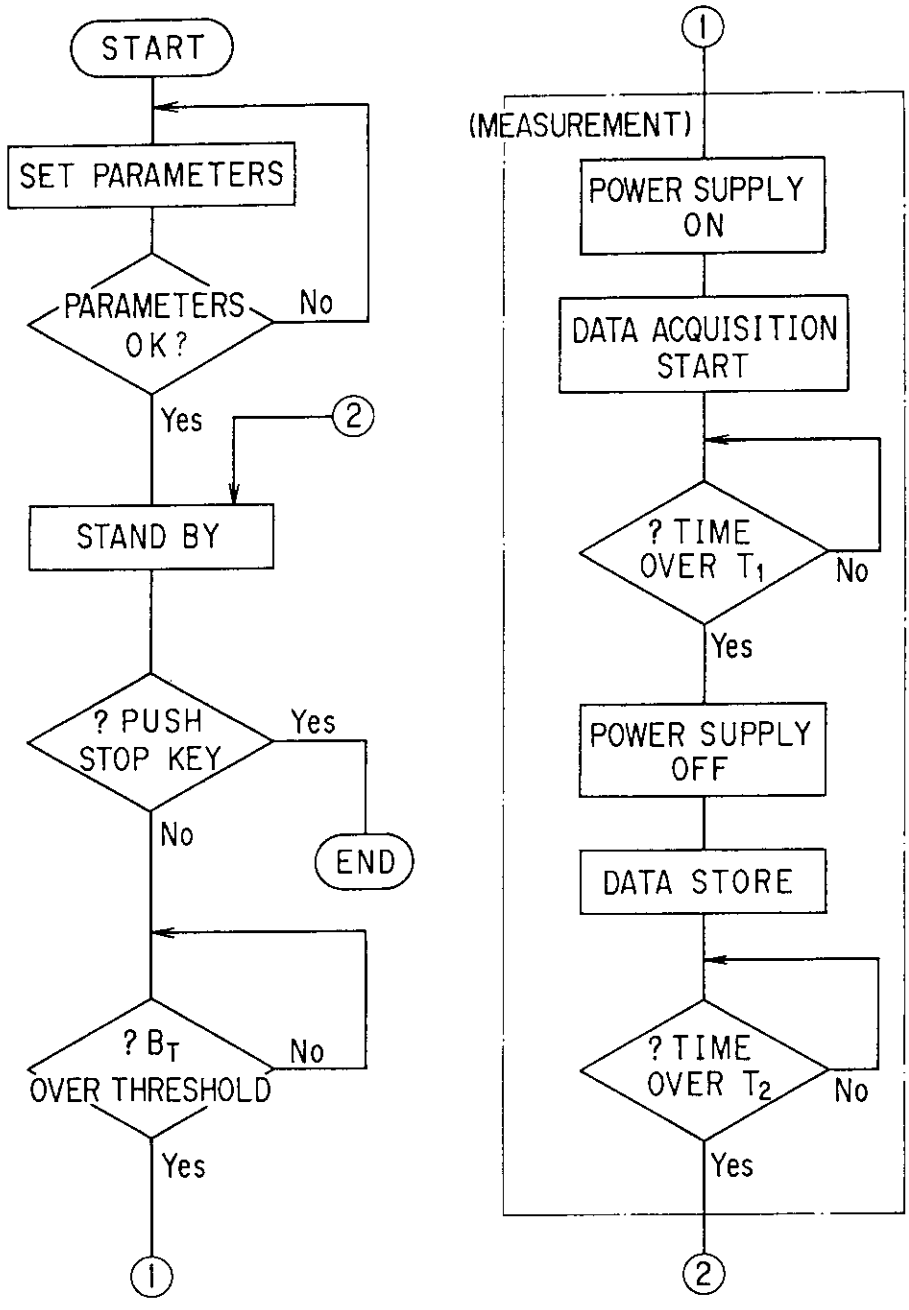

Fig. 4.4 Control flow diagram.

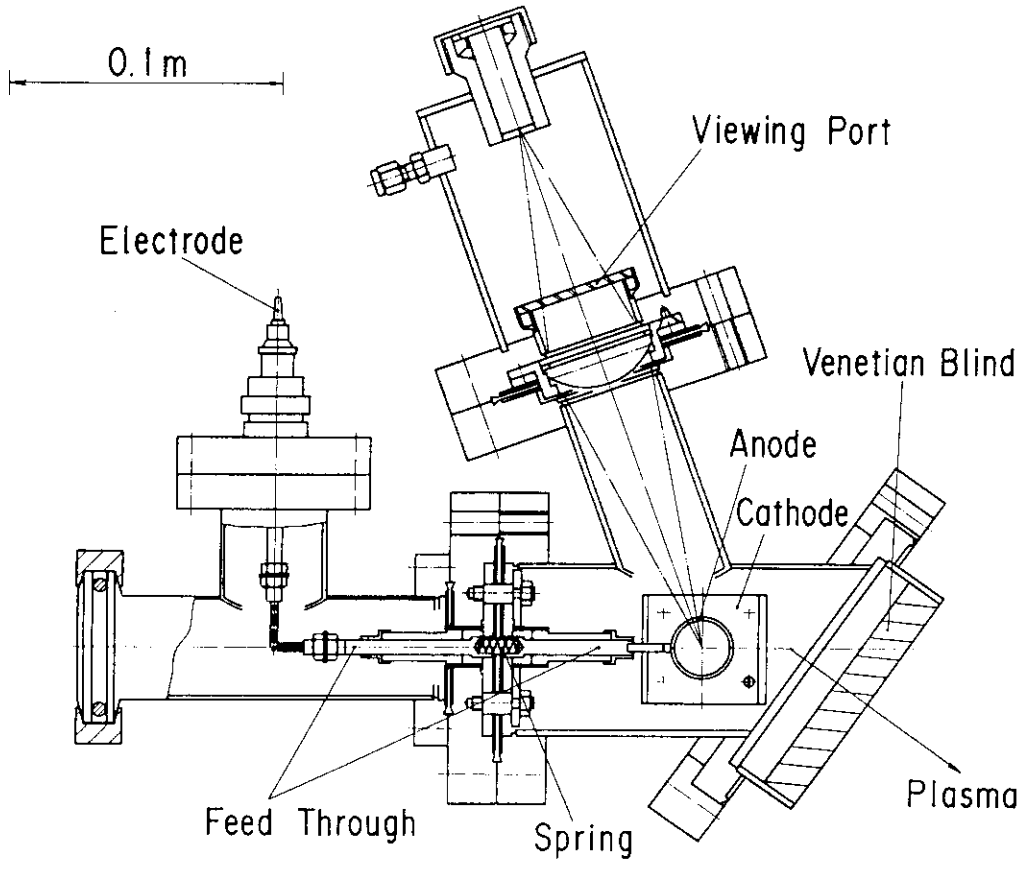

Fig. 4.5 Details of the gauge head. The Venetian blind is placed between the Penning cell (anode and cathodes) and the plasma.

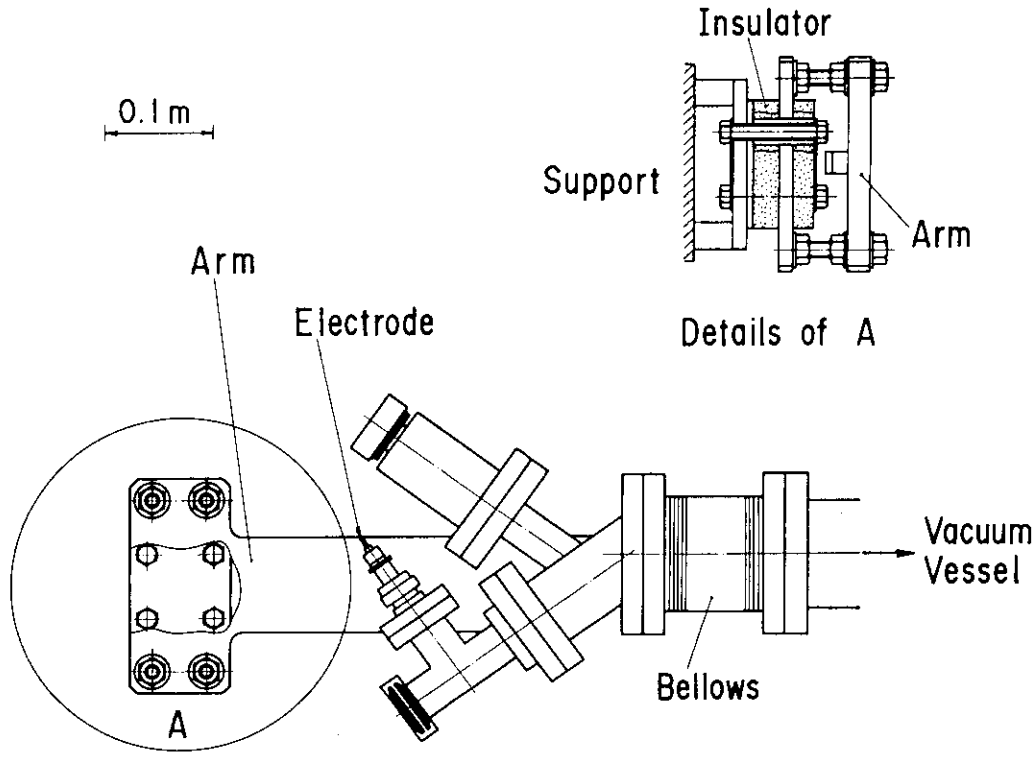

Fig. 4.6 Support structure for the heads at S4U and S4L ports. Bellows break the vibrations of the vacuum vessel.

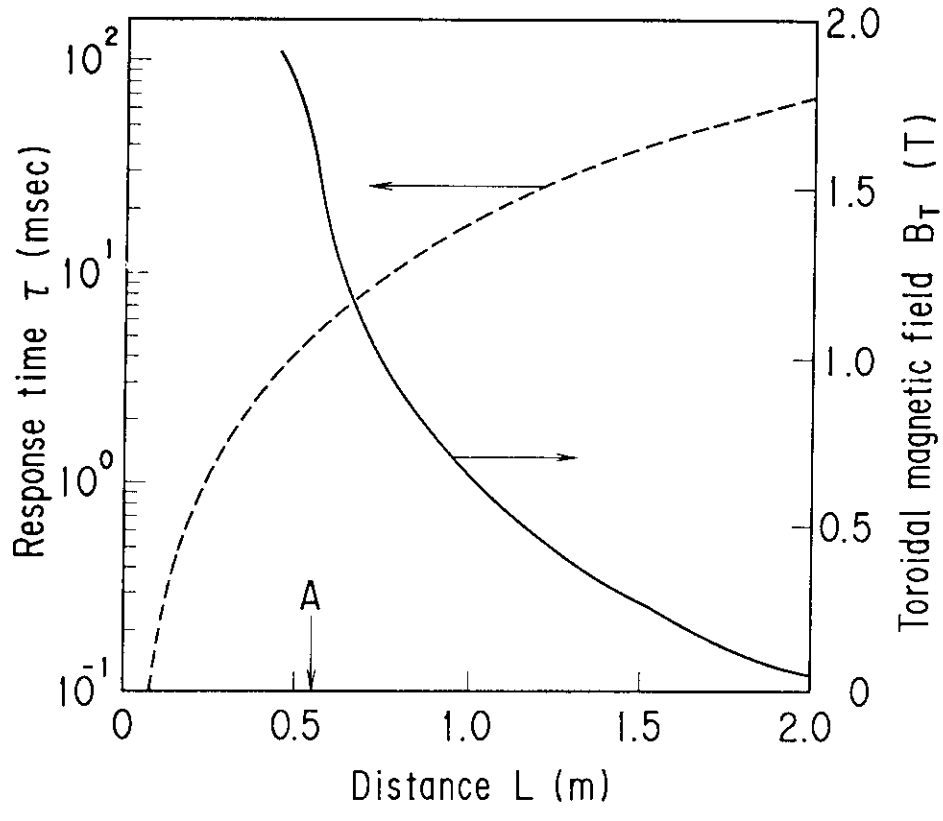

Fig. 4.7 Response time for H_2 and toroidal magnetic field as a function of distance from the first wall of JT-60. Point "A" indicates the distance to the flange of IN2LS.

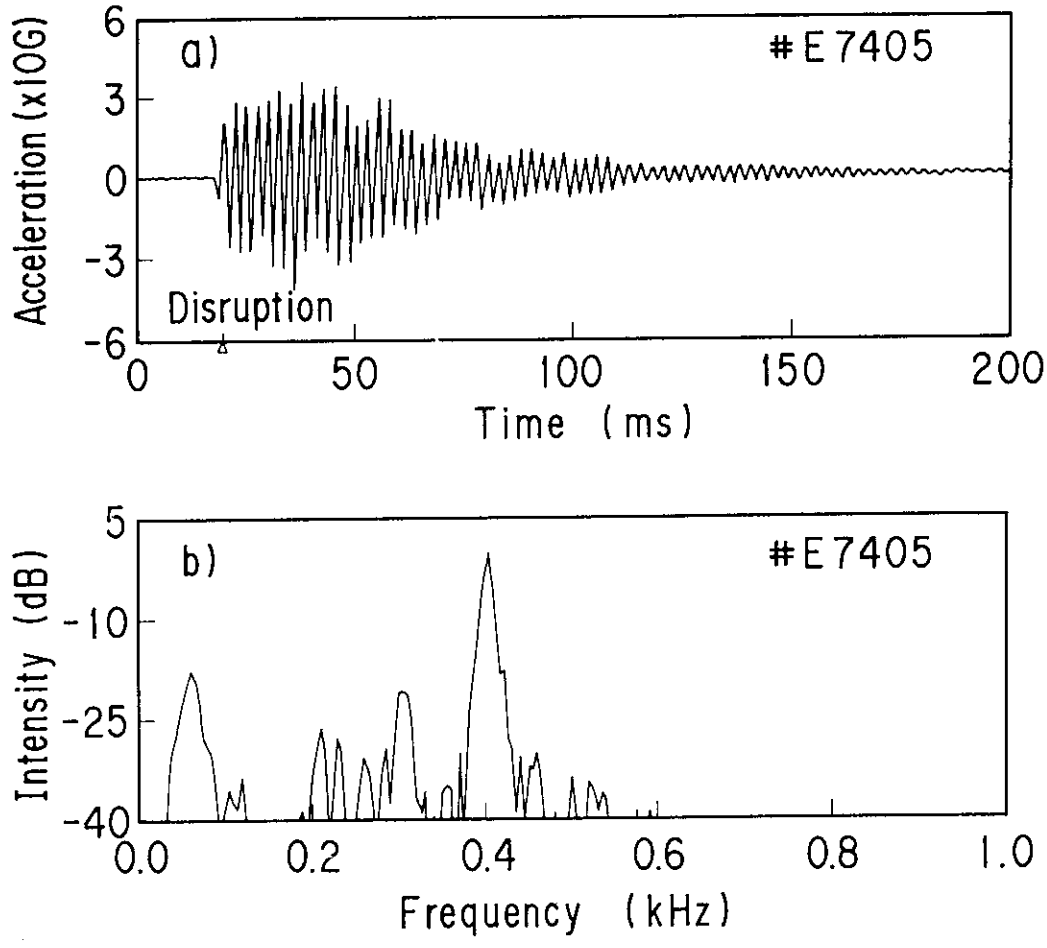

Fig. 4.8 Typical acceleration and frequency components in the vibration of IN2LS port just after the plasma disruption.

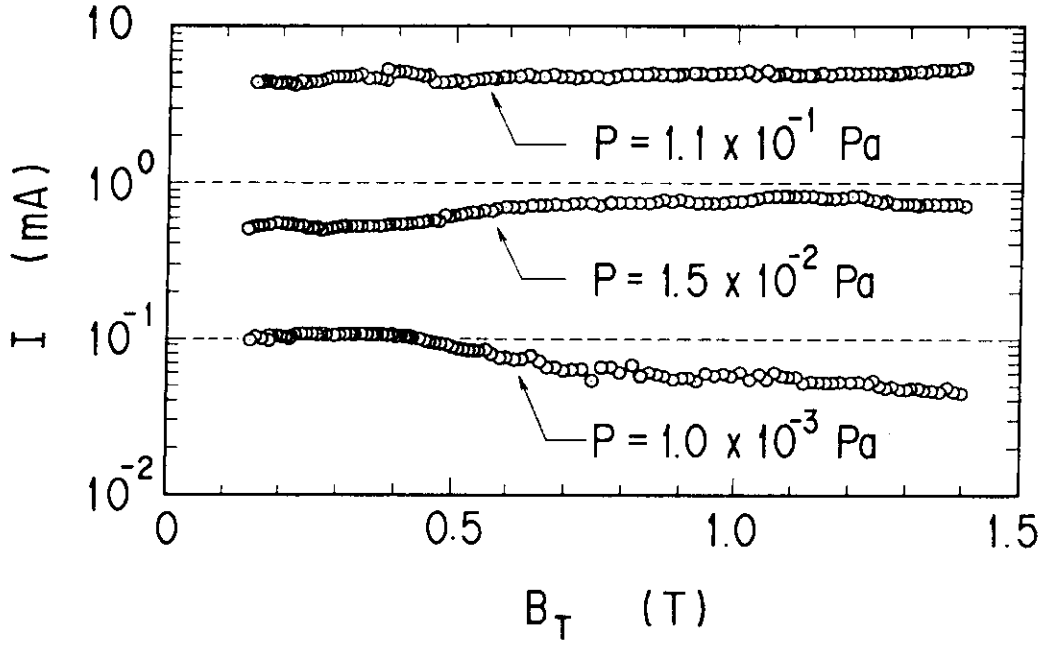

Fig. 4.9 Typical variation of the Penning discharge current I with the toroidal magnetic field strength B_T in constant pressures. The discharge current reaches a saturation level with the increasing magnetic field strength.

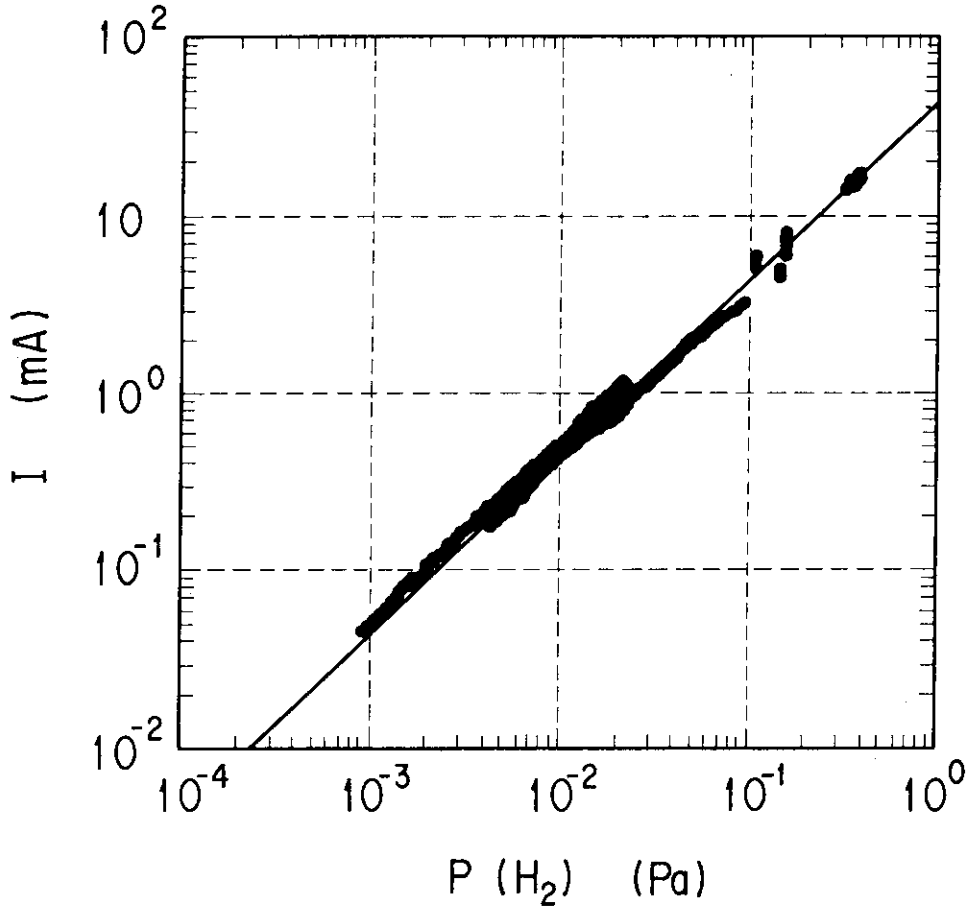

Fig. 4.10 Variation of the Penning discharge current I as a function of the pressure of hydrogen P(H_2) above 0.7 T. The ion current is approximately proportional to the pressure.

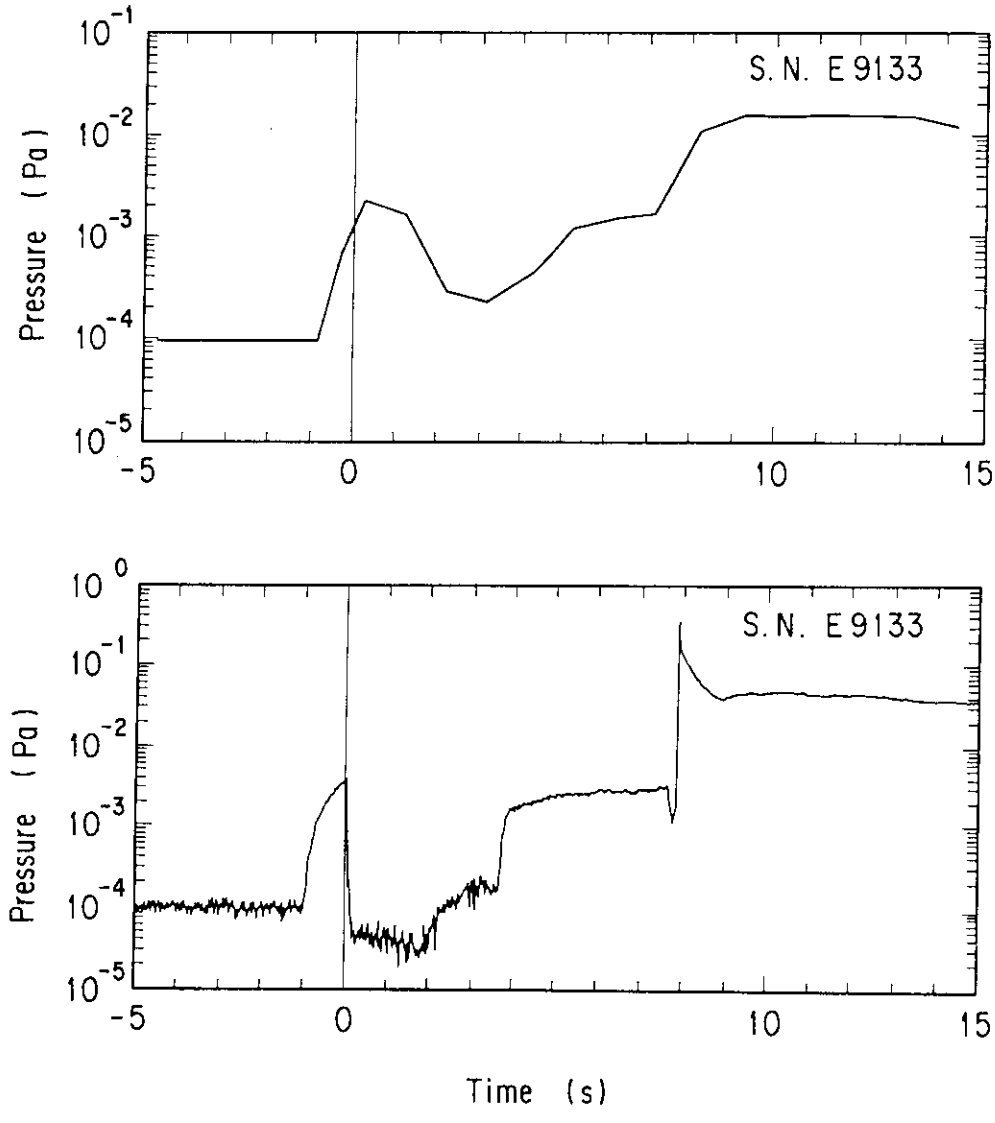

Fig. 4.11 Typical change in the pressure for ~20 s including the plasma discharge. The top is that measured with a BA gauge which is placed ~5 m from the plasma. The bottom is that measured with the Penning configuration gauge at the IN2LS port.

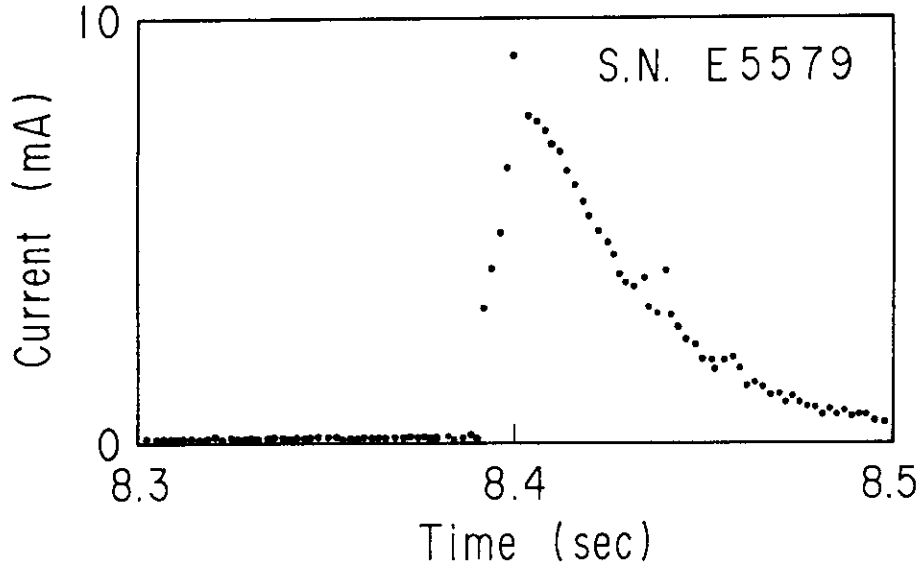

Fig. 4.12 Typical time response of the gauge at the IN2LS port just after 1 ms contact of a plasma with the inner wall near the gauge.

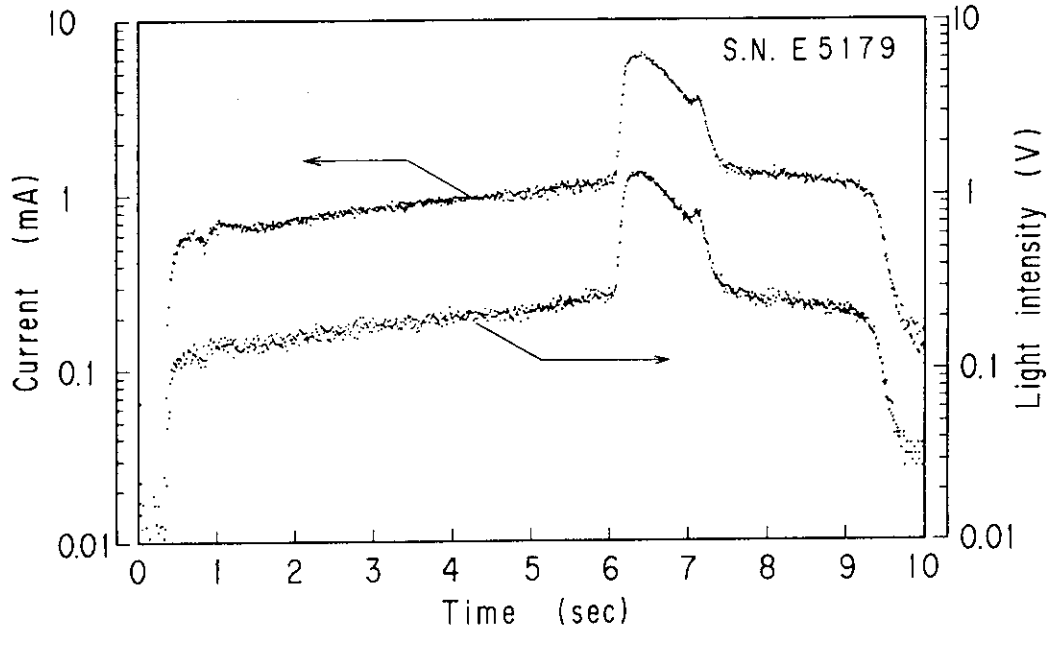

Fig. 4.13 Typical output of the gauge at the S4L port for a plasma with outer divertor configuration. Plasma current is 1.0 MA and neutral beam of 19 MW is injected from 6.0 to 7.0 s.

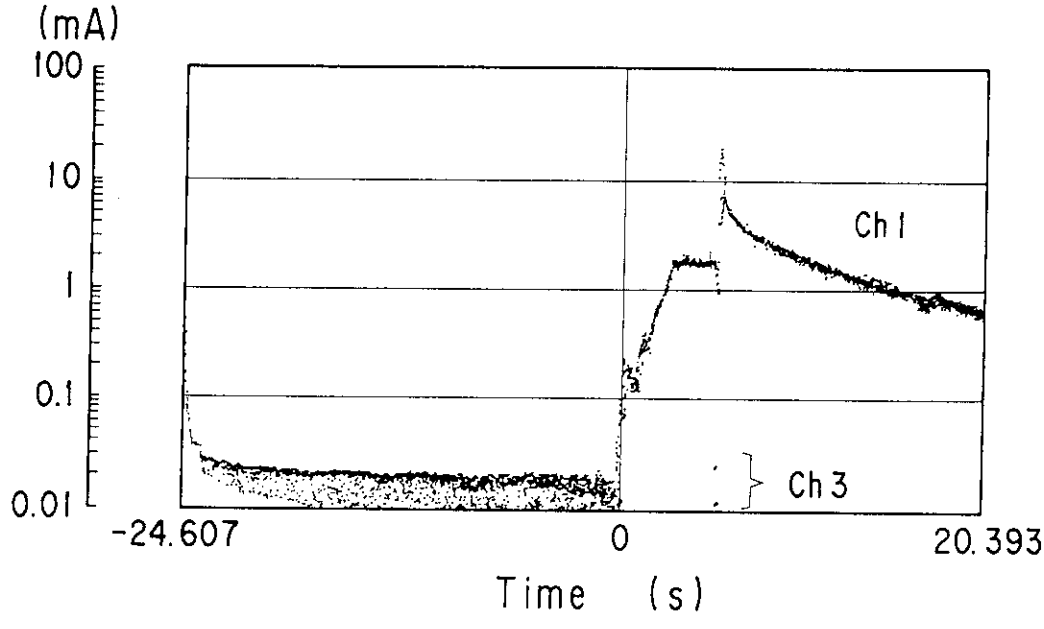

Fig. 4.14 Change in the discharge current for the two gauges during a plasma discharge. The gauge at S4U (ch 1) is operated at the anode voltage of 5 kV. The other at IN2LS (ch 3) is not ignited at 5 kV. The plasma is disrupted at t = ~5.5 s. Maximum of the spurious current is found to be 0.03 mA at the plasma disruption.

5. Outgassing mechanism after current decaying phase in disruptive and normal discharges in a tokamak

5.1 Introduction

Tokamak device components are known to retain particles. Recycling properties are largely affected by the gas release from the wall. Too high a plasma density can give rise to density-limit plasma disruption.[1,2] The inventory of tritium will be one of the most important problems in future deuterium-tritium (DT) burning experiments in fusion devices.[3]

Many attempts are being made to reduce the hydrogen or its isotope retention level in the first wall. Recently, He glow and He discharge cleaning were successfully used to reduce recycling and edge neutral pressure.[4,5] It would be desirable to develop a simple method for exhausting the gases from the wall.

In order to develop a new method for inventory control, we have studied the outgassing from the graphite first wall during and just after the discharge in the JT-60 fusion device. It is widely known that large amounts of gases are released when the plasma is disrupted.[6] Recently "disruptive discharge cleaning" was employed in TFTR especially to achieve super shots.[7] However, the details of the outgassing mechanism have been little studied. Therefore we paid attention to the mechanism after the plasma disruption. The mechanism of the outgassing after the disruption differs considerably from that after the gradual ending of the plasma. In this paper, we demonstrate the differences between the outgassing mechanisms.

In section 5.2, the experimental apparatus is described. A newly developed pressure gauge is mentioned. Results and discussion are given in section 5.3. A new method for reducing the hydrogen content is proposed. Finally we summarize the experiments.

5.2 Experimental apparatus

5.2.1 The first wall and the vacuum system of JT-60

The JT-60 plasma device is a large tokamak which can be operated with the plasma boundary defined by either material limiters or a magnetic separatrix (Fig. 5.1(a)). The plasma major and minor radii are 3.0 m and 0.9 m, respectively. The top view of the experimental apparatus related to this experiment is shown in Fig. 5.1(b). Details of the machine parameters are described elsewhere.[8] The Inconel wall of the vacuum vessel is covered with the first wall, which is composed of toroidal limiters, liner plates, and divertor plates. The limiters and the divertor plates are made of graphite (ETP-10 fabricated by Ibiden and HCB-18S by Hitachi-Chemical).[9] The liner plates are made of TiC-coated Inconel because they hardly come into contact with the plasma. The distance between the graphite limiters and the plasma center is 930 mm at the inner side and 940 mm at the outer side, respectively. The 3500 kg of graphite is composed of 13000 pieces. The total surface area of the graphite is about 200 m^2. The area facing the plasma is about 70 m^2. The vacuum vessel is held at a temperature of 200-350^{o}C to protect the first wall from absorbing water vapor.[9] The area above 200^{o}C is ~2000 m^2. The pumping manifold (which is made of type 304 stainless steel) is held at room temperature (RT). Its area is ~150 m^2.

The vacuum vessel with a volume of 160 m^3 is evacuated by four identical pumping units as shown in Fig. 5.1(a).[10] Each set has a manifold and four turbomolecular pumps with a liquid-nitrogen trap. Total pumping speed for H_2 is 29.0 m^3/s at the pumping port of the vacuum vessel and 43.5 m^3/s at the manifold

where the turbomolecular pumps are connected. This pumping speed is maintained from 10^{-1} to 10^{-5} Pa. The ultimate pressure at the vacuum vessel is below $1x10^{-6}$ Pa. The base pressure in this experiment was $\sim 5x10^{-5}$ Pa because of the outgassing from the hot wall.

5.2.2 A fast-response gauge and the pressure measurement

The outgassing from the first wall has been investigated with a newly developed gauge. This gauge can measure the pressure P_v in the vacuum vessel in a short response time (<10 ms). We have also accurately measured the pressure P_m in the manifold for evaluating the gas quantity exhausted by the vacuum pumping system. Two types of gauges have been employed. One is a newly developed gauge (G_1) (Fig. 5.1) with a short response time, and the other is a calibrated Bayard-Alpert gauge (G_2) with a magnetic shield. Gauge G_1 is directly connected with the vacuum vessel far from the pumping port. Gauge G_2 is located in the pumping manifold. The accuracy of the measurement with gauge G_2 is within ±5%.

The newly developed gauge G_1 is a type of Penning configuration gauge. The schematic of the gauge is shown in Fig. 5.2. The dimensions of the Penning cell are as follows: (a) the anode (made of SUS 304) is a tube 20 mm in diameter and 10 mm in length; (b) cathode plates are made of a square Mo sheet of 250 mm^2 area, and the distance between the cathodes is 25 mm. A Penning discharge in the cell is sustained by the magnetic field (toroidal magnetic field) which confines the tokamak plasma. A Venetian blind is placed in front of the cell to prevent the fast particles from impinging into the cell. The Penning cell is

located in a diagnostic box between the toroidal magnetic field coils, as schematically shown in Fig. 5.1(a). Since the cell is ~1 m from the first wall, we measure the pressure of the thermalized gases in the diagnostic box. As shown in Fig. 5.1(b), gauge G_1 is far from the puffing valves and the pumping ports. In addition, there is a rather large clearance between the plasma and the outer first wall especially during the plasma-current decaying phase, because the plasma is connected to the inner board of the first wall (limiter configuration) or to the divertor plates (divertor configuration). The conductance between the neighboring diagnostic boxes is evaluated to be greater than ~30 m^3/s. Thus we assume toroidal uniformity of the pressure around the plasma and that the pressure is measured with gauge G_1. The gauge was calibrated at a test stand over a wide range of pressures from 0.5 to 10^{-4} Pa. The influence of the magnetic field strength was also investigated as reported previously.[11] The gauge is calibrated again with JT-60 for H_2. The relationship between the pressure $P(H_2)$ and the discharge current I is approximately expressed by the following equation:

$$P(H_2) = C\ I, \qquad (17)$$

where the constant C is 21.5 (Pa/A). The deviation of the data is within ± 20% of equation (17). This gauge is controlled by a personal computer, which acquires the pressure and magnetic field data. The gauge is switched on above 0.7 T. Thus the pressure P_v in the vacuum vessel is measured for ~50 s including the duration of the discharge. The response time of the pressure measurement is simulated to be 8 ms.

The evacuated quantity Q_{out} is estimated from the pressure P_m and the effective pumping speed S_{eff} by the following equation:

$$Q_{out} = \int_0^T S_{eff}(P_m)\ P_m(t)dt. \qquad (18)$$

Here, we set the origin of the time at the start of the build up of the plasma current. After a large quantity of gases is evacuated routinely, the effective pumping speed may be reduced perhaps owing to the outgassing from the pumps themselves. When all the high-vacuum valves (HVV) shown in Fig. 5.1 were closed, the inlet pressure of the TMP became less than 1×10^{-6} Pa within 1 min. Thus the outgassing from the pumps is found to be negligible for calculating Q_{out}. However, as we ignore the outgassing from the vacuum vessel at the base pressure P_b ($\sim5\times10^{-5}$ Pa), we assume to express the effective pumping speed S_{eff} by the following equation,

$$S_{eff} = S_{nom}(1 - P_b/P). \qquad (19)$$

Here, the notations S_{nom} and P refer to the nominal pumping speed and measured pressure, respectively. The accuracy of Q_{out} is estimated to be within ±20 %. This is mainly due to the inaccuracy of the effective pumping speed.

In this paper, both the pressures P_v and P_m are described as those at room temperature. The gas input and the evacuated quantity are also expressed by the unit of Pam^3 at room temperature.

5.2.3 Outgassing rate

The variation of the total fuel atom number N in the vacuum vessel (excluding ones in the wall) is expressed by

$$\frac{dN}{dt} = \frac{dN_p}{dt} + 2\frac{d\{P(V_T - V_p)\}}{dt}$$

$$= 2\,Q_{in} + 2\,q - (1 - \beta)N_p/\tau_p - 2\,PS, \quad (20)$$

where N_p = total number of protons in the plasma volume,

P = gas pressure around the plasma case,

V_T = volume of the vacuum vessel,

V_p = plasma volume (50-60 m^3),

Q_{in} = total gas input (molecules),

q = outgassing rate, i.e., number of thermalized molecules coming into the vacuum per unit time from the wall,

β = recycling coefficient, i.e., the ratio of the (energetic) atoms directly entering from the wall into the plasma to the number of neutral particles incident upon the wall,

τ_p = gross particle confinement time in the plasma,

S = pumping speed.

Here, we introduce an effective outgassing rate q_{eff} because in this experiment we cannot discriminate the particles which are released from the wall with enough energy to go directly into the plasma from those with thermal energy. The definition of the effective outgassing rate q_{eff} is given by

$$q_{eff} = q - (1 - \beta)\ N_p/(2\tau_p). \quad (21)$$

Of course, the rate q_{eff} becomes the outgassing rate q without the plasma. The value of q is, in general, greater than that of

q_{eff} because β is less than 1. From equations (20) and (21), we explicitly describe the effective outgassing rate q_{eff};

$$q_{eff} = \frac{1}{2}\frac{dN_p}{dt} + \frac{d\{P(V_T - V_p)\}}{dt} - Q + PS. \quad (22)$$

The value of N_p is calculated by the relation $N_p = \bar{n}_e V_p / Z_{eff}$, where, $\bar{n}_e$ and Z_{eff} refer to the average electron density and the effective nuclear charge, respectively. The other parameters are directly measured. We cannot measure the plasma volume only during ~10 ms just before the end of the plasma. Therefore we assume that the plasma volume becomes zero at 10 ms just before the end of the plasma with the normal discharge and at the time of the start of the current quench with the disruptive discharge. For this short period of time, we underestimate the effective outgassing rate. The error is within 30%.

Hereafter, we use the term "outgassing rate" as the effective outgassing defined by equation (21). Moreover, the outgassing rate is expressed by the units of Pam^3/s at room temperature instead of molecules/s.

5.3 Results and discussion

We show the results for the hydrogen plasma. Virtually the same results were obtained for both plasma configurations (limiter configuration and divertor configuration).

5.3.1 Changes in the evacuated gas quantity with discharges

Retention of the fuel gases has been studied extensively. Here all 29 discharges (shots) in a day are examined as an

example. All the shots are carried out with the limiter configuration. The plasma current I_p ranges from 1 to 2.5 MA. Typical time behaviors of the pressure P_m at I_p=2.5 MA are shown in Fig. 5.3. The dotted and solid lines in the figure show the pressures in the disruptive and normal discharges, respectively. For a period of 0-30 s the pressure is higher in the disruptive discharge than in the normal discharge. The two pressures decrease in a similar manner at t>30 s. Thus the difference of the evacuated quantity (output) between the disruptive and normal discharges is mainly that of the first 30-s output, which is defined as equation (18) with T=30 s.

The total gas input Q_{in} is a sum of gas input by gas puffing, neutral beam injection and pellet injection. The output Q_{out} is evaluated using equation (18) with T=7 min. The changes in Q_{in} and Q_{out} with the shots are shown in Fig. 5.4(a). The first 30-s output is shown by the filled output bar. Q_{out} is nearly equal to or greater than Q_{in} in all the disruptive discharges, which are expressed by the notation D. Q_{out} in the disruptive shots is likely to increase with I_p. On the other hand, Q_{out} in the normal discharges, except the third shot (#E9197), is smaller than Q_{in}. This is because the first 30-s output is rather small in the normal discharges. The ratio of the first 30-s output to Q_{out} is $\gtrsim$0.5 in all the disruptive shots and $\lesssim$0.4 in all the normal shots including the conditioning ones. The conditioning discharge, which is shown by the notation C in Fig. 5.4(a), is employed for the wall conditioning. It is a type of ohmic heating plasma with a current of 1 MA and gas puffings of 0.4-1 Pam^3. The conditioning discharges have outputs of 3-5 Pam^3.

The summation of the difference between Q_{in} and Q_{out} gives the relative change in the hydrogen content in the wall with the discharges (Fig. 5.4(b)). The hydrogen content decreases or does not change with disruptive shots. On the other hand, the content increases with normal discharges. Hydrogen of ~30 Pam^3 is stored in the wall after the 29 shots. The conditioning discharges also reduce the amount of retained hydrogen because of the small input (0.4-1 Pam^3).

If the input is as small as that of shot #E9203 in Fig. 5.4(b), the disruptive discharge is most likely to reduce the hydrogen content.

5.3.2 Differences between the outgassing mechanisms after the disruptive and normal discharges

The pressure P_m in the manifold always changes in a similar way at t>30 s, as shown in Fig. 5.3. Therefore, the outgassing mechanism at t>30 s is strongly suggested to be the same for all the discharges. On the other hand, the mechanism just after the disruptive discharges is quite different from that after the normal discharges.

The change in P_v has been examined just after the discharges. Figure 5.5 shows the typical evolution of the discharge and the change in P_v for the disruptive shot (#E9220). Figure 5.6 shows them for the normal discharge (#E9219). The sampling time of gauge G_1 is set at 10 ms. The disruptive discharge has a current decay of 2.5 MA/15 ms at t=6.9 s. The normal discharge has a decay of 1.3 MA/1.2 s. Other conditions are as follows: the maximum of the plasma current is 2.5 MA for the two discharges. The neutral beam auxiliary heating of 16 MW

supplies a gas input of 12.9 Pam^3 for the normal shot (#E9219) and 8.3 Pam^3 for the disruptive shot (#E9220). The gas input by pellet injection is 5.5 Pam^3 for shot #E9219 and 5.8 Pam^3 for shot #E9220.

The time behaviors of P_v are shown in Figs. 5.5(b) and 5.6(b) for a period of 0-25 s. The pressure in the disruptive shot rises abruptly at the same time as the disruption (t=6.9 s). It then decays from 7 to 8 s with a time constant τ=0.6 s. At t>10 s the pressure decays with τ=7.0 s, which is nearly equal to the value of 6.95 s obtained from the simulation of the vacuum pumping characteristics. On the other hand, the pressure in the normal shot rises after the end of the plasma and its peak appears at t=13 s. It then decays with τ=11 s.

These observations are explained well in terms of the outgassing rate, as shown in Figs. 5.5(c) and 5.6(c). As a negative rate of outgassing indicates that the gases in the vicinity of the wall are pumped out by the wall and/or the plasma, the outgassing behavior is as follows for the disruptive discharge (Fig. 5.5(c)):

(a) The abrupt gas release occurs at the disruption owing to the abrupt heat flux (see section 5.3.3). In the disruptive shot (#E9220), 40 Pam^3 of gases are released within ~50 ms.

(b) About three quarters of all the released gases return to the wall for ~1 s after the disruption because of the adsorption on the wall. A possible mechanism is that the outgassed wall pumps the gases with decreasing temperature. The rest (~10 Pam^3) of the released gases are evacuated for 0-30 s by the pumping system.

(c) Then, no more large amounts of gases are released. However, outgassing continues with rates less than ~1 Pam^3/s. The rates

gradually decrease to become less than 0.1 Pam^3/s at t>30 s. This is probably due to gas release from two parts. The first is that from the graphite surface which did not suffer the abrupt heat load during the disruption. The second is that from the RT area (~150 m^2). The latter is likely to be prevalent at t>2 min because of a large time constant (τ=450 s).

In the case of the normal discharge (#E9219), negative outgassing is observed from 7 to 10 s in Fig. 5.6(c). This indicates that the wall pumps out the particles which come from the plasma because the electron density decreases during the current decaying phase (Fig. 5.6(a)). The energetic particles from the plasma to the wall are believed to penetrate into the bulk. The gases are released after the end of the plasma. Therefore it takes ~1 s or more until the particles are desorbed from the surface after impinging into the wall. The following summarizes these results:

(a′) The particles from the plasma impinge into the wall while the plasma current decays. In this phase, the wall works as a pump.

(b′) The gases are then slowly and continuously released as shown in Fig. 5.6(c). The gases from the bulk of the graphite are probably dominant at $t \lesssim 30$ s, and the ones from the RT area are prevalent at t>2 min.

5.3.3 Details of the outgassing mechanism just after the disruption

The heat flux leading to the abrupt gas release during the disruption is examined. Figure 5.7(a) shows the typical time behaviors of the near-central chord integrated soft X-ray

emissivity SXR and the plasma current I_p during the disruption. The soft X-ray emissivity decreases rapidly from 7.820 to 7.833 s. This crash indicates the heat flux due to the loss of the plasma thermal energy (thermal quench).[12,13] After the soft X-ray crash, the plasma current decays from 7.836 to 7.850 s. The heat flux to the wall in this current decay phase is well recognized to be due to the release of the plasma magnetic energy.[14,15] Large amounts of gases will be released in two stages during the disruption if the two kinds of heat fluxes to the wall are high enough. This is because hydrogen atoms are desorbed very rapidly from the graphite wall when the temperature increases above ~1000^{o}C.[16-19] Figures 5.7(b) and 5.7(c) show the time behaviors of the pressure P_v and the outgassing rate in the vacuum vessel, respectively. Here, the pressure P_v has been measured in the short response time (<10 ms). Two peaks clearly appear in the outgassing rate. The gas release occurs two times within 30 ms during the disruption. The first gas release corresponds to the soft X-ray crash, and the second occurs during the plasma current decay phase. Thus we clearly observe the abrupt gas release due to both the thermal quench and the release of the plasma magnetic energy.

The heat flux leading to the abrupt gas release is unlikely to be ascribed to radiation loss and runaway electrons for the following reasons:

(a) Even if the whole plasma energy of ~7 MJ is dumped as radiation loss onto the entire wall area for 10 ms, the temperature rise is only 40 degrees.

(b) The runaway electrons have large enough energy to desorb the gases by direct collision with the particles. However, most of

their energy is given to the wall as thermal energy. Therefore, the runaway electrons could hardly desorb such large amounts of gases as 10^{21} molecules (see Table 5.1), because the total energy of the runaway electrons is evaluated to be ~200 kJ from the expression[13] by Jarvis et al.

5.3.4 Gas release after the normal discharge

The graphite first wall pumps out the fuel gases during the plasma current decay phase, as shown in Fig. 5.6(c). We discuss the small but continuous gas release after the normal discharge. If the temperature of the graphite was above ~1500°C during the constant current phase and then decreased rapidly during and after the current decay phase, the change in the permissible retention[20] of hydrogen might give an explanation of the gas-release behavior. However, the maximum temperature was less than 450°C in the normal discharges. Thus a probable mechanism is bulk diffusion, since above 300°C, the hydrogen atoms migrate on the graphite surface too rapidly to explain the outgassing behavior.[21]

Making use of a disruption with a residual plasma current, we estimate the activation energy of bulk diffusion. The plasma disruption is controlled so as to terminate with a residual plasma current having a duration of several hundred milliseconds (Fig. 5.8(a)). The pressure P_v rises abruptly and then decays with the plasma current I_p, as shown in Fig. 5.8(a). In the current decay phase, the graphite wall exhausts the particles from the plasma, as described in Sec.III.B. Most of the particles from the plasma are believed to impinge into the wall with the average implant depths of 20-50 Å.[22] The maximum density of

hydrogen atoms in the graphite is probably located at the implant depth at the time of the most rapid decrease of the pressure. Figure 5.8(b) shows that it takes 0.8 s from the start of the diffusion to the maximum outgassing rate. Thus we can estimate the diffusion coefficient. Since the diffusion coefficient D is taken to be $D_0 \exp(-E_D/kT)$,[22] the activation energy is evaluated to be less than 1.5 eV. Here, the maximum value of the preexponential factor D_0 is adopted to be 5×10^{-2} cm^2/s from the reported values[23,24] for isotropic pyrolytic carbon. The wall temperature was ~350°C from the thermocouple measurements.

5.3.5 Controlled disruption

We discuss a new method for using the disruption to reduce the hydrogen retention level in the first wall. If we terminate the plasma current in a disruption, the hydrogen content is smaller than that after the quiet ending of the plasma. Conditioning discharges with disruptions will be more useful because of the small gas input.

There are two concerns about the use of the disruptive discharge. The first is the damage to the vacuum vessel and other components. This is induced by the electromagnetic forces due to the rapid current decay.[25] The design criteria of JT-60 allow the elements, except those made of graphite, more than 10000 disruptions. The first wall made of graphite has been strong enough for more than 500-1000 disruptions of the plasma with currents of 1-2.5 MA, although it is difficult to estimate the strength of the graphite components against the electromagnetic forces. We have also observed the abrupt gas release during the disruption of the plasma with a current of 0.5 MA. Since the

electromagnetic force decreases with the plasma current when the current decays during a constant time, we can select a lower current disruption which produces large amounts of released gases.

The second is concerned with the outgassed area. To reduce the hydrogen content, it is necessary to outgas a large area. Let us survey the area of the graphite wall which releases the gases during the disruption. The rapid decrease of pressure is observed just after the disruption, as shown in Fig. 5.7(b). The wall outgassed by the disruption absorbs gases on its surface. The outgassed area is estimated from the rate of the pressure decay, assuming that the sticking probability of the hydrogen molecules is unity. The evaluated value, which is a lower limit of the area outgassed by the disruption, is shown in Table 5.1 for the disruptions of 1 MA plasmas. An area of ~10 m^2 is found to be outgassed. The areal density of the atoms ejected in the disruptions is also evaluated to be $1\text{-}3\times10^{21}$ atoms/m^2, which is comparable to the near-surface areal density of the hydrogen isotope from the TFTR and PDX limiter.[26] Although the surface area outgassed by a disruption is smaller than the whole area, we can outgas most of the first wall by controlling the position of the plasma. If we force the plasma to move toward a certain direction of the wall, then the plasma will disrupt, and the gases will be released from the area approached by the plasma.

The choice of the gas species is important for making the controlled disruption more effective for inventory control. This is because the cleaning efficiency of various kinds of techniques is affected by the gas species.[5,27] Helium is perhaps preferable to hydrogen from the viewpoints of solubility, sticking

probability and chemical reactivity.

Thus the controlled disruption, which is defined as the one that is permissible for the damage against the electromagnetic forces and whose position is controllable, will be useful to suppress and reduce the inventory of the fuel gases.

5.4 Conclusions

We have developed a new gauge with a fast response time (< 10 ms) to study the outgassing mechanisms. The following were found.

(1) The evacuated gas quantity after a typical disruption is almost equal to or greater than the input. On the other hand, the evacuated quantity after a gradual ending of the plasma is less than the input.

(2) Large amounts of gases are abruptly released in two stages during the disruption of the plasma. The first gas release occurs at the time of the soft X-ray crash. This is ascribed to the abrupt heat flux due to the loss of the plasma thermal energy (thermal quench). The second appears during the decay of the plasma current. The heat flux due to the loss of the plasma magnetic energy causes the second gas release.

(3) The disruptions of 1 MA plasmas outgas a surface area of ~10 m^2. Gases of 30-80 Pam^3 are released within 30 ms. Three quarters of them then return to the wall. This return of the gases to the wall will have to be examined in order to efficiently use the disruption for the reduction of hydrogen content.

(4) The gases are released after the end of the plasma current in the normal discharges. The hydrogen atoms probably diffuse in the bulk to the surface. The activation energy is estimated to be

less than 1.5 eV.

Finally, we discussed the use of the controlled disruption for reducing the content of fuel particles in the first wall. We hope that the controlled disruption will be one of the useful techniques for inventory control.

References

[1] M. Murakami, J.D.Callen, and L.A.Berry, Nucl. Fusion 16, 347 (1976).

[2] S.J.Fielding, J.Hugill, G.M.McCracken, J.W.M.Paul, R.Prentice, and P.E.Stott, Nucl. Fusion 17, 1382 (1977).

[3] K.L.Wilson and W.L.Hsu, J. Nucl. Mater. **145/147**, 121 (1987).

[4] H.F.Dylla, P.H.LaMarche, M.Ulrickson, R.J.Goldston, D.B.Heifetz, K.W.Hill, and A.T.Ramsey, Nucl. Fusion 27, 1221 (1987).

[5] G.L.Jackson, T.S.Taylor, S.L.Allen, J.Ferron, G.Haas, D.Hill, M.A.Mahdavi, H.Nakamura, T.H.Osborne, P.I.Petersen, R.Seraydarian, M.Shimada, E.J.Strait, and P.L.Taylor, J. Nucl. Mater. **162/164**, 489 (1989).

[6] J.Ehrenberg, J. Nucl. Mater. **162/164**, 63 (1989).

[7] H.F.Dylla and the TFTR Team, J. Nucl. Mater. **145/147**, 48 (1987).

[8] JT-60 Team (presented by M.Yoshikawa), in Proc. 11th Int. Conf. on Plasma Physics and Controlled Nuclear Fusion Research, Kyoto, 1986, vol.1 (IAEA, Vienna, 1987) p.11.

[9] T.Arai, H.Takatsu, H.Ninomiya, R.Yoshino, N.Hosogane, M.Yamamoto, K.Kodama, A.Kaminaga, M.Shimizu, and the JT-60 Team, J. Nucl. Mater. **162/164**, 743 (1989).

[10] N.Ogiwara, T.Arai, M.Shimizu, T.Takizawa, and F.Kimijima, in Proc. 13th Symp. on Fusion Technology, Varese, September 1984, p.381.

[11] N.Ogiwara and M.Maeno, J. Vac. Sci. Technol. A7, 2804 (1989).

[12] S.M.Kaye, G.L.Jahns, A.W.Morris, S.Sesnic, K.Bol, M.S.Chance, P.Couture, R.J.Fonck, G.Gammel, W.W.Heidbrink, R.Kaita, H.W.Kugel, B.LeBlanc, J.Manickam, N.Ohyabu, M.Okabayashi, M.F.Reusch, and H.Takahashi, Nucl. Fusion 28, 1963 (1988).

[13]O.N.Jarvis, G.Sadler, and J.L.Thompson, Nucl. Fusion **28**, 1981 (1988).

[14]M.Ulrickson, M.Bell, F.C.Jobes, and D.Long, Bull. Am. Phys. Soc. **31**, 1448 (1986).

[15]M.Ulrickson, F.C.Jobes, D.K.Owens, and D.Long, Bull. Am. Phys. Soc. **32**, 1806 (1987).

[16]B.L.Doyle, W.R.Wampler, and D.K.Brice, J. Nucl. Mater. **103/104**, 513 (1981).

[17]K.Ashida, K.Ichimura, M.Matsuyama, and K.Watanabe, J. Nucl. Mater. **128/129**, 792 (1984).

[18]K.Nakayama, S.Fukuda, T.Hino, and T.Yamashina, J. Nucl. Mater. **145/147**, 301 (1987).

[19]V.Philipps, E.Vietzke, M.Erdweg, and K.Flaskamp, J. Nucl. Mater. **145/147**, 292 (1987).

[20]R.A.Causey, M.I.Baskes, and K.L.Wilson, J. Vac. Sci. Technol. A4, 1189 (1986).

[21]D.R.Olander and M.Balooch, J. Catal. **60**, 41 (1979).

[22]D.B.Heifetz, M.I.Baskes, H.F.Dylla, and M.Ulrickson, J. Nucl. Mater. **145/147**, 326 (1987).

[23]M.Saeki, J. Nucl. Mater. **131**, 32 (1985).

[24]H.D.Röhrig, P.G.Fischer, and R.Hecker, J. Am. Ceram. Soc. **59**, 316 (1976).

[25]B.J.Merrill and S.C.Jardin, J. Nucl. Mater. **145/147**, 881 (1987).

[26]A.E.Pontau, W.R.Wampler, B.E.Mills, B.L.Doyle, A.F.Wright, M.A.Ulrickson, P.H.LaMarche, H.F.Dylla, and S.Fukuda, J. Vac. Sci. Technol. A4, 1193 (1986).

[27]H.F.Dylla, J. Vac. Sci. Technol. A6, 1276 (1988).

Table 5.1 Area outgassed by the disruption of a 1 MA plasma.

All the discharges in this table are operated with the divertor configuration.

Shot no.	Decay time of plasma current	Pumping speed S just after disruption	Outgassed area estimated from S	Hydrogen atoms ejected during disruption
	ms	x 10^3 m^3/s	m^2	x 10^{21} atoms/m^2
E9118	14	7.4	11	3.4
E9121	15	8.4	13	2.2
E9125	17	6.1	9.3	2.1
E9132	12	8.9	13	3.1
E9133	15	9.0	14	2.5
E9146	12	4.4	6.7	2.8
E9148	13	8.7	13	2.0
E9152	22	6.3	9.5	1.0

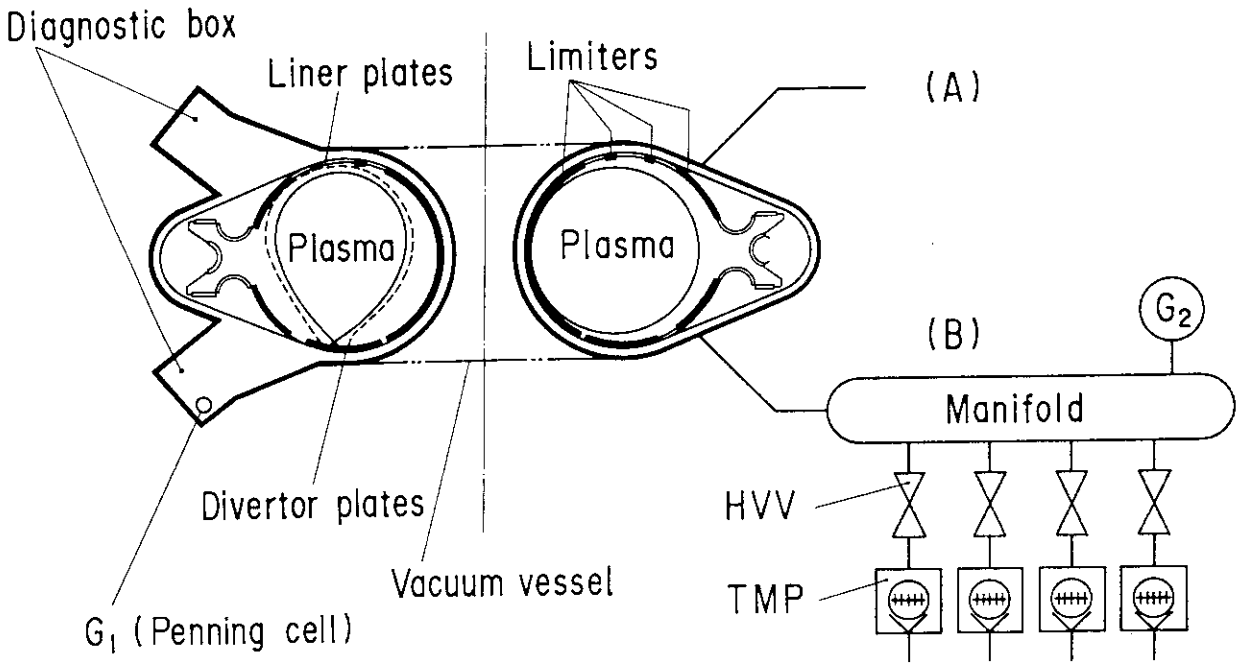

(a)

Fig. 5.1 (a) Schematic diagram of the first wall and the vacuum system of JT-60. The first wall is made up of the toroidal limiters, divertor plates, and the liner plates. The limiters and the divertor plates are made of graphite, and the liner plates are TiC-coated Inconel. The total pressure P_v in the vacuum vessel is measured with a type of Penning configuration gauge G_1, and the pressure P_m in the manifold is measured with a magnetically shielded Bayard-Alpert gauge G_2. The vacuum vessel is pumped out by four identical systems. Each has a manifold and four turbomolecular pumps (TMP) with a liquid-nitrogen trap (omitted in this figure). TMPs are connected by high vacuum valves (HVV). Two types of plasma configuration are also shown in this figure: (right) limiter configuration; (left) divertor configuration.
(b) Top view of the experimental apparatus. Gas input is summation of input by gas puffing (Gas), neutral beam injection (NB) and pellet injection (Pellet). Gauges G_1 and G_2 are explained in (a).

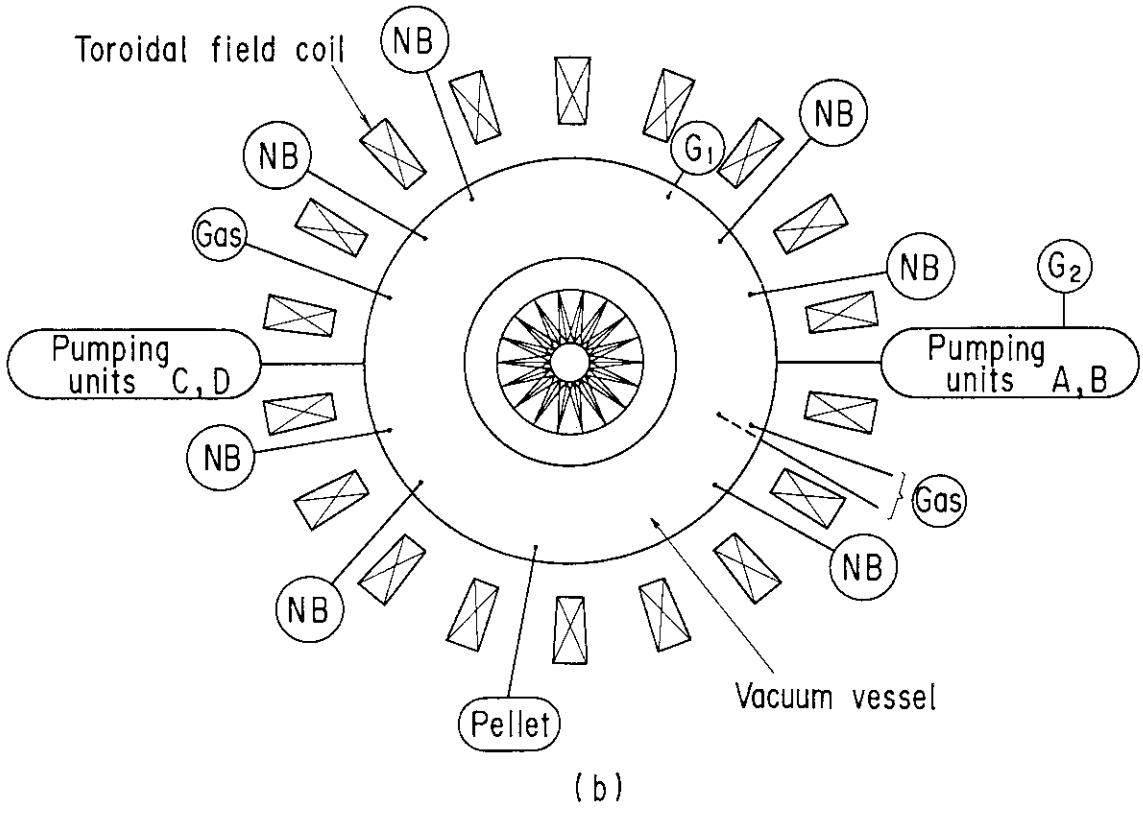

Fig. 5.1 (Continued)

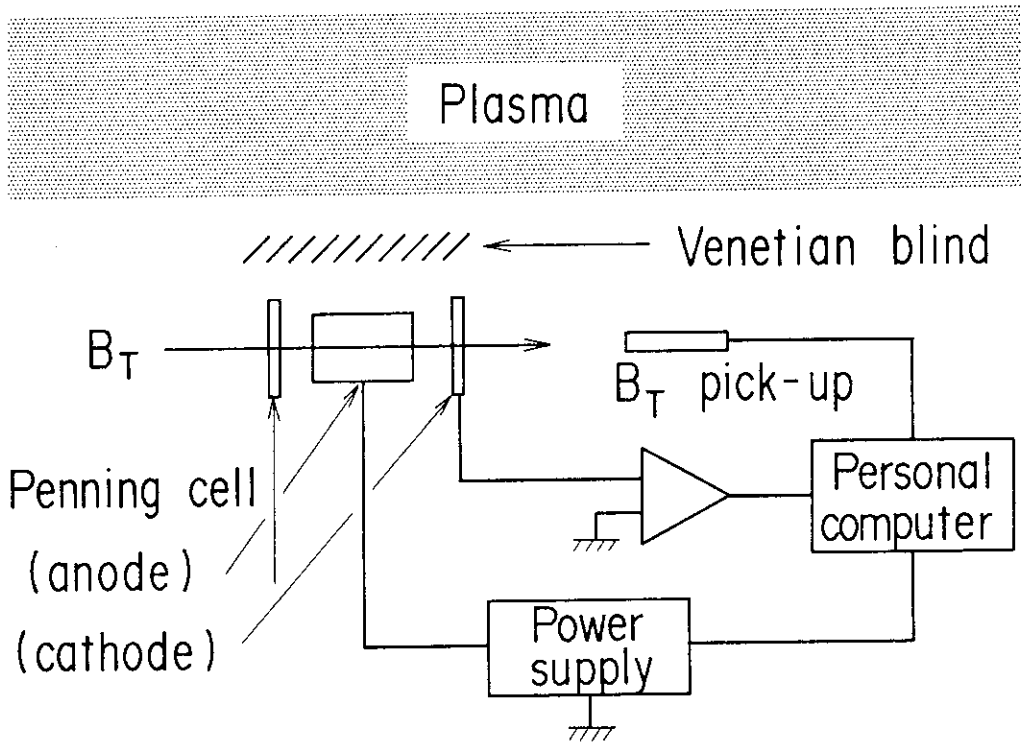

Fig. 5.2 Schematic diagram of gauge G_1. This is a type of Penning configuration gauge. A Penning discharge is sustained by the magnetic field (B_T) which is used for confining the tokamak plasma. This gauge is controlled by a personal computer. If the value of B_T is greater than 0.7 T, the gauge is switched on.

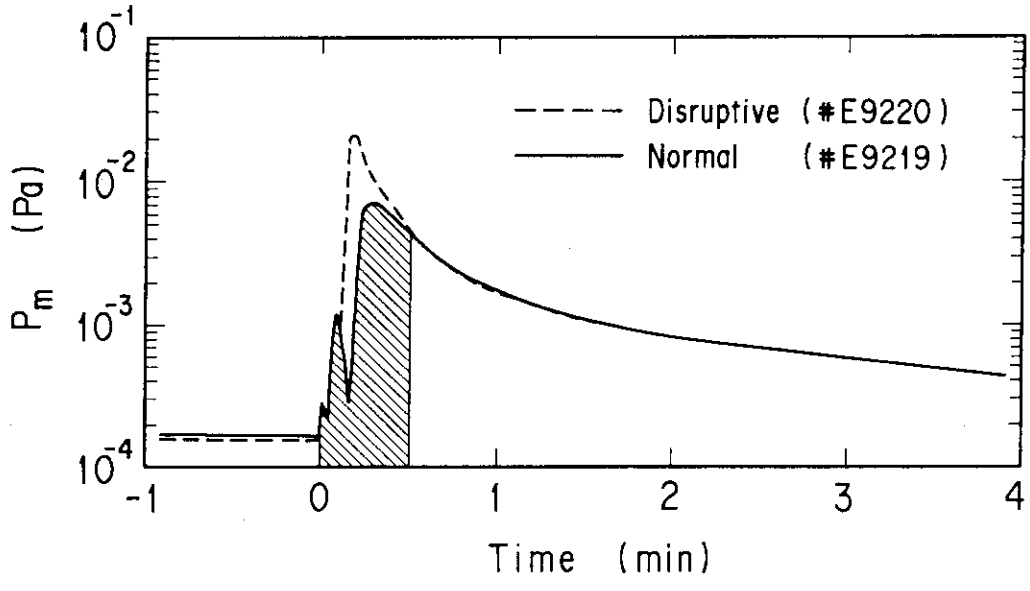

Fig. 5.3 Typical changes in the pressure P_m for normal (#E9219) and disruptive (#E9220) discharges. The hatched portion refers to the evacuated gases for 0-30 s in the case of the normal discharge (#E9219). The time evolution of the plasma is shown in Figs. 5.5(a) and 5.6(a) for the disruptive (#E9220) and normal (#E9219) discharges, respectively. Both the discharges have the limiter configuration.

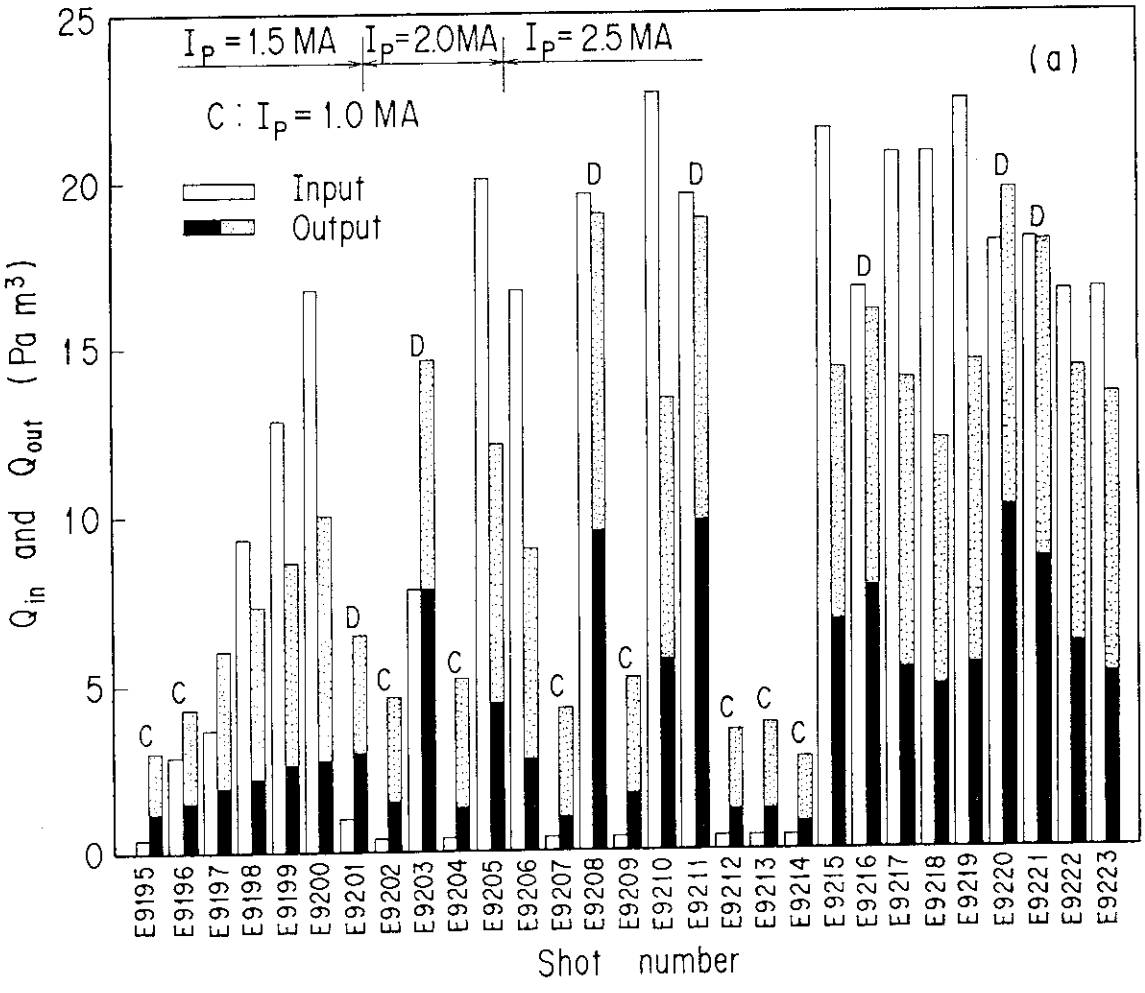

Fig. 5.4 (a) Bar chart of the gas input Q_{in} and the evacuated quantity Q_{out} with the discharges. The input is a sum of the one by gas puffing, neutral beam injection and pellet injection. The output is estimated by the pressure in the manifold and the effective pumping speed. The filled bar refers to the output for 0-30 s. Notations C and D refer to the conditioning and disruptive discharges, respectively. The conditioning discharges are ohmic heating plasmas with a current of 1 MA and small amounts of gases (0.4-1 Pam^3).
(b) Change in the accumulated gas quantity in the wall with the discharges. All the discharges shown in this figure have the limiter configuration.

Fig. 5.4 (Continued)

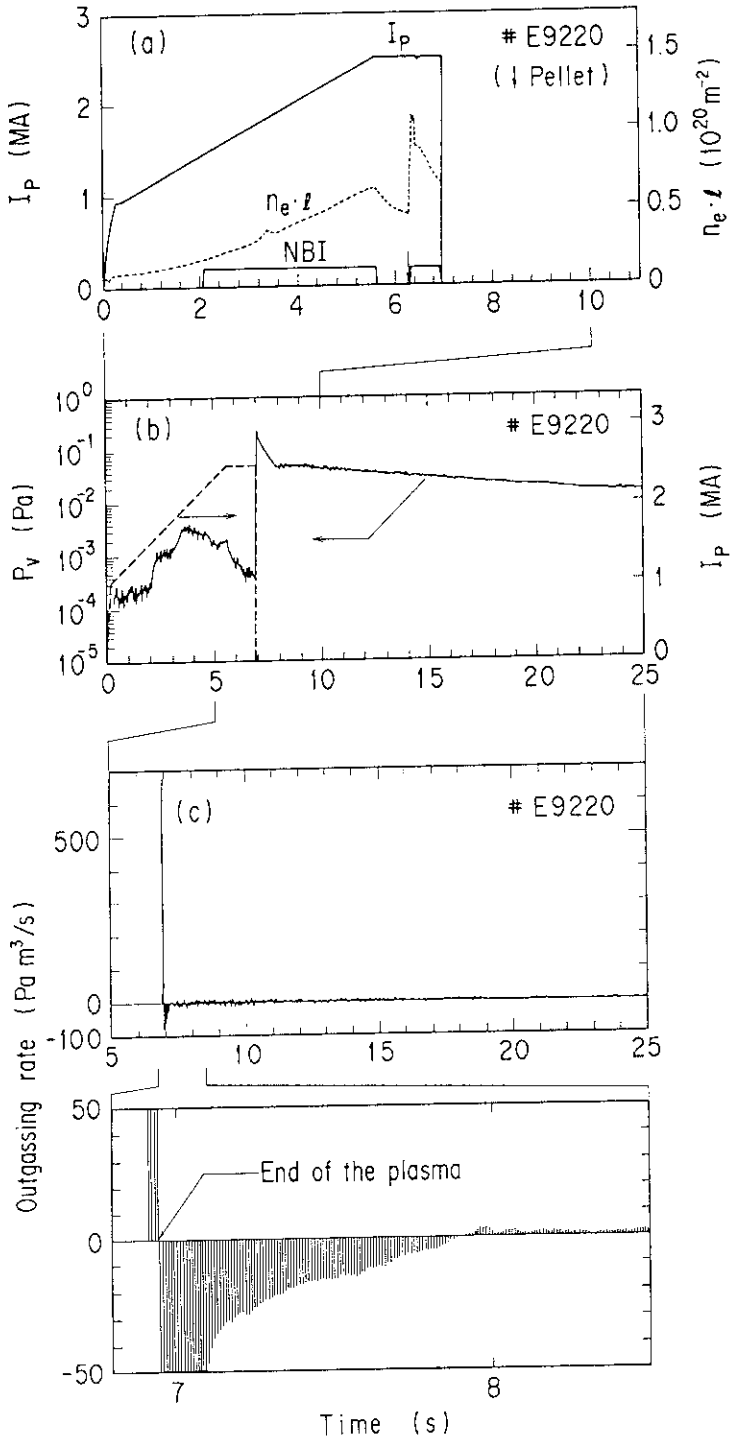

Fig. 5.5 Typical changes in the pressure and the outgassing rate after the disruptive discharge: (a) the evolution of the plasma; (b) the pressure P_v in the vacuum vessel just after the disruption; and (c) the outgassing rate near and after the end of the plasma. This discharge has the limiter configuration.

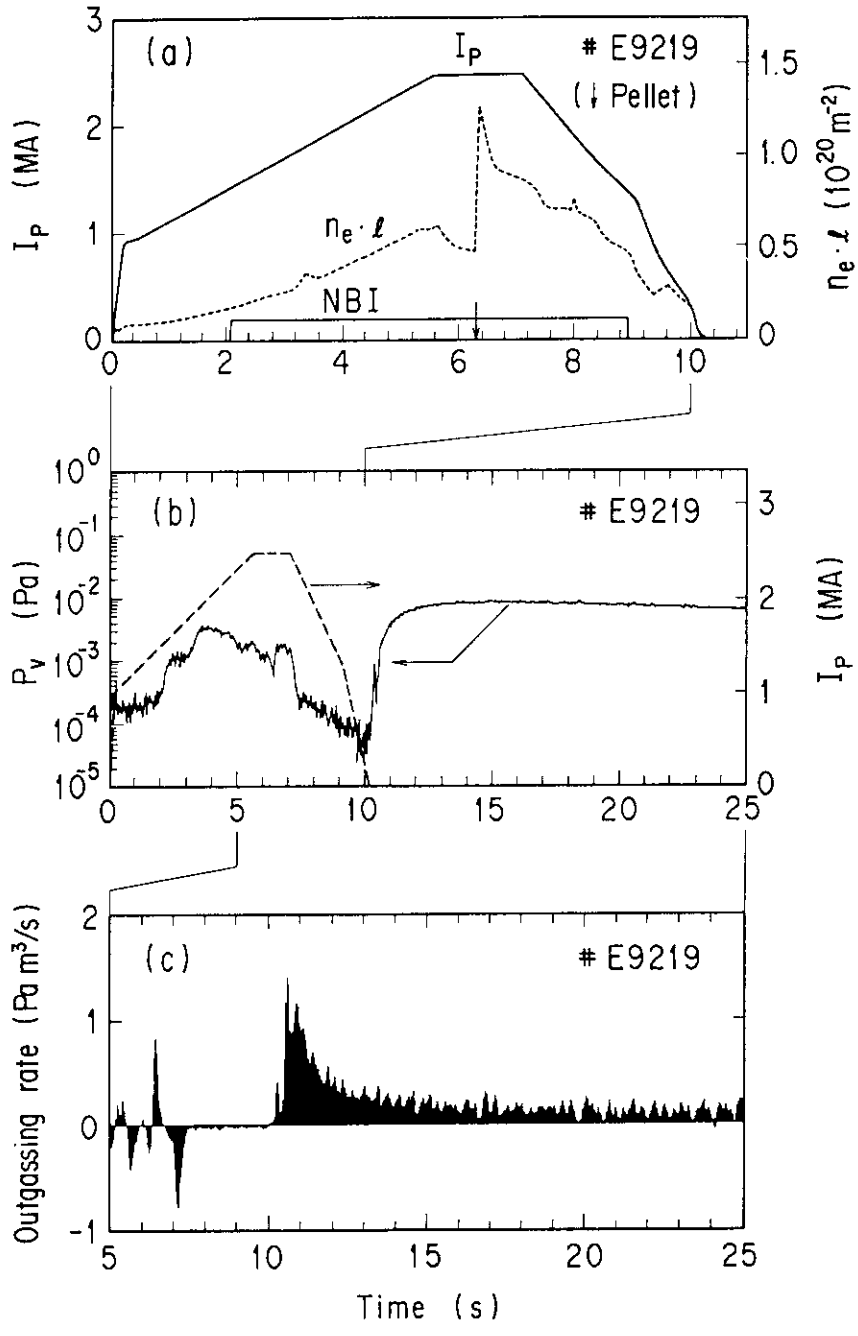

Fig. 5.6 Typical changes in the pressure and the outgassing rate after the normal discharge: (a) the evolution of the plasma; (b) the pressure P_v in the vacuum vessel after the gradual ending of the plasma; and (c) the outgassing rate near and after the end of the normal plasma. This discharge has the limiter configuration.

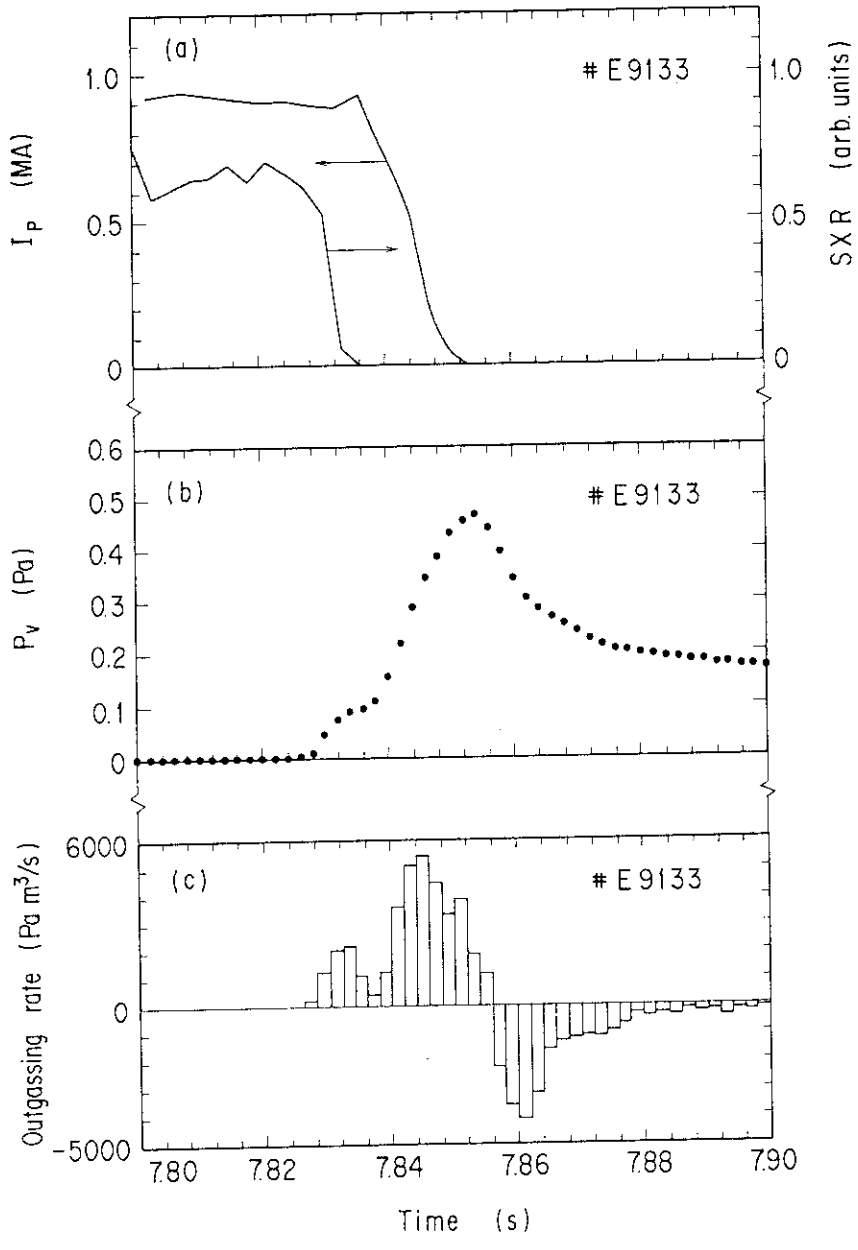

Fig. 5.7 Plasma features and the pressure change near and during the typical disruption: (a) changes in the plasma current I_p and the soft X-ray emissivity SXR; (b) change in the pressure P_v; and (c) outgassing rate. The pressure P_v is measured in a short response time (t<10 ms). This discharge has the divertor configuration.

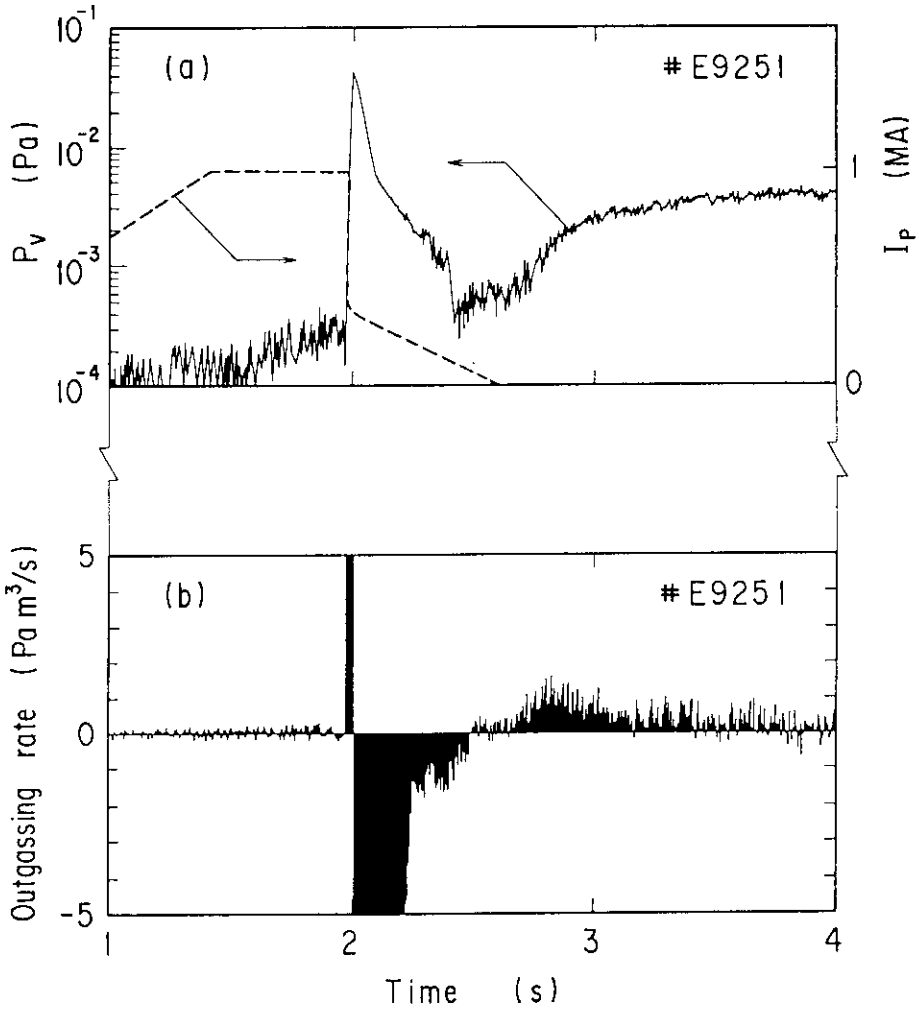

Fig. 5.8 Typical changes in the pressure and the outgassing rate after the disruptive discharge with a residual current for 0.6 s: (a) changes in the pressure P_v and the plasma current I_p; and (b) outgassing rate. The disruption occurs at t=2.0 s. Then the plasma current is successfully controlled to decrease gradually to zero. This discharge has the divertor configuration.

6. Conclusions

6.1 Summary of the present work

This report has described the studies on development of the pressure measurement methods, which are necessary to develop and confirm the particle control method for a long-pulse break-even plasma.

We first developed a new type of hot cathode ionization gauge with spherical symmetry to measure the neutral gas pressure in a high magnetic field. Its performance is summarized as follows:

(1) The gauge has a linear relation between the ion current and the pressure ranging from 10^{-4} to 1 Pa for N_2 and Ar.

(2) The changes in the sensitivity are small; within + 20% in a field of 0 - 1.2 T. The main reasons are that the collection probability of ions is unaffected by the magnetic field, and that the emitted electrons have almost the same probability of ionizing gas molecules as in zero magnetic field, owing to the spherical symmetry.

(3) The lower pressure limit is ascribed to the x-ray limit. On the other hand, the collective motion of ions gives an explanation to the upper pressure limit.

Then we describe a new method for using a Penning gauge to measure pressure in high magnetic fields. The intensity of the H_α and H_β Balmer lines emitted from a Penning discharge is a function only of the discharge ion current: their intensity is independent of anode voltage and magnetic fields from 0.1 to 2.0 T. The light intensity is proportional to the ion current below ~ 0.1 Pa. The ratio of the light intensity to the ion current increases by 40% for pressures above ~ 0.1 Pa because of a change

in the type of discharge. The higher pressure discharge probably has a lower electron temperature. In addition, we demonstrated the possibility of the partial pressure measurement with the light emitted from the Penning discharge. The following results are obtained:

(1) The spectral line intensity is proportional to the pressure if the cathode current increases with the pressure.

(2) The line intensities are individually linear to the partial pressure in the gas mixture of H_2 and He.

Next we have constructed the fast pressure monitoring system with the newly developed gauges. The gauges are used to monitor the pressure near the JT-60 plasma. The main features of the gauges are as follows:

a) The response time is fast (less than 10 ms) because of the Penning discharge which is sustained by the confining magnetic field of the plasma.

b) The structure is very simple; the necessary electrodes are an anode and cathode (two plates). Therefore the gauges are reliable for use in severe conditions in a fusion device.

Finally, the usefulness of the fast response gauge is demonstrated. The outgassing mechanisms are studied in the JT-60 tokamak. The following points are noted:

(1) The evacuated gas quantity after a typical disruption is almost equal to or greater than the input. On the other hand, the evacuated quantity after a quiet ending of the plasma is less than the input.

(2) Large amounts of gases are abruptly released in two stages during the disruption of the plasma. The first gas release occurs at the time of the soft x-ray crash. This is ascribed to the

abrupt heat flux due to the loss of the plasma thermal energy (thermal quench). The second appears during the decay of the plasma current. The heat flux due to the loss of the plasma magnetic energy causes the second gas release. The energetic particles are most likely to focus on the limited area of the first wall.

(3) The disruptions of 1 MA plasmas outgas a surface area of ~10 m^2. The gases of 30-80 Pam^3 are released within 30 ms; three quarters of them return to the wall. This return of the gases to the wall must be examined in order to efficiently use the disruption for the reduction of hydrogen content.

(4) The gases are released after the end of the plasma current in the normal discharges. The hydrogen atoms probably diffuse in the bulk to the surface. The activation energy is estimated to be less than 1.5 eV.

(5) Finally, we discuss the use of the controlled disruption for reducing the content of fuel particles in the first wall. We hope that the controlled disruption will be one of the useful techniques for the inventory control.

6.2 Future investigation

In order to realize a quasi-steady-state fusion reactor, we must develop and confirm a technique for fueling and particle control. Fuel particles will be injected by a newly developed pellet injector. The speed of the pellet will be ~10 km/s for reaching the plasma center. Because we have a density limit due to the limitation of β value, we must operate the plasma in the

fixed region of the electron density. Therefore, we have to evacuate the particles (fuel particles and He ash particles) from the plasma boundary in order to maintain the plasma. We can measure the particle density at any plasma boundary with the newly developed methods, therefore we will examine the particle flow from the plasma to the ordinary pumping system to develop and perfect the fuel control technique. First, we must study the pump limiter and divertor (open and closed) with JT-60 upgrade to determine whether they have the ability to evacuate the particles during a long-pulse break-even plasma. In addition, we will examine the He ash exhaust in order not to dilute the fuel and not to degrade the fusion reactivity.

We hope that these new methods will prove of fundamental use in the operation of the fusion reactor.

Acknowledgments

The author would like to express his sincere appreciation to Professor A. Kawazu of Tokyo University for his continuous guidance and affectionate encouragement.

The author also wishes to express his appreciation to Professor A. Kimbara, Professor F. Shimizu, Professor N. Inoue, and Professor T. Okano of Tokyo University for their encouragement and kind advice.

The author expresses his sincere gratitude to Drs. M. Yoshikawa, T. Iijima, Y. Tanaka, and H. Shirakata for their continuous support and encouragement.

The author is most grateful to Drs. I. Kondo and M. Maeno for their valuable insight and suggestion to this work. All the

fixed region of the electron density. Therefore, we have to evacuate the particles (fuel particles and He ash particles) from the plasma boundary in order to maintain the plasma. We can measure the particle density at any plasma boundary with the newly developed methods, therefore we will examine the particle flow from the plasma to the ordinary pumping system to develop and perfect the fuel control technique. First, we must study the pump limiter and divertor (open and closed) with JT-60 upgrade to determine whether they have the ability to evacuate the particles during a long-pulse break-even plasma. In addition, we will examine the He ash exhaust in order not to dilute the fuel and not to degrade the fusion reactivity.

We hope that these new methods will prove of fundamental use in the operation of the fusion reactor.

Acknowledgments

The author would like to express his sincere appreciation to Professor A. Kawazu of Tokyo University for his continuous guidance and affectionate encouragement.

The author also wishes to express his appreciation to Professor A. Kimbara, Professor F. Shimizu, Professor N. Inoue, and Professor T. Okano of Tokyo University for their encouragement and kind advice.

The author expresses his sincere gratitude to Drs. M. Yoshikawa, T. Iijima, Y. Tanaka, and H. Shirakata for their continuous support and encouragement.

The author is most grateful to Drs. I. Kondo and M. Maeno for their valuable insight and suggestion to this work. All the

members of JT-60 Facility Division II are gratefully acknowledged for their help in operating the machine.

This work was performed at Japan Atomic Energy Research Institute as one of the works in JT-60.

Publication list

(1) N. Ogiwara and M. Maeno, J. Vac. Sci. Technol. A6, 2870 (1988). (Chapter 2)

(2) N. Ogiwara and M. Maeno, J. Vac. Sci. Technol. A7, 2804 (1989). (Chapter 3,4)

(3) N. Ogiwara and M. Maeno, Shinku [J. Vac. Soc. Jpn.] 32, 292 (1989). (Chapter 3)

(4) N. Ogiwara, Y. Yamashita, H. Yokomizo, M. Maeno, T. Shimada, and F. Kimijima, Shinku [J. Vac. Soc. Jpn.] 31, 406 (1988). (Chapter 4)

(5) N. Ogiwara and M. Maeno, Shinku [J. Vac. Soc. Jpn.] 33, 381 (1990). (Chapter 5)

(6) N. Ogiwara and M. Maeno, J. Vac. Sci. Technol. A8, 3855 (1990). (Chapter 4,5)

(7) N. Ogiwara and M. Maeno,"Large amounts of gas release just after disruptive discharges in the JT-60 tokamak", to be published in J. Nucl. Mater. (1990). (Chapter 3,5)